

**Influence of Atmospheric Processes and Chemical Transformations  
on Nitrogen Deposition to Coastal Regions**

Dissertation

zur Erlangung des Doktorgrades  
der Naturwissenschaften im Fachbereich  
Geowissenschaften  
der Universität Hamburg

vorgelegt von

Laura M. Klein

aus

Bloomington, Indiana, USA

Hamburg

2002

Als Dissertaton angenommen vom Fachbereich Geowissenschaften  
der Universität Hamburg  
auf Grund der Gutachten von Priv. Doz. Dr. K. Heinke Schlünzen  
und Prof. Dr. Guy. Brasseur

Hamburg, den 1. November, 2002

Prof. Dr. J. O. Backhaus  
Prodekan  
des Fachbereichs Geowissenschaften

## Abstract

To understand the mechanisms governing the dispersal, transformation and deposition of pollutants from the atmosphere to coastal waters, coastal meteorology must first be considered. This study focuses on the deposition of atmospheric inputs of inorganic nitrogen compounds (NO, NO<sub>2</sub>, HNO<sub>3</sub>, NH<sub>3</sub>) into the southern North Sea. The three-dimensional Eulerian mesoscale transport model METRAS is used in this study to simulate meteorology in the coastal regions and the SEMA box model and the chemistry transport model MECTM were applied to determine the impact of meteorology and chemical transformations on deposition and the resultant nitrogen loads into the coastal waters. The studies are performed for the 1998 ANICE field campaign.

The results of the METRAS meteorology runs were validated against observations using a series of programs developed for that purpose. With the model system METRAS/MECTM the influence of meteorological phenomena and gas phase chemical transformations on nitrogen deposition are studied and total N deposition loading to the study area is calculated.

This study shows that even though emissions play a large role in nitrogen loading, the secondary pollutants arising from the chemical transformations have a much greater impact on deposition. It is also shown that meteorology can direct an input event (June 20<sup>th</sup>), but a combination of meteorological influences such as wind speed and wind direction, and chemical transformations can also have a significant impact (June 18<sup>th</sup>).

The aerosol box model SEMA study shows that aerosol formation in the coastal region would greatly alter the input calculated from gas phase-only chemical transport models, and is an important contributing process.

## Zusammenfassung

Um die Mechanismen zu verstehen, die Ausbreitung, Umwandlung und Deposition von Schadstoffen aus der Atmosphäre in küstennahe Gewässer bestimmen, muss zunächst die Meteorologie in den Küstengebieten betrachtet werden. Die hier vorgestellte Studie beschäftigt sich insbesondere mit der Deposition von atmosphärischen Einträgen anorganischer Stickstoffverbindungen ( $\text{NO}$ ,  $\text{NO}_2$ ,  $\text{HNO}_3$ ,  $\text{NH}_3$ ) in die südliche Nordsee. Das dreidimensionale mesoskalige Eulersche Transportmodell METRAS wird verwendet, um die Meteorologie in den Küstengebieten zu simulieren. Mit Hilfe des Aerosol-Boxmodells SEMA und des Chemie-Transport Modells MECTM wird der Einfluss von meteorologischen Prozessen und chemischen Umwandlungen auf die Deposition und den daraus resultierenden Stickstoffeintrag in küstennahe Gewässer bestimmt. Die Untersuchungen beziehen sich auf die 1998 durchgeführte Feldkampagne ANICE.

Die Ergebnisgüte des meteorologischen Modells METRAS wird anhand eines Vergleichs mit Beobachtungen beurteilt. Zu diesem Zweck wurden eigens Evaluierungsprogramme entwickelt. Mit dem Modellsystem METRAS/MECTM wird der Gesamtbetrag der Stickstoffdeposition im Untersuchungsgebiet berechnet und der Einfluss von chemischen Umwandlungen in der Gasphase und meteorologischen Prozessen untersucht.

Die Untersuchungen zeigen, dass Emissionen eine große Rolle im Stickstoffhaushalt spielen, dass aber die sekundären Schadstoffe, die bei chemischen Umwandlungen entstehen, einen wesentlich stärkeren Einfluss auf die trockene Deposition haben. Darüber hinaus zeigt die Studie, dass Meteorologie bereits ohne wesentlichen Beitrag der Atmosphärenchemie zu einem Depositionsereignis führen kann (20. Juni), dass aber auch das Zusammenwirken meteorologischer Einflussgrößen wie Windgeschwindigkeit und Windrichtung mit chemischen Umwandlungen große Bedeutung haben kann (18. Juni).

Die Untersuchungen mit dem Aerosol-Boxmodell SEMA zeigen, dass die Bildung von Aerosolen im Küstengebiet zu Stickstoffeinträgen führt, die sich wesentlich von Ergebnissen der nur mit Gasphasenchemie durchgeführten Modellrechnungen unterscheiden. Somit leistet die Aerosolbildung einen wichtigen Beitrag zur Stickstoffdeposition.

# Table of Contents

<b>ABSTRACT</b> .....	<b>I</b>
<b>ZUSAMMENFASSUNG</b> .....	<b>II</b>
<b>TABLE OF CONTENTS</b> .....	<b>III</b>
<b>TABLE OF FIGURES</b> .....	<b>V</b>
<b>TABLE OF TABLES</b> .....	<b>VII</b>
<b>1. INTRODUCTION</b> .....	<b>1</b>
<b>2. INVESTIGATING NITROGEN DEPOSITION IN A COASTAL ENVIRONMENT</b> .....	<b>4</b>
2.1 PHYSICAL COASTAL PROCESSES .....	4
2.1.1 Coastal Meteorology.....	4
2.1.2 Coastal Meteorological Effects on Pollutants .....	6
2.2 CHEMICAL COASTAL PROCESSES .....	7
2.2.1 Gas Phase Chemistry.....	7
2.2.2 Aerosol Phase Chemistry.....	8
2.2.2.1 Physical Aerosol Processes.....	8
2.2.2.2 Aerosol Chemistry processes .....	9
2.2.2.3 Aerosols in Coastal Regions .....	11
2.2.2.4 Aerosol Behavior over the North Sea .....	12
2.3 DRY DEPOSITION .....	13
2.3.1 Dry Deposition of Gases.....	13
2.3.2 Dry Deposition of Aerosols.....	14
2.4 AEROSOL MODELING.....	15
<b>3. MODELS AND INPUT DATA</b> .....	<b>19</b>
3.1 THE METRAS/MECTM MODEL SYSTEM.....	19
3.1.1 Mesoscale Model METRAS.....	19
3.1.2 Mesoscale Chemistry Model MECTM.....	21
3.1.3 Sectional Aerosol Model SEMA.....	24
3.2 DATA SOURCES AND PRE-PROCESSING .....	26
3.2.1 Input for METRAS.....	26
3.2.2 Emission Data and Photolysis Rates for MECTM.....	29
3.2.3 Initial Values for METCM .....	30
3.2.4 Initial Values for SEMA Box Model.....	30
<b>4. THE INFLUENCE OF COASTAL METEOROLOGICAL PHENOMENA</b> .	<b>32</b>
4.1 EVALUATION OF METRAS METEOROLOGY RESULTS.....	32
4.2 INFLUENCE OF METEOROLOGY ON POLLUTION DISPERSION MECHANISMS .....	36
4.3 INFLUENCE OF METEOROLOGY ON PASSIVE TRANSPORT .....	39

<b>5.</b>	<b>INFLUENCE OF CHEMICAL TRANSFORMATIONS.....</b>	<b>43</b>
5.1	INFLUENCE OF GAS PHASE CHEMISTRY .....	43
5.2	INFLUENCE OF AEROSOL PHASE CHEMISTRY.....	48
<b>6.</b>	<b>INFLUENCE OF PHYSICAL AND CHEMICAL PROCESSES ON DEPOSITION .....</b>	<b>53</b>
6.1	PASSIVE TRACER DEPOSITION STUDIES .....	53
6.2	GAS PHASE CHEMISTRY DEPOSITION STUDIES .....	55
6.3	PASSIVE TRACER VS. CHEMISTRY DEPOSITION.....	59
<b>7.</b>	<b>DISCUSSION AND CONCLUSIONS.....</b>	<b>62</b>
	<b>APPENDIX A: DEPOSITION FACTORS .....</b>	<b>65</b>
	<b>APPENDIX B: MECTM CHEMICAL SPECIES.....</b>	<b>71</b>
	<b>APPENDIX C: CHEMICAL MECHANISM REACTIONS .....</b>	<b>73</b>
	<b>APPENDIX D: LANDUSE CLASSES.....</b>	<b>79</b>
	<b>APPENDIX E: EMISSION CHEMICAL SPECIES.....</b>	<b>81</b>
	<b>APPENDIX F: STAR PHOTOLYTIC REACTIONS .....</b>	<b>82</b>
	<b>APPENDIX G: SEMA BOX-MODEL SENSITIVITY ANALYSIS.....</b>	<b>84</b>
	<b>LIST OF SYMBOLS .....</b>	<b>85</b>
	<b>ACKNOWLEDGEMENTS .....</b>	<b>86</b>
	<b>REFERENCES .....</b>	<b>87</b>

## Table of Figures

Figure 1-1. METRAS model domain (boxed area) and NO <sub>x</sub> emissions for June 16, 1998. (Figure taken from the emission data set, description provided by Wickert (2000)) ....	2
Figure 2-1. Coastal Boundary Layers .....	4
Figure 2-2. Simplified Scheme of the Sea Breeze Circulation .....	5
Figure 2-3. Simplified Scheme of the Land Breeze Circulation.....	6
Figure 3-1. Overview of the Model System METRAS/MECTM.....	19
Figure 3-2. Surface (S, solid lines) and Geostrophic (G, dashed lines) backward wind trajectories in 3-hour increments for June 16, 1998. The maximum life times of the air parcels represented is 60 hrs, the minimum is 24 hrs for G winds, and 60 hrs for S winds.....	27
Figure 3-3. Surface (S, solid lines) and Geostrophic (G, dashed lines) backward wind trajectories for WAO in 3-hour increments for June 20, 1998. The maximum life times of the air parcels represented is 60hrs, the minimum is 58 hrs for G winds, and 23 hrs for S winds. ....	28
Figure 3-4. Surface (S, solid lines) and Geostrophic (G, dashed lines) backward wind trajectories for WAO in 3-hour increment for June 21, 1998. The maximum life times of the air parcels represented is 60 hrs, the minimum is 19 hrs for G winds, and 60 hrs for S winds. ....	28
Figure 3-5. Measured Concentrations at WAO, June 16, 1998. The original measurements were redistributed to create an input for the SEMA box model. (WAO-12, 8:02h-16:02h, June 16).....	31
Figure 4-1. Stability vs. height based on rawindsonde data for Hemsby, UK, 12Z June 16th, 1998. ....	34
Figure 4-2. West-east vertical cross-section to 1500m height of vertical exchange coefficient in m <sup>2</sup> /s at 53° North during the day (a) and during the night (b) for June 16, 1998. The North Sea is situated in the center and is bounded by England and the Netherlands. (Figure not to scale).....	36
Figure 4-3. Vertical cross-section of potential temperature (shaded area) and specific humidity (contour lines) to 2500m height, June 16, 22:00. The cross-section is taken at the same latitude as the MPN site (figure is not to scale). The eastern coast of England is on the far left, and the western coast of the Netherlands on the right side of the plot. ....	38
Figure 4-4. Boundary layer heights at sites MPN, WAO, and a continental site. ....	38
Figure 4-5. Minimum concentrations at a height of 10m, June 16, 1998 (ppb). Runs included emissions and deposition but no chemical reactions.....	40
Figure 4-6. Hourly concentrations at a height of 10m, June 16, 1998 (ppb). Runs included emissions and deposition but no chemical reactions. ....	41
Figure 4-7. SO <sub>2</sub> maximum hourly concentration (ppb), 23:00 (scaled to a max of 20 ppb) at a height of 10m, June 16, 1998. Runs included emissions and deposition but no chemical reactions.....	42
Figure 5-1. Minimum hourly concentrations at a height of 10m, June 16, 1998 (ppb) when including chemical reactions.....	44
Figure 5-2. Same as in Figure 5-1, except for O <sub>3</sub> and SO <sub>2</sub> . ....	45

Figure 5-3. Maximum hourly concentrations at 10m, June 16, 1998(ppb) when including chemical reactions. ....	46
Figure 5-4. Same as in Figure 5-3, except for O <sub>3</sub> and SO <sub>2</sub> . ....	47
Figure 5-5. SEMA results using a relative humidity of 95%, temperature of 15°C, and completing the ion budget with H <sup>+</sup> . ....	49
Figure 5-6. SEMA results using a relative humidity of 95%, temperature of 15°C, and completing the ion budget with Na <sup>+</sup> . ....	49
Figure 5-7. MPN-9 measurements taken from 13:12h - 20:44h June 16, 1998. ....	50
Figure 5-8. MPN-10 measurements taken from 21:38h June 16, 1998 to 12:06h June 17, 1998. ....	50
Figure 6-1. Daily deposition values for various nitrogen compounds with no gas phase chemistry (only passive tracers), June 16 1998 (mg/m <sup>2</sup> /day).....	54
Figure 6-2. Daily deposition values for various nitrogen compounds, June 16, 1998 (mg/m <sup>2</sup> /day, scaled to a maximum of 1 mg/m <sup>2</sup> /day N). ....	55
Figure 6-3. Hourly deposition values for N-NO <sub>2</sub> and S-SO <sub>2</sub> , 14:00, June 16, 1998 (µg/m <sup>2</sup> /hour, scaled to a maximum of 5 µg/m <sup>2</sup> /hour).....	56
Figure 6-4. Daily deposition values for N-HNO <sub>3</sub> and N-NH <sub>3</sub> , June 17, 1998 (mg/m <sup>2</sup> /day, scaled to a max of 2 mg/m <sup>2</sup> /day N). ....	56
Figure 6-5. Daily deposition values for N-HNO <sub>3</sub> and N-NH <sub>3</sub> , June 18, 1998 (mg/m <sup>2</sup> /day). (N-HNO <sub>3</sub> scaled to a max of 4 mg/m <sup>2</sup> /day N, N-NH <sub>3</sub> scaled to a max of 2 mg/m <sup>2</sup> /day. ....	57
Figure 6-6. Daily deposition values for N-HNO <sub>3</sub> and N-NH <sub>3</sub> , June 19, 1998 (mg/m <sup>2</sup> /day, scaled to a max of 2 mg/m <sup>2</sup> /day N). ....	57
Figure 6-7. Daily deposition values for N-HNO <sub>3</sub> and N-NH <sub>3</sub> , June 20, 1998 (mg/m <sup>2</sup> /day, scaled to a max of 4 mg/m <sup>2</sup> /day). ....	58
Figure 6-8. Total N Deposition to the southern North Sea as Modeled by METRAS/MECTM (region covers 83,520 km <sup>2</sup> ).....	59
Figure 6-9. Total N Deposition to the southern North Sea as Modeled by METRAS/MECTM for the Chemistry and No Chemistry cases, June 16th, 1998.....	60

## Table of Tables

Table 2-1. Comparison of Thermodynamic Equilibrium Aerosol Models from Literature .....	18
Table 4-1. Forecast accuracy of METRAS for the period June 16-20, 1998. ....	33
Table 4-2. Forecast accuracy of METRAS correlated to the ANICE stations. ....	33
Table 5-1. Total Concentrations, Box-Model Results vs. Observations.....	51
Table A-1. Conversion factor $\hat{r}_s^{species}$ and surface parameters $r_s$ for gaseous species.....	65
Table A-2. Parameters $r_{s,min}$ , $r_{s,max}$ , and $r_{s,wet}$ for SO <sub>2</sub> .....	66
Table A-3. Parameters $r_{s,min}$ , $r_{s,max}$ , and $r_{s,wet}$ for PAN.....	67
Table A-4. Parameters $r_{s,min}$ , $r_{s,max}$ , and $r_{s,wet}$ for PAA.....	68
Table A-5. Conversion factor $\hat{r}_s^{species}$ (same equations as those above, but using values of $r_s^{Pb}$ , Table A-6) and surface parameters $r_s$ for particulate species .....	69
Table A-6. Parameters $r_{s,min}$ , $r_{s,max}$ , and $r_{s,wet}$ for Pb .....	70
Table B-1. MECTM Species List .....	71
Table C-1. MECTM's Modified RADM2 Mechanism Reactions.....	73
Table D-1. METRAS/MECTM Landuse Classes.....	79
Table D-2. STAR photolysis rate Landuse classes (adapted from Ruggaber, 1991) .....	79
Table D-3. Biogenic Emission Factors Landuse Classes (Adapted from McKeen et al., 1991) .....	80
Table D-4. Relation Matrices for METRAS/MECTM Landuse Classes with Photolysis Rates (STAR) and Biogenic Emission Factors.....	80
Table E-1. Emission Species used for MECTM.....	81
Table F-1. STAR photolytic reactions and relation to the MECTM chemistry.....	82
Table G-1. SEMA Results vs. Measurements (hit rates based on deviations <50% of measured data in 8 sections) .....	84



## **1. Introduction**

The study of coastal zones and the associated processes is essential when considering that 71% of the earth's surface is covered by water delineated by 436,800 km of coastline. Throughout history, the human population has shown a tendency to settle along the world's coastal zones and the effects of humans inhabiting shores and coastlines have become increasingly apparent. Coastal pollution is creating ecosystem problems and costing government and industry billions of dollars remediation efforts. This pollution includes the atmospheric pollution resulting from emissions that originate in the coastal regions.

Of particular interest is the atmospheric nitrogen input to coastal waters due to dry deposition that accounts for a major fraction of the total atmospheric nitrogen deposition to natural bodies of water. It is estimated that 27% of the total nitrogen input to the North Sea is from direct atmospheric deposition to the water. This percentage does not include the deposition to the watershed that is eventually runoff into the sea (Duce, 1998). Dry deposition of particulate contaminants to natural waters contributes to the degradation of aquatic ecosystems; for example, excess inputs of biologically available nitrogen ( $\text{NO}^-$ ,  $\text{NH}_3/\text{NH}_4^+$ ) may enhance algae growth leading to eutrophication.

Shallow coastal waters are particularly susceptible to human-induced eutrophication due to their proximity to large sources of inorganic and organic anthropogenic emissions. The combination of these emissions with complex meteorology results in atmospheric inputs to the coastal waters that are highly variable in space and time in comparison to the fluvial inputs, which are confined to river mouths and deltas. Most notably, specific meteorological situations have been identified where this combination has resulted in high deposition events (Spokes et al., 1993). Understanding the mechanisms governing the dispersal, transformation, and deposition of pollutants from the coastal atmosphere is essential for the development of a strategy to reduce the input of nutrients, which promote eutrophication, into the water from dry deposition.

The first step in fully comprehending the process of nutrient deposition into coastal regions is understanding the coastal meteorology and its impact on pollutants. Pollution dispersion is dependent on meteorological parameters such as atmospheric stability and windspeed and the cases where high pollution concentrations are observed near the ground can often be related to the meteorological conditions occurring at that time, including advection. Local emissions undergo chemical and physical transformations that are influenced by the meteorological parameters listed above, as well as with humidity and solar radiation.

This study attempts to determine those physical and chemical processes that have the greatest effect on the nitrogen deposition to the coastal region. For this purpose meteorology and chemical transport models were applied to the southern North Sea region. The im-

## 1. Introduction

impact of coastal meteorology and gas phase chemistry on deposition and the resultant nitrogen loads into a water body has been determined.

The southern North Sea area was selected due to its combination of coastline, open water, and urban and agricultural emission sources. The southern North Sea area (Figure 1-1) is mostly low-level land and most of the industrial activity is located in the eastern region (Belgium, The Netherlands, Germany). The emissions in the western part of the modeled area originate in London and are mainly industrial and transportation in nature. The eastern land region is also highly agricultural and there is a great influx of ammonia emissions in the lowlands. Measurements are available for both sides of the water body from the ANICE (Atmospheric Nitrogen Input to the Coastal Environment) experiment, which ran from June 15-20, 1998. Other available data for that region includes routine measurement data and routine weather forecasts.

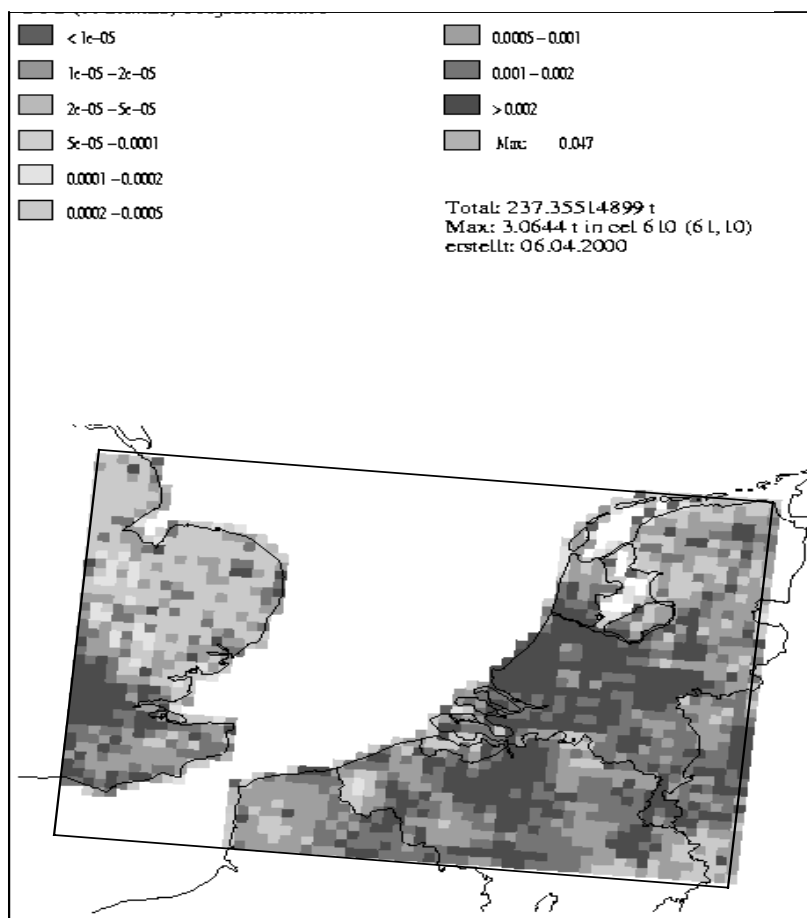


**Figure 1-1.** METRAS model domain (boxed area) and NO<sub>x</sub> emissions for June 16, 1998. (Figure taken from the emission data set, description provided by Wickert (2000))

Large changes occur in both the physical and chemical properties of an air mass advected from land over sea. For example the humidity increases, the surface properties change, and the emission sources change from mostly anthropogenic to mostly biogenic. When modeling this area it is necessary to resolve short time scales to capture the characteristics of such gaseous species as  $\text{NH}_3$  and  $\text{HNO}_3$  because of their relatively short residence time attributable to both their reactivity and scavenging by sea salt aerosols. These factors lead to the hypothesis that a significant part of the nitrogen compounds may be removed from the atmosphere in the first 10 to 20 km of the maritime atmosphere where high nitrogen concentration continental air moves over the North Sea. Taking into account physical and chemical processes in the transport-chemistry models aids in estimation of nitrogen deposition in these areas.

The MEscale TRANsport and fluid (Stream) model, METRAS (Schlünzen, 1990; Schlünzen et al., 1996) has been applied to simulate these coastal atmospheric meteorological phenomena during the period of June 15-20, 1998. METRAS is a multi-layer meteorology model that can generate three-dimensional meteorology fields. The results from the meteorology runs were then used with the MEscale Chemistry Transport Model (MECTM) (Müller et al., 2001) which includes the RADM2 gas phase chemistry mechanisms (Stockwell et al., 1990). The MECTM was run with full chemistry and also with emissions and deposition but no chemical reactions in order to study the influence of both pure meteorology and chemical reactions on concentrations and deposition. The aerosol box-model SEMA (von Salzen, 1997; von Salzen and Schlünzen, 1999a,b) was also applied to this study region to obtain a general idea of the influence of aerosol chemistry on nitrogen deposition. SEMA combines a thermodynamic equilibrium approach with a kinetic approach to predict the condensation and evaporation of gases at the surface of the aerosol.

These models are applied to the southern North Sea in order to investigate the dominant meteorological parameters that are affecting the gas phase pollutant concentrations in the coastal regions and also to investigate those impacting the nitrogen loads into the water body through dry deposition. Before the influence of meteorological phenomena (Chapter 4) and gas phase chemical transformations (Chapter 5) on deposition (Chapter 6) are discussed, the nitrogen transport in coastal environments is discussed in more detail (Chapter 2) and the models are introduced (Chapter 3). In the final chapter, Chapter 7, the results will be discussed and conclusions will be drawn.

## 2. Investigating Nitrogen Deposition in a Coastal Environment

### 2.1 Physical Coastal Processes

The amounts of nitrogen deposited to the coastal waters are not driven by chemical emissions and transformation processes alone, but are also strongly influenced by the physical processes (Owens et al., 1992; Michaels et al., 1993; Spokes et al., 1993, Angevine et al., 1996b, Aneja et al., 2001). Pollutants are transported through advection, dispersed by diffusion, and removed through precipitation scavenging and deposition, which are all results of meteorological phenomena. Since mesoscale meteorological processes are dependant upon parameters as orography and land use, coastal meteorological conditions vary greatly from those conditions found in an inland region.

#### 2.1.1 Coastal Meteorology

One of the principle areas of coastal meteorological study has been the growth of the Internal Boundary Layer (IBL), mainly concerning the influence of this boundary layer on coastal pollution from industrial sites. The IBL can develop at the coastline below the planetary boundary layer (PBL) due to the difference in aerodynamic roughness changes and the differences in surface temperature between land and water resulting in an interface (Figure 2-1).

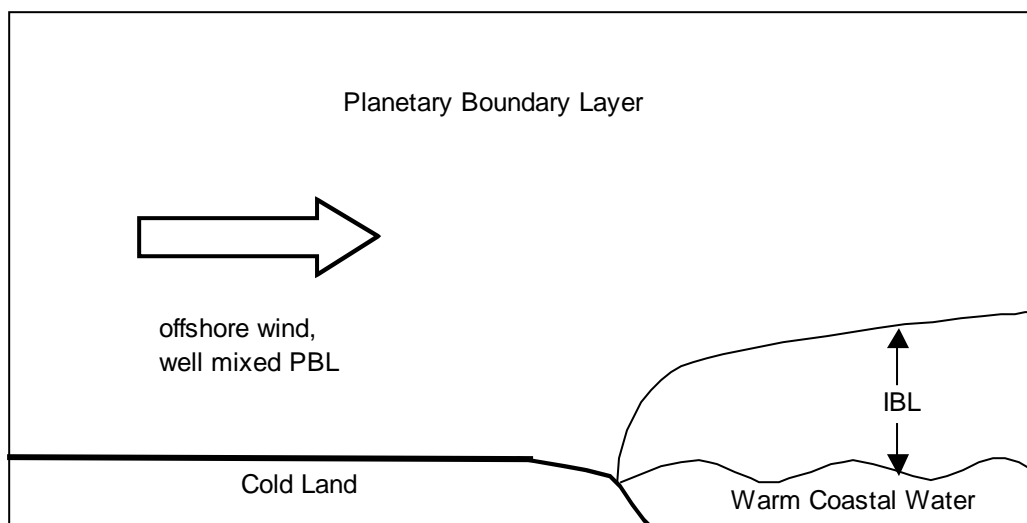


**Figure 2-1.** Coastal Boundary Layers

The surface layer is a region of strong wind shear that comprises the bottom 10 percent of the boundary layer and ranges from about 10-100m thick and is lower than the IBL. There

is a shear stress in this layer due to friction at the surface and wind in the atmosphere, and this shear stress enhances motion on a molecular scale and creates eddies which transfer momentum and energy vertically and horizontally, thus creating turbulence (Jacobson, 1999a). Surface layer turbulence in coastal regions is impacted by the meeting of land and water shorelines because, similar to the IBL development, there is an abrupt change in physical parameters such as land use and orography which in turn leads to local differences in heat absorption and reflection as well as surface friction. These dynamic and thermal differences can either maintain or reduce the energy of the turbulence, which enhances or limits advection and dispersion within the surface layer.

The thermal differences at a coastline can also generate local wind fields. During the morning as the land surface heats a horizontal temperature gradient between the land and sea surfaces develops. The warm air over the land begins to rise due to thermal advection and as it rises it generates a horizontal pressure gradient above the surface. At the surface over land low pressure is developing while over the sea high pressure is developing, generating a horizontal pressure gradient force at the surface acting from over the ocean towards the land. This generates a flow from the sea towards land. A return flow brings the warm air aloft back towards the sea where it cools and returns to the surface closing the circulation. To replace the surface air moving from over the water towards land, the warm air sinks from above, and the cool sea air flows in-land (Defant, 1950; Atkinson, 1981). The circulation is sketched in Figure 2-2.

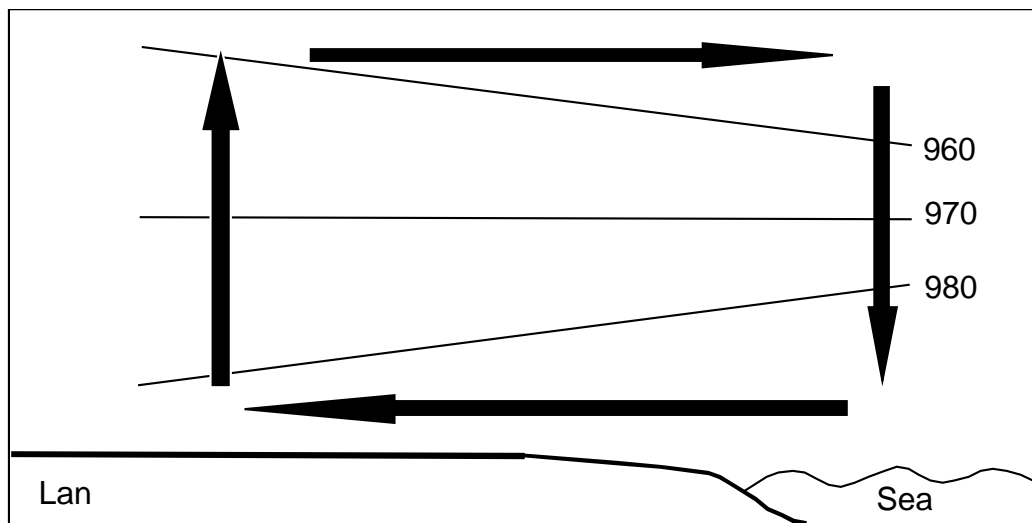


**Figure 2-2.** *Simplified Scheme of the Sea Breeze Circulation*

During the evening and at nighttime, the land cools faster than the water and the process is reversed during night (Figure 2-3). The net result is a land breeze, surface winds blow from the land out to sea.

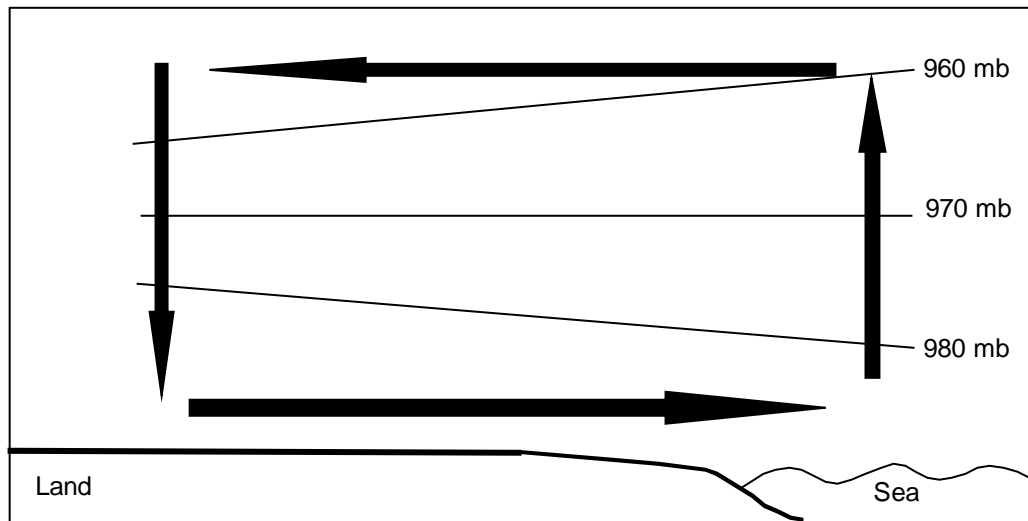


**Figure 2-3.** *Simplified Scheme of the Land Breeze Circulation*

In front of the inland moving maritime air a sea breeze front develops marked by a low-level convergence, a temperature drop, an increase in humidity, and upward vertical winds. The position of the convergence line that defines the frontal edge of the sea breeze varies with the orography and time of day, penetrating further inland when the land surface is relatively flat and also as afternoon progresses. In the mid-latitudes this can range from 20-50 km. In the mid-latitudes the summer sea breeze starts usually between 0800-0900 LT with a lifetime of from six to eighteen hours (Lyons, 1972; Atkinson, 1981; Schlünzen, 1990; Melas et al., 2000a; Millan et al. 2000).

### 2.1.2 Coastal Meteorological Effects on Pollutants

The meteorology described above greatly effects pollutant transport, deposition, and chemical transformations in the coastal region. Examples of effects are mixing ratio differences that can influence which chemical reactions are relevant and cloudiness, which will effect the photolytical reactions. Serious pollution events can result from unfavorable meteorological conditions that diminish the dispersive ability of the atmosphere (Katsoulis, 1988; Merrill and Moody, 1996; Angevine et al., 1996b; Melas et al., 2000b). For example, sea breeze circulations can present a situation where the recirculating wind field prevents long-range horizontal and vertical dispersion of plumes. In the case where there are emissions in the vicinity of the coast line and sea breezes are present, the primary pollutants are transported inland, go through photochemical transformations, are vertically transported then carried back to the sea by the return flow. Land based emissions can cause more injections of pollutants to add to the concentrations in the return flow and the subsidence to the sea create layers of secondary pollutants in the air far off shore (Angevine et al., 1996a; Millan et al., 2000). The next day the aged pollutants are transported by the sea breeze back over the land and then mixed with the new emissions (Andronopoulis et al., 2000). These recirculation processes are important while, for example, the daily observed  $O_3$  might result from fumigation from reservoir layers and advection within the recirculating air mass.

The local meteorology also impacts deposition of pollutants. Dry deposition refers both to the process and to the amount deposited and is the transfer of airborne components to the land and sea surface by atmospheric turbulence. Since the atmospheric turbulence is different over land than over sea due to the convective heating of land during the day and the different roughness lengths over land and water, the gases and particles are transported at different rates to the land surface and sea surface. Also, developing sea breeze circulations that may trap the pollutants and increase the local concentrations may also increase the deposition at the coastline (Schlünzen and Pahl, 1992).

## 2.2 Chemical Coastal Processes

### 2.2.1 Gas Phase Chemistry

Atmospheric chemistry is highly complex and comprised of many sub-groups of chemistry. Some examples are: photochemistry which is driven by solar radiation, heterochemistry which includes aqueous phase transformations, anthropochemistry, that chemistry directly influenced by human activities such as combustion or emissions of chlorofluorocarbons, and geochemistry, geochemical processes including dry deposition and dissolution from oceans (sea salt emissions). Each of these processes plays a role in the entire atmospheric chemistry system since they have feedback effect. This discussion will concentrate on gas phase chemistry and in particular of those nitrogen species which when input in large amounts may result in short term blooms of algae.

Nitrogen components are important nutrients that can be the limiting factor for algal growth in the maritime environment. There are two groups that are important for eutrophication and those are ammonia and its reaction products and nitrogen oxides and their reaction products. The ammonia group,  $\text{NH}_x$ , consists of gaseous ammonia ( $\text{NH}_3$ ) and ammonium in particles ( $\text{NH}_4^+$  aerosol). The nitrogen oxides ( $\text{NO}_y$ ) consists of the gaseous components nitrogen monoxide ( $\text{NO}$ ), nitrogen dioxide ( $\text{NO}_2$ ), nitric acid ( $\text{HNO}_3$ ), nitrous acid ( $\text{HNO}_2$ ), peroxyacetyl nitrate (PAN), nitrate in particles ( $\text{NO}_3^-$  aerosol) and nitrate radicals ( $\text{NO}_3$ ). The dominating atmospheric  $\text{NO}_y$  components over the sea are  $\text{NO}_2$ ,  $\text{HNO}_3$ , PAN, and  $\text{NO}_3^-$  aerosol (Asman and Berkowicz, 1994). The full speciation of gaseous nitrogen compounds has rarely been done for the North Sea atmosphere because of the difficulty in separating oxidized nitrogen compounds and because of their low detection limits. Most monitoring stations measure total  $\text{NO}_x$ , including other indefinable nitrogen species (Schulz, 2001). This is useful information for general nitrogen values, but makes it difficult to compare the individual nitrogen species such as  $\text{NO}$ ,  $\text{NO}_2$ , and  $\text{HNO}_3$ .

Photochemistry is a main driver for chemical activity in the atmosphere. The most well known reactions in a photochemical model are the chemistry of ozone, nitrogen, and sulf-

## 2. Investigating Nitrogen Deposition in a Coastal Environment

ur-containing species. Through a chain of photolytical reactions ozone reacts with H<sub>2</sub>O to produce the hydroxy radical (HO), which in turn reacts with both inorganic and organic species. The reactions of HO with SO<sub>2</sub> and with NO<sub>2</sub> are the major gas phase sources of H<sub>2</sub>SO<sub>4</sub> and HNO<sub>3</sub>, which is a very important loss process for NO<sub>x</sub>, and both play a role in the formation of coastal aerosols.

NH<sub>3</sub>, after N<sub>2</sub> and N<sub>2</sub>O is the most abundant compound of nitrogen in the atmosphere (Seinfeld and Pandis, 1998). NH<sub>3</sub> can react with OH, but as it is highly soluble and reactive with atmospheric acids, that is the preferable route for the removal of the gas phase nitrogen from the atmosphere. NH<sub>3</sub> and SO<sub>2</sub> are rapidly taken up by aerosols and are therefore relevant when investigating deposition in coastal areas.

### 2.2.2 Aerosol Phase Chemistry

Atmospheric particulates, or aerosols, have a large number of sources. In general the characterization of aerosols involves a specification not only of their spatial and temporal distributions, but also of their multicomponent composition, particle size distribution, and physical properties such as composition, particles size distribution, and physical properties. Tropospheric aerosols have short lifetimes (~ days to several weeks) and exhibit enormous spatial variability. Atmospheric aerosols can be broadly divided into two categories - primary particles that are injected directly into the atmosphere, and secondary particles that are formed in the atmosphere by chemical and microphysical processes. This work focuses on secondary aerosols.

#### 2.2.2.1 Physical Aerosol Processes

Aerosols can also be categorized by size and as maritime or continental. The size ranges for aerosols are usually divided into 3 modes; nucleation ( $D_p < 0.2\mu\text{m}$ ), accumulation ( $0.2 < D_p < 1.0 \mu\text{m}$ ) and large or coarse ( $1.0 \mu\text{m} < D_p$ ) are distinguished (Fitzgerald, 1991; Jacobson, 1999a) but the distributions can be highly variable depending upon the chemical make-up of the aerosol.

##### *Maritime Aerosol Size Distributions*

In the absence of significant transport of continental aerosols, particles over the remote oceans are largely of marine origin (Savoie and Prospero, 1989). Maritime atmospheric particle concentrations are normally in the range of 100 to 300 cm<sup>-3</sup>. The fine mode particles are depleted mainly by coagulation (Turco, 1993). Typically, the coarse mode particles, comprising 95% of the total mass but only 5 to 10% of the particle number, result from the evaporation of sea spray produced by bursting bubbles or wind-induced wave breaking (Blanchard and Woodcock, 1975; Monahan et al., 1983). Maritime aerosol com-

position consists mainly of  $\text{H}_2(\text{SO}_4)$ ,  $(\text{NH}_4)_2\text{SO}_4$ , and sea salt. A high presence of  $(\text{NH}_4)_2\text{SO}_4$  is usually the result of continental influence. Typical sea-salt aerosol number concentrations in the maritime boundary layer (MBL) without continental influence are around 5 to 30  $\text{cm}^{-3}$  (Blanchard and Cipriano, 1987; O'Dowd and Smith, 1993).  $\text{H}_2(\text{SO}_4)$  number concentrations can be from 0 to 12  $\text{cm}^{-3}$  and  $(\text{NH}_4)_2\text{SO}_4$  is negligible.

### *Continental Aerosol Size Distributions*

Continental aerosols can be grouped as either urban or rural. Urban aerosols are mixtures of primary particulate emissions from industries, transportation, power generation, and natural sources and secondary material formed by gas-to-particle conversion mechanisms. The number distribution is dominated by particles smaller than 0.1  $\mu\text{m}$ . The size distributions in urban areas are quite variable, usually high concentrations of fine particles (less than 0.1  $\mu\text{m}$  in diameter) are found close to sources but their concentrations decrease with distance from sources.

Aerosols in rural areas are mainly of natural origin but with a moderate influence of anthropogenic sources (Hobbs and McCormick, 1988). The number distribution is characterized by two modes at diameters about 0.02 and 0.08  $\mu\text{m}$  (Jaenicke, 1993), while the mass distribution is dominated by the coarse mode centered at around 7  $\mu\text{m}$ . The mass distribution of rural aerosol if not influenced by local sources has a small accumulation mode and no nuclei mode.

Remote continental aerosols (i.e. dust, pollen) are mainly primary particles and secondary oxidation products. Their number concentrations average around 2,000 to 10,000  $\text{cm}^{-3}$  and  $\text{PM}_{10}$  (particulate matter > 10  $\mu\text{m}$  in diameter) are around 10  $\mu\text{g}/\text{m}^3$  (Seinfeld and Pandis, 1998).

### **2.2.2.2 Aerosol Chemistry Processes**

Aerosol chemistry can be broken into several distinct areas; multiphase thermodynamics, deliquescence, aerosol growth, and sea-salt aerosol processes, with several significant state variables; water content, and relative humidity. Although many studies have been carried out, the enormous variability inherent in these processes and variables hinders simple classification. Reactions in aqueous solution have been studied for many years, and the application of basic data to atmospheric chemistry problems is well established (Seinfeld, 1986; Seinfeld and Pandis, 1998; Jacobson, 1999a).

Chemical reactions on aerosols can indirectly alter the concentrations and distributions of climatologically important gases such as ozone. The chemical transformations of gases into particles has both direct and indirect climate implications: direct, because the build-up of aerosols affects the radiation balance; indirect because aerosols are involved in the formation of clouds, which affect atmospheric radiation at all wavelengths.

## 2. Investigating Nitrogen Deposition in a Coastal Environment

Water content (WC) and relative humidity (RH) are integral factors in aerosol structure and growth. Each inorganic salt is a solid until the ambient RH reaches a certain value called the relative humidity of deliquescence (DRH), at which the substance absorbs atmospheric moisture to produce a saturated aqueous solution. As the RH continues to increase, additional water condenses onto the salt solution to maintain thermodynamic equilibrium. As the RH over a salt solution decreases, evaporation of the water occurs. It is important to note that the solution will, most likely, not crystallize at the deliquescence point. Instead it will remain supersaturated until a much lower humidity, the relative humidity of crystallization (CRH), at which point crystallization finally occurs. This is called the hysteresis process. Multi-component salts have a more complicated deliquescence and hysteresis pattern and depending upon its composition may contain both a solid and an aqueous phase. It has also been shown that the DRH of a multicomponent particle is lower than that of its components (Pilinis et al., 1989; Wexler and Seinfeld, 1991; Tang and Munkelwitz, 1993; Ansari and Pandis, 1999; Jacobson, 1999a).

There is a basic thermodynamic assumption used in determining aerosol growth. It is assumed that using the concentration of a group of chemical constituents that comprise a gas-aerosol system, i.e. total  $\text{HNO}_3$ ,  $\text{NH}_3$ ,  $\text{NaCl}$ , and  $\text{H}_2\text{SO}_4$ , as well as the ambient temperature and RH, the gas and liquid phases are considered to be in equilibrium, while a solid phase is non-existent. The condition of chemical equilibrium in a closed system, such as the one above, at constant temperature  $T$  and pressure  $P$ , is that the total Gibbs free energy of the system,  $G$ , is a minimum (Pilinis et al, 1989). This assumption leads to the conclusion that unbound water is an important component of atmospheric aerosols and its existence depends on meteorological conditions, as well as the ambient concentrations of the aerosol species. Also, the time scales for the gas and aerosol phases to equilibrate depend crucially on the ambient conditions and the composition and state of the aerosol (Wexler and Seinfeld, 1990).

The most significant microphysical processes are nucleation, condensation/evaporation, coagulation and sedimentation (Pruppacher and Klett, 1978; Gelbhard and Seinfeld, 1980; Seinfeld, 1986; Turco, 1993). To include aerosol physics in a model the compositional differences between aerosol types and the size distribution of the particles must be treated. Such details are needed to define the chemical, microphysical and radiative properties of the aerosols.

Nucleation represents the formation of aerosol particles from vapors that are supersaturated. Homogeneous nucleation, or new particle production, involves the condensation of a pure vapor into a pure aerosol of that material; heterogeneous nucleation involves the deposition of a vapor onto a substrate particle of fundamentally different composition and origin adding mass. Condensation/evaporation refers to the deposition of a vapor onto, or evaporation from, a pre-existing aerosol of similar material. The rate of condensation or evaporation depends on the difference between the vapor pressure and the partial (ambient)

pressure of the condensing gas. Coagulation refers to a family of processes by which one aerosol particle dynamically encounters another and the two particles coalesce. The process is described quantitatively by a coagulation (or collision/coalescence) kernel. Finally, sedimentation is the process in which the terminal fall speed of a macroscopic particle under the influence of gravity is balanced by the aerodynamic drag of the atmosphere. The fall speeds of individual particles are determined by the kinematics of gas-particle interactions as a function of particle size and gas density. This differs from dry deposition, which occurs when particles diffuse to, or are transported by diffusion, towards the surface.

Vertical profiles of aerosol particle concentrations indicate on average, a decrease with altitude. It has also been observed that there is a mechanistic connection between the reduction of water vapor concentration at about the same rate. Both substances have a near-surface source and different deposition processes remove both. As air is lifted above the boundary layer it cools and condensation takes place removing available water vapor and absorbing soluble substances in the process. This results in a decrease in the concentration of aerosol particles and soluble trace gases (Kleinman et al., 1996; Schimmel, 1999).

### 2.2.2.3 Aerosols in Coastal Regions

In clean maritime areas, aerosol number concentration is frequently dominated by sea-salt particles, but in coastal regions influenced by offshore transport of continental air masses the small coastal aerosols (i.e.  $D_p < 0.25 \mu\text{m}$ ) may contain nitrate, sulfate, and other chemical compounds not usually found in the ocean (Ottley and Harrison, 1992; Harrison et al., 1994; O'Dowd et al., 1997). Chloride depletion is caused by a reaction of nitric or sulfuric acid with the sea-salt aerosol, NaCl, resulting in the formation of  $\text{NaNO}_3$  or  $\text{Na}_2\text{SO}_4$  and  $\text{HCl(g)}$  (Savoie and Prospero, 1989). The smaller aerosols are first depleted because of their higher surface area. The resultant HCl is then available to react with  $\text{NH}_3$  to form secondary  $\text{NH}_4\text{Cl}$  aerosols (Pio et al., 1992). Chloride depletion is an important process in the coastal zone, as it effects the aerosol formation and also the quality of the bulk nitrogen deposition.

Sea-salt production is a function of wind speed. O'Dowd and Smith (1993) found that there is a strong exponential dependence of sea salt aerosol ( $0.1 \mu\text{m} < D_p < 3.0 \mu\text{m}$ ) upon the prevailing wind speed. The assumption here is that the aerosol number concentration increase results from the increased bubble bursting associated with enhanced whitecap coverage at high wind speeds. Higher wind speed also increases the flux of DMS from the ocean surface, and the higher DMS emissions eventually lead to larger concentrations of  $\text{SO}_2$  (Katoshevski et al., 1999). This increased amount of  $\text{SO}_2$  is then available for uptake by the increased quantity of sea salt. In a ship experiment performed in the Mediterranean, measurements of DMS concentrations, chemical composition of aerosol particles, and size distribution of aerosol composition was collected (Despiau et al., 1999). The high DMS events were generally associated with high  $\text{NO}_3^-$  concentrations in aerosol particles possibly because of oxidation of DMS by  $\text{NO}_3^-$ . In other words, this study showed again

## 2. *Investigating Nitrogen Deposition in a Coastal Environment*

that sea salt is likely to act as a significant sink for vapors like sulfuric acid and methane sulfonic acid (MSA), and secondary organics.

### 2.2.2.4 *Aerosol Behavior over the North Sea*

Schulz (2001) has compiled a comprehensive overview of the projects and data resources for inorganic atmospheric compounds, including aerosols, in the North Sea region for the period 1972-1999. These projects have been comprised of field measurement campaigns and of numerical simulations and each attempts to add to the body of knowledge for atmospheric pollutant processes in the region.

Aerosol activity (formation and loss) in the marine boundary layer is the subject of experimental studies such as the EUROTRAC North Sea Experiment which took place in September 1991 (Harrison et al., 1994) and the ANICE study with field campaigns in 1998 and 1999 (deLeeuw et al, 1999a,b,c, 2000).

In the EUROTRAC Experiment two research ships, the Alkor and Belgica, took up position 200km apart, and moved around the circumference of a circle such that the Belgica was always 200km downwind of the Alkor. Measurements of atmospheric composition were made on both ships and changes are interpreted in terms of chemical transformations, surface exchange and entrainment loss to the free troposphere. This experiment showed the difficulty of interpreting data from analysis of an air mass advected between two sampling points in the marine boundary layer. Harrison et al. concluded that for nitrate species the formation from NO<sub>2</sub> oxidation approximately balanced losses by deposition to the sea surface. For ammonium species appreciable loss occurs by deposition, and it appears that no substantial interconversion of the two species takes place. They also concluded that overall there were appreciable losses of trace gaseous and particulate species due to entrainment losses, chemical reactions and dry deposition.

The European Union project ANICE (Atmospheric Nitrogen Input to the Coastal Environment) endeavored to quantify the amounts of nitrogen deposited to the southern North Sea. The 1998 measuring campaign for ANICE comprised two observation sites, the MPN and Weybourne Atmospheric Observatory (WAO) as well as the southern ferry route from Hamburg (Germany) to Harwich (UK). The MPN platform lies 9 km off shore from the Dutch Coast and the WAO is 75m inland from the coast. The 1998 measuring campaign ran during the month of June. The chemical parameters collected at the two observation sites were sulfate, %nss sulfate, ammonium, nitrate, chloride, and sodium. Both aerosol concentrations and size distributions were collected, as well as rain samples analyzed for the wet deposition values. The sampling periods ranged from 8h - 16h, at an average of 12h. Time series data of NH<sub>3</sub>, HNO<sub>3</sub>, NO<sub>x</sub>, and O<sub>3</sub> were collected at the MPN platform and WAO.

During a different measurement experiment in the North Sea coastal zone, bulk deposition and through flow were measured at three sites in the Dutch coastal dune area Meijndel near The Hague (Harkel, 1997) with the objectives to calculate the total atmospheric deposition and the contribution of atmospheric deposition to eutrophication and acidification of coastal dry dune grasslands. A sodium deposition model was developed to study the influence of the changing particle size distribution of sodium aerosols on the deposition and it was found that there was chloride depletion of the sea-salt aerosol up to 75 or 95%.

Von Salzen and Schlünzen (1999c) applied the 3-D numerical model METRAS which included sea salt generation and the Sectional Multicomponent Aerosol Model SEMA to investigate the dynamics and composition of aerosol in the German Bight. Their study showed that the production rate of nitrate compounds in coarse sea-salt aerosol is of the same order as the reduction of the produced coarse nitrate by dry deposition.

Atmospheric bulk deposition at coastal sites is largely influenced by the distance to the seashore (Harkel, 1997). The study in the region of The Hague showed sodium bulk deposition decreased by 50% within the interval from 0.5 to 2.0 km inland from the coastline. The modeled sodium aerosol diameter distribution showed that more than 50% of the sodium aerosols deposited at a coastal site are larger than 20  $\mu\text{m}$ . Harkel also showed that the sea-salt neutralizes part of the  $\text{NO}_3^-$  and  $\text{SO}_2^{4-}$  close to the sea, which concurs with findings that the ammonium nitrate and ammonium chloride present in terrestrial aerosols dissociate rapidly over the sea due to the lower levels of ammonia present (Ottley and Harrison, 1992). This neutralizing effect decreases very quickly with increasing distance inland.

### 2.3 Dry Deposition

#### 2.3.1 Dry Deposition of Gases

Dry deposition is the process by which atmospheric trace chemicals are transferred by turbulence to the surface. Deposition of a chemical tracer depends upon its composition and the surface that it is being deposited to. Deposition velocities may be computed as the inverse of the sum of resistances (Wesley and Hicks, 1977; Slinn and Slinn, 1980):

$$v_d = \frac{1}{r_a + r_b + r_s} \quad (2-1)$$

Where:

$v_d$  = deposition velocity

$r_a$  = aerodynamic resistance

$r_b$  = viscous sub layer resistance

## 2. Investigating Nitrogen Deposition in a Coastal Environment

$r_s$  = surface resistance

The aerodynamic resistance,  $r_a$ , is the resistance to transport of air above the viscous sub layer over the surface. The vertical transport through this layer is due to turbulence and this will differ over water and over land mainly due to the differences in turbulence in the surface layer. An example of this difference is the dependence upon the atmospheric conditions; the stability could cause a convective situation over water, but still be stable over land resulting in a larger turbulence over water. Gases are transported through the viscous sub layer,  $r_b$ , by molecular diffusion. The surface resistance,  $r_s$ , sometimes called canopy resistance, varies with surface type and chemical properties.

Apart from the resistance due to turbulence, there is a resistance for the uptake of a gas in the water. For the highly soluble nitrogen gases such as  $\text{NH}_3$ ,  $\text{HNO}_3$  and  $\text{HNO}_2$  this resistance is negligible. For poorly soluble gases, i.e.  $\text{NO}$  and  $\text{NO}_2$ , the reactivity of the gas in the water phase is important. For these gases only a slow reaction, if any, takes place and the surface resistance becomes very large and dominates.

### 2.3.2 Dry Deposition of Aerosols

Dry deposition of an aerosol depends upon its size, composition, and the surface that it is being deposited on to, similar to the dry deposition of gases. The equation is also similar to Equation 2-1 except for the inclusion of gravitational settling velocity.

$$v_d = \frac{1}{r_a + r_b} + v_g \quad (2-2)$$

Where  $v_g$  = gravitational settling velocity

Processes for the transport of particles through the viscous sub layer,  $r_b$ , are: Brownian diffusion, interception, impaction and transport due to gravitation. Brownian diffusion in the viscous sub layer is important for the smallest particles (radius  $< 0.01\mu\text{m}$ ). Particles of this size do not, however, contribute much to the total mass of nitrogen in particles. For airborne particles with a radius less than about  $5\mu\text{m}$ , settling due to gravitation is not important compared to the transport due to turbulence (Asman and Berkowicz, 1994).  $\text{NH}_4^+$  and  $\text{NO}_3^-$  containing particles usually have a radius less than  $5\mu\text{m}$  and the deposition can be described by the same aerodynamic resistance,  $r_a$ , as for gases (Equation 2-1). For larger particles impaction and transport due to gravitation play an important role. As size and mass increase the gravitational force becomes stronger and deposition velocity increases.

Hygroscopic aerosols undergo a change in particle size as they approach a water surface. This change is less in a metastable (wet) aerosol than in a dry aerosol, and it can be as-

sumed that for deposition of wet aerosols over water hygroscopic growth is relatively unimportant when determining deposition velocities (Kermin and Wexler, 1997; Zufall et al., 1998).

## 2.4 Aerosol Modeling

An atmospheric chemistry transport model that includes meteorology can provide the representation of the transport of chemical compounds. Such a model may use the output from a reliable meteorological model, and a more complete picture is given by one including aerosol phase chemistry. The chemical reactions on aerosols can indirectly alter the concentrations and distributions of gases, so the inclusion of aerosols is necessary to broaden the understanding of what is really occurring in the environment.

A common approach to aerosol modeling is to first address thermodynamic equilibrium. It has been stated that in order to present quantitative results on the basis of thermodynamic equilibrium it is necessary to specify a group of chemical compounds that comprise the gas-aerosol system and actually carry out the equilibrium calculation. Aerosol modules usually simulate the partitioning of chemical species among gas, aqueous, and solid phases (Kim et al., 1993a,b; Sun and Wexler, 1998; Jacobson, 1999a; Nenes et al., 1999; von Salzen and Schlünzen, 1999a).

Transports, as well as the thermodynamic properties of the aerosol population govern the distribution of aerosols (Wexler and Seinfeld, 1990). For example an accurate prediction of the quantity of ammonium salt in atmospheric aerosol and its distribution with respect to particle size can only be obtained by explicitly modeling the transport of  $\text{NH}_3$ ,  $\text{HNO}_3$ , and  $\text{HCl}$  between the gas and aerosol phases. Whether there is a thermodynamic preference for ammonium salt condensate to appear in one size particle over another depends on the state of the condensed ammonium salt (aqueous or solid), the osmotic dominance of the ammonium salt if it exists in the aqueous phase, and the relative magnitude of the time scales for the aerosol and the gas phase to equilibrate if the ammonium salt is not osmotically dominant.

A sectional approach to modeling refers to dividing the size distribution into a number of sections with size-independent values within each section. A full-stationary size structure is one in which particles in a given size bin have a fixed volume, and each size bin contains any number of particles, all of which have the same composition and volume as each other particle in the size bin. When particles grow, their volumes do not change; instead, the number of particles in the original size bin decreases, and the number of particles in a larger size bin increases. Similarly, when two particles coagulate, particle numbers in each size bin, not volumes, change. Testing has shown that the method is highly accurate in predicting the aerosol behavior, conserve the particle mass and the particle number and follow the growth characteristics (Pilinis, 1990, von Salzen and Schlünzen, 1999b).

## 2. Investigating Nitrogen Deposition in a Coastal Environment

Coupled gas phase/aerosol models solve several equations. Among these are (a) the continuity equations for trace gas number concentration, water vapor, particle number concentration, particle volume concentration, and air; (b) the conservation of energy equation; (c) the horizontal equations of motion; and (d) the radiative transfer equation. In many cases the continuity equations for air and water vapor, the conservation of energy equation, and the equations of motion, which includes the hydrostatic equation are solved with the meteorological model. Vertical and horizontal velocities are also predicted from the meteorological model and are used to advect gases and aerosol components.

Several inorganic aerosol thermodynamic models have been developed over the past years to predict the composition and physical rate of inorganic aerosol formation. Many of these modules require host gas-phase models to provide gas-phase chemistry and transport. Table 2-1 presents thermodynamic equilibrium modules that are currently used in 3-D simulations and summarizes some of the major numerical characteristics. The table does not include all equilibrium modules because it is difficult to get exact model descriptions from the open literature.

The primary assumption in the chemistry of a thermodynamic aerosol module is that the aerosol is internally mixed (all the particles of a given size have the same composition) (Zhang et al., 2000). The particle composition is only a function of particle size. The modules attempt to predict impactor-based measurements of particle composition by mixing the particles of a given size. When developing the governing equations the processes considered are advection, turbulent diffusion, condensation and evaporation, coagulation, nucleation, aerosol-phase chemical reactions, gravitational settling, emissions and deposition. The resulting equation is usually used with a host gas-phase model to predict both the gas-phase pollutant concentrations and the size and composition of particulate pollutants (Table 2-1). The condensation and evaporation terms are solved in the aerosol module while the remaining terms are solved using numerical methods available in the host gas-phase model. Stand-alone versions of most modules are used in intercomparison studies when it is desirable to avoid differences due to the host models.

The Zdanovskii-Stokes-Robinson (ZSR) water equation (Stokes and Robinson, 1966) is often chosen to calculate the water content of the aerosols since it is easy to use and has comparable accuracy with other more computationally demanding methods (Table 2-1). The ZSR method is solved to predict liquid water content due to hydration when the relative humidity is less than 100%.

Kim et al. (1993b) evaluated the sensitivity of results to different approaches for treating the weak electrolytes, ammonia and bisulfate ions. The results of their analysis shows that the inclusion of associated ammonia does not increase the accuracy of predictions, but the inclusion of the bisulfate ion is essential to estimate concentrations accurately, especially particle acidity. They also compared three activity coefficient estimation methods, and then

compared the SCAPE model to the AIM gas-particle equilibrium model. The Pitzer (1981) method for multicomponent activity coefficients is not applicable for systems of ionic strength exceeding about 30M and in those cases, which are the sulfate-poor cases, the K-M and the Bromley methods should be used. It was also found that particulate concentrations, ammonium, nitrate, and chloride, are generally similar with the two models and are not a particularly sensitive indicator of model performance. Instead, the acidity and the solid concentrations are more sensitive indicators of model performance.

An aerosol growth process that is simulated, aside from condensation and evaporation, is coagulation. Jacobson et al. (1994) have set out to develop a technique for simulating coagulation among any number of aerosol types. The scheme is volume conserving and unconditionally stable, uses any time-step, and solves over any size-bin structure. The equations shown for multiple particle types assume that whenever a particle of one type coagulates with a particle of another type, the resulting particle enters a multicomponent mixture representing all particle types. Single component particles quickly heterocoagulate with particles of other types when the air is particle-rich.

Sedimentation and deposition are aerosol features that should be included in the module to simulate realistic processes. Particle sedimentation is included by permitting size-distributed particles to fall from one layer of the atmosphere down to any layer below or to the surface.

Particle dry deposition to the sea surface is most often treated using the formulation of Slinn and Slinn (1980) which determines the deposition velocity as a function of particle size and neglects hygroscopic growth (Kermin and Wexler, 1997; Zufall et al., 1998; Katohevski et al., 1999). When it is desirable to include hygroscopic growth the approach of Fairall and Larsen can be applied (von Salzen and Schlünzen, 1999c), or a hybrid deposition function can be tailored to the modeler's purpose (Pryor and Barthelmie, 2000).

Aerosol modeling is an evolving process. Recent advances include the development of models for dry aerosols and the integration of aerosol modules on a global scale. These were not included in this section, as they do not pertain to this investigation.

## 2. Investigating Nitrogen Deposition in a Coastal Environment

**Table 2-1. Comparison of Thermodynamic Equilibrium Aerosol Models from Literature**

Model Name	Equisolv II	SCAPE2	SEMA	AIM2	SEUILIB	MADE
<b>Gas-phase Host Model</b>	GATOR	CIT	METRAS/MECTM	UAM-IV	SAQM-AERO UAM-AERO	EURAD system: MM5, EEM, CTM2
<b>Species</b>	NO <sub>3</sub> <sup>-</sup> , Cl <sup>-</sup> , SO <sub>4</sub> <sup>2-</sup> , NH <sub>4</sub> <sup>+</sup> , Na <sup>+</sup> , H <sub>2</sub> O, K <sup>+</sup> , Ca, Mg, CaCO	NO <sub>3</sub> <sup>-</sup> , Cl <sup>-</sup> , SO <sub>4</sub> <sup>2-</sup> , NH <sub>4</sub> <sup>+</sup> , Na <sup>+</sup> , H <sub>2</sub> O, K <sup>+</sup> , Ca, Mg, CaCO	NO <sub>3</sub> <sup>-</sup> , Cl <sup>-</sup> , SO <sub>4</sub> <sup>2-</sup> , NH <sub>4</sub> <sup>+</sup> , Na <sup>+</sup> , H <sub>2</sub> O	NO <sub>3</sub> <sup>-</sup> , Cl <sup>-</sup> , SO <sub>4</sub> <sup>2-</sup> , NH <sub>4</sub> <sup>+</sup> , Na <sup>+</sup> , H <sub>2</sub> O	NO <sub>3</sub> <sup>-</sup> , Cl <sup>-</sup> , SO <sub>4</sub> <sup>2-</sup> , NH <sub>4</sub> <sup>+</sup> , Na <sup>+</sup> , H <sub>2</sub> O	NO <sub>3</sub> <sup>-</sup> , SO <sub>4</sub> <sup>2-</sup> , NH <sub>4</sub> <sup>+</sup> , HSO <sub>4</sub> <sup>-</sup> , H <sub>2</sub> O
<b>Multi-Component Activity Coefficient</b>	Bromley	K-M <sup>1</sup> or Pitzer	Pitzer	K-M	Bromley	2.
<b>Binary Activity Coefficient</b>	Hmaer and Wu, Goldberg, Bassett and Seinfeld, Filippov et a., Pitzer	K-M	Pitzer	K-M	Pitzer	2.
<b>Water Activity</b>	ZSR Method	ZSR Method	ZSR Method	ZSR Method	ZSR Method	Spann and Richardson, Nair and Vohra, Tang, Cohen et al.
<b>Notes</b>	Uses a mass flux iteration method	2.	Uses a full stationary size structure	2.	2.	The aerosol Liquid Water Content is fit to experimental data
<b>References</b>	Jacobson (1997) Jacobson (1999a, b)	Kim et al., (1993a, b) Kim and Seinfeld (1995) Meng et al. (1995)	von Salzen et al., (1997 a,b) vonSalzen and Schlünzen, (1999a,b)	Clegg et al. (1992, 1994, 1995, 1998a,b)	Pliinis and Seinfeld (1987)	Binkowski and Shankar, (1995) Ackermann et al., (1995) Ackermann et al., (1998)
1. Kermin and Wexler Method						
2. Information not in reference						

### 3. Models and Input Data

The METRAS/MECTM model system includes the mesoscale model METRAS, the chemistry transport model MECTM, and preprocessors for; large scale meteorology data, emissions, biogenic emissions, landuse data, and photolysis rates. A simple schematic is shown in Figure 3.1 and described in detail in the following sections.

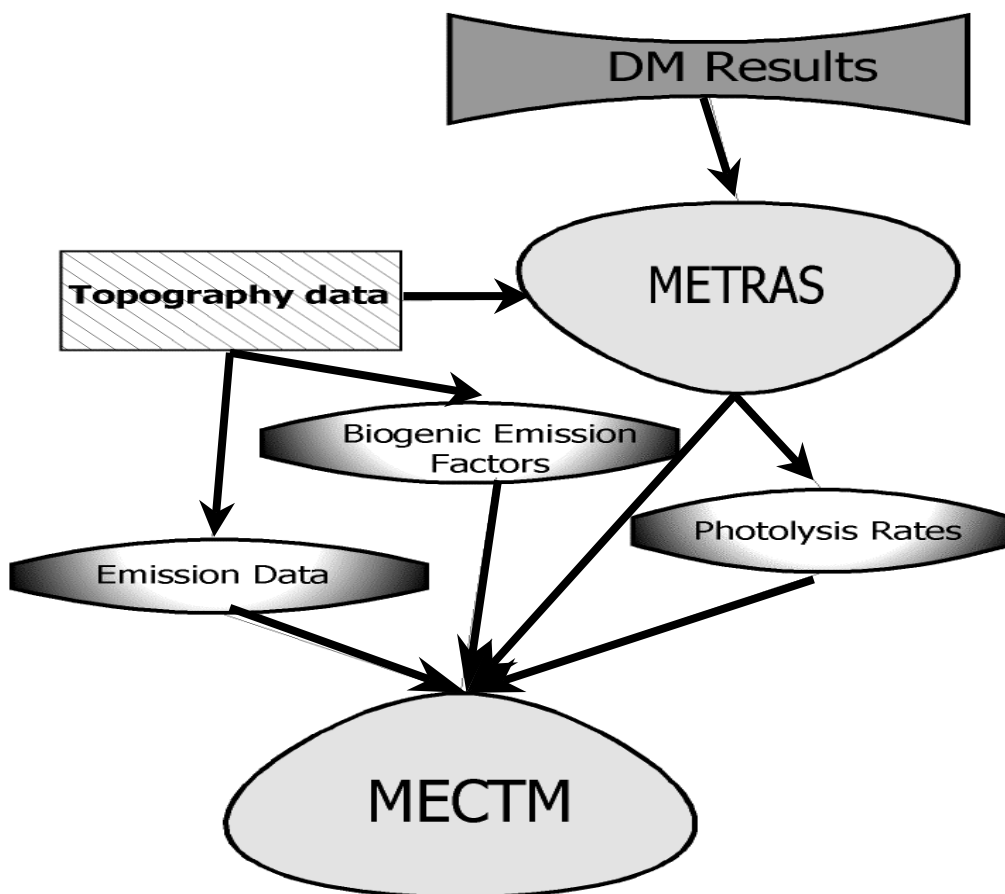


**Figure 3-1.** Overview of the Model System METRAS/MECTM

#### 3.1 The METRAS/MECTM model system

##### 3.1.1 Mesoscale Model METRAS

METRAS, the MESoscale TRANsport and fluid (Stream) model is based on the conservation laws for mass, momentum, and energy. The equations are solved three dimensionally in a terrain-following co-ordinate system. Only few approximations are applied, which ensure a wide range of model applications.

### 3. Models and Input Data

There are no principal restrictions to the time and spatial variability of the synoptic fields. METRAS (Schlünzen 1990; Schlünzen et al. 1996) can be used for simulations of wind, temperature and humidity over areas up to 500 km x 500 km. The use of a non-uniform grid allows high resolution in model areas with highly varying orography. Wind, temperature, humidity, cloud- and rainwater content are derived from prognostic equations, whereas density and pressure are calculated from diagnostic equations. METRAS utilizes the anelastic approximation, which is valid throughout the entire mesoscale. Other approximations like the hydrostatic approximation  $\partial p / \partial z = -g\rho$  and the geostrophic approximation  $\mathbf{v} = \mathbf{v}_g$  can only be applied to larger scale phenomena and therefore not employed. Processes linked to relatively small areas (e.g. sea-breezes) are solved explicitly.

The model equations are integrated over the grid volume, the model time step is between 1s and 1 min (maximum) and the output time interval  $\Delta t = 15$  min. The micro-scale density variations are neglected. In the averaged equations the averages of temperature, humidity, pressure and density are further decomposed into a mesoscale part and a large-scale part. The sub-grid scale turbulent transport terms in the model equations are parameterized by a first order closure. The most important parameters for the transport of chemical concentrations are the exchange coefficients (especially in the vertical) and the determination of the planetary boundary layer (PBL) height.

The vertical exchange coefficient ( $K_{vert}$ ) parameterization used in these METRAS/MECTM model runs is the scheme described by Lüpkes and Schlünzen (1996). For unstable stratification a countergradient approach is employed, based on the formulations of Holtslag and Moeng (1991). The parameterization for vertical exchange coefficient of any scalar ( $K_{vert,\chi}$ ) is

$$K_{vert,\chi} = \frac{\kappa u_* z_p}{\left( \Phi_h - \frac{\kappa z_p}{\Theta_*} \Gamma|_{z_p} \right)} \left( \frac{z_i - z}{z_i - z_p} \right)^2 \frac{u_* \kappa z + w_f z_i (z / z_i)^{4/3}}{u_* \kappa z_p + w_f z_i (z_p / z_i)^{4/3}} \quad \text{for } z_i \geq z \geq z_p$$

where  $z_p$  is the height of the first grid level,  $\chi$  represents any scalar variable,  $\kappa$  is the von Kármán constant,  $u_*$  is friction velocity,  $w_f$  is vertical velocity and  $\Phi$  is the stability function. To calculate the vertical exchange coefficient for momentum  $K_{vert}$  METRAS employs

$$K_{vert} = \left[ \frac{\Phi_h|_{z_p}}{\Phi_m|_{z_p}} + 3 \frac{w_f u_* \kappa z_p}{\Phi_m|_{z_p} w^2|_{z_p} z_i} \right] K_{vert,\chi}$$

The height of the convective boundary layer  $z_i$  is determined as the level where the heat flux maintains a minimum. For stable stratification a mixing length approach is used. The application of this combined scheme results in higher values of the mixed layer heights during the day, and lower heights during the evening as will be shown in Chapter 4.

METRAS has been used in a number of meteorological studies over the past decade. Simulations of sea wind circulations (Schlünzen, 1990; Wu and Schlünzen, 1992) have been investigated. Arctic circulations (Lüpkes and Schlünzen, 1996) and ice simulations (Dierer and Schlünzen, 1999) are another growing use of the METRAS model and have been validated successfully. The deposition of chemical compounds in coastal regions was investigated by Schlünzen and Pahl (1992); Schlünzen and Krell (1994); and Schlünzen et al. (1997).

In this work METRAS was used with MECTM to study deposition in the southern North Sea. The meteorological input is described in Section 3.2.1, and the results of the meteorology runs are presented in Chapter 4. The MECTM is described in further detail in the following section.

### ***3.1.2 Mesoscale Chemistry Model MECTM***

Besides the meteorological model the other important component of any regional air quality model is its chemical mechanism. A transport-transformation model must include a gas phase chemical mechanism that incorporates all significant reactions, but must also be simple by comparison with the very complex chemistry of the real atmosphere.

The METRAS/MECTM system solves:

- Equation of 3D motion in a surface following co-ordinate system,
- Conservation of energy,
- Budget equation for water,
- Advection/diffusion part of MECTM is the same as METRAS, and
- Budget equation for the gas phase species that includes emissions, transport, transformations and deposition.

The MECTM that was used in previous studies (Müller et al., 2000) was modified and adapted for this southern North Sea study. The model uses the gas phase chemical mechanism from the Regional Acid Deposition Model (RADM2) as described in Stockwell et al. (1990). The MECTM comprises 58 gas phase species (Appendix B) and 201 reactions. All reactions are categorized and listed in Appendix C. In the MECTM calculations are made with consideration to gaseous emissions, vertical and

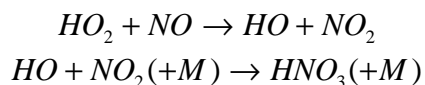
### 3. Models and Input Data

horizontal dispersion, chemical transformations, and removal of species due to deposition.

The RADM2 mechanism is a gas phase chemical mechanism developed for polluted environments. The gas phase reactions are lumped through a reactivity lumped molecular approach. For example, organic compounds are grouped into classes based on similarity in oxidation reactivity and emission magnitude. Inside each category several model species that span the reactivity range are used to represent that class of reactions (Stockwell et al. 1990). The number of intermediates and stable species in a class is relative to the range of reactivity within that class.

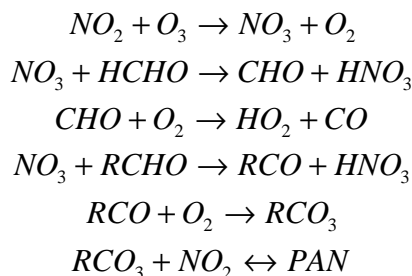
The inorganic chemistry in RADM2 contains most of the nitrogen species that are the focus of the deposition study, mainly  $\text{NO}_2$ ,  $\text{NO}$ , and  $\text{HNO}_3$ . The mechanism does not include  $\text{NH}_3$ , which has been included as a passive tracer for the nitrogen input studies. In the gas phase chemistry the major source of  $\text{HNO}_3$  is the reaction of  $\text{HO}$  with  $\text{NO}_2$ .

In daytime:

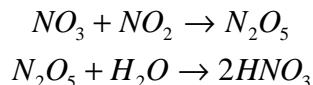


The gas phase production of  $\text{HNO}_3$  is a major loss process for  $\text{NO}_x$ .

The nighttime production of  $\text{HNO}_3$  is more complicated:



$\text{NO}_2$  also reacts with  $\text{NO}_3$  to form  $\text{N}_2\text{O}_5$ , which then reacts with water as another production of nitric acid.



The production of  $\text{HNO}_3$  is strongly related to the amount of  $\text{NO}_2$  in the atmosphere and thus  $\text{NO}$  and  $\text{NO}_2$  emissions. It is expected that the deposition simulations using the chemical mechanism will show lower  $\text{NO}_2$  deposition, and increased nitric acid deposition. The regions of the differences will depend on the meteorological parameters wind direction, wind speed, temperature, and humidity. Chapters 5 and 6 show

the results of the deposition from passive tracer model runs, and model runs with full chemistry and the effects that the reactions listed above have on the form that the nitrogen takes when it is deposited from the atmosphere.

At each time step MECTM selects the photolysis rates for each species from the table that was developed by a preprocessor using the STAR mechanism (Section 3.2.2). The initial chemical concentrations for each grid point are determined by calculating the contribution from the direct sources (emissions), contribution from vertical diffusion, contribution or loss due to the chemical reactions, and loss from deposition. The integration time for the initialization is 24 hours in order to develop concentration fields that are in balance and representative background concentrations for the situation being simulated.

The form of the differential equation expression used in MECTM is:

$$\partial C_i / \partial t = a(C_i, t) - b(C_i, t) * C_i$$

where the left hand side represents the local change of the species  $i$  concentration due to chemical reactions, emissions, and dry deposition. The first term on the right hand side represents the corresponding production terms and the second term is the loss. The initial time step is 3-4 minutes and is greater than the reactions rates, so the corresponding equations are considered to be stiff. These stiff equations are treated with a very stable method that dampens out the small oscillations caused by the very small time constants. The convergence of each of the individual equations is determined by using the relative error criterion of  $\pm 10^{-3}$ . The maximum number of iterations is kept to 10, and if convergence is not obtained the cycle is restarted and the time step is reduced by a value of 0.7. The limits are set so that  $\Delta t_{\min} \geq 10^{-5}$  s and  $\Delta t_{\max} \leq 5$  min. The previous values of  $a$  and  $b$  are not stored from one cycle to the next. When convergence is achieved the new values of  $C(\partial t)$  are set. In this solver, the iteration procedure is continued until the convergence criterion is satisfied for all species.

For solving the stiff chemical equation system the hybrid solver was selected for use in the chemistry model since it has been shown to better predict  $\text{NO}_x$  concentrations (as well as others) (Müller et al., 2000). The hybrid method in MECTM is based on the work of Young & Boris (1977) and adapted for the use with METRAS (Müller et al. 2000; Müller personal communication 2001). It is stable for practical time step sizes and has a high level of accuracy. This method recognizes the stiff equations and integrates them by some very stable method while the remainder of the equations are treated by the faster classical polynomial methods. The polynomial methods have a tendency to be unstable for differential equations with time constants much shorter than the integration time step, as in chemical reactions, so are used sparingly. Computing time and storage requirements are kept low by using a low-order method, and this method can adapt to changes in the chemical reaction rate code easily.

The dry deposition in this model system is calculated using the resistance method where the deposition velocity is the reciprocal sum of the three characteristic resistances, aerodynamic resistance  $r_a$ , viscous sub layer resistance  $r_b$ , and surface resistance  $r_s$  (eq. 2-1). A detailed description and tables of the  $r_s$  values used in this study are presented in Appendix A. The resistance values used here are updated from the previous values used in METRAS. The factors for gaseous species were updated for  $\text{NH}_3$ ,  $\text{H}_2\text{O}_2$ ,  $\text{HCHO}$ ,  $\text{RO}_2$ , and  $\text{PAA}$ . The values were made consistent for the particulates  $\text{Pb}$ ,  $\text{S(VI)}$ ,  $\text{NH}_4\text{NO}_3$ ,  $\text{NH}_4\text{SO}_4$ , and  $\text{NO}_3$ . The updates were based on new findings in literature (Wesely & Hicks 2000).

The MECTM was originally developed for a vectorized computing platform, but due to the limited access and computing problems facing the local computer center, the program used here was re-written for a parallel platform. The code was parallelized using the OpenMP (multi processing) programming system. OpenMP is a set of extensions to Fortran, which specifies shared memory parallels. The parallel computing improved the required computing time per run, on the vector computer the turn-around time was 24 days to simulate 1 day of chemistry, the parallel computer only requires 8 hours for a one day simulation. As the code was being re-written, modifications needed to be made to the code and in the process it was found that more updates and corrections were needed in various sections of the chemistry code. The model did not previously include  $\text{NH}_3$  in the gas phase, which is a species that is very important for this study of nitrification in the coastal waters.  $\text{NH}_3$  was included, as well as  $\text{HCl}$  and  $\text{H}_2\text{SO}_4$  in the gas phase. Once the code was completed further test runs had to be made to ensure that the quality of the output was satisfactorily reflecting the natural environment.

#### 3.1.3 Sectional Aerosol Model SEMA

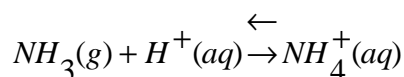
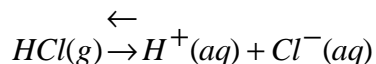
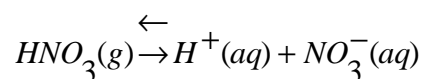
The Sectional Multicomponent Aerosol model (SEMA) (von Salzen, 1997; von Salzen and Schlünzen, 1999 a, b) is a model that uses both a thermodynamic approach for gas and internally mixed aerosol species concentrations at the aerosol surface, and a non-equilibrium approach for the size-dependence of condensation and evaporation of inorganic aerosol precursors. A sectional approach is applied to solve the size specific fundamental equations. The model includes condensation and evaporation, and considers surface partial pressures of the gaseous precursors.

The system being considered in SEMA consists of the following components:

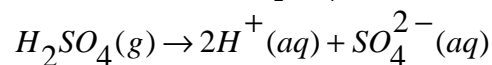
Aerosol phase:  $\text{H}^+$ ,  $\text{SO}_4^{2-}$ ,  $\text{NO}_3^-$ ,  $\text{Cl}^-$ ,  $\text{NH}_4^+$ ,  $\text{Na}^+$

Gas phase:  $\text{H}_2\text{SO}_4$ ,  $\text{HNO}_3$ ,  $\text{HCl}$ ,  $\text{NH}_3$ ,  $\text{H}_2\text{O}$

The equilibria that are allowed to exist are:



The dissolution of  $H_2SO_4$  is assumed to be uni-directional:



The equilibrium compositions of the aerosols are calculated by using the Gibbs free energy minimum condition. When the temperature, pressure and RH of a closed chemical system are kept constant this will keep the total Gibbs free energy to a minimum and then the equilibrium equations can be derived. The equilibrium constants necessary for the aerosol chemistry are then calculated for  $HNO_3$ ,  $HCl$ , and  $NH_3$  and these values are held constant throughout the model calculations for the individual time steps. In order to close the system electrolyte pairs have been assumed to exist:  $NaCl$ ,  $(NH_4)_2SO_4$ ,  $NH_4NO_3$ ,  $Na_2SO_4$ ,  $NaNO_3$ , and  $NH_4Cl$ .

When the sectional grid is initialized the diffusion coefficients, dependant upon temperature, are calculated. During the initialization the boundaries and mids of the sections are derived using a bimodal mass distribution based on mean diameters and size variance that are input to the model. The two modes represent continental and maritime aerosols. Continental aerosols are roughly generalized to be those particles in the model that have a mean diameter of  $0.6 \mu m$ . The mean diameter for the maritime aerosols in the SEMA simulations performed here is  $7 \mu m$ . This information, combined with the number of sections required, is used to derive the size section boundaries.

The model then calculates the relative concentrations of the continental aerosol species per section. Activity coefficients are derived using the Pitzer method (1981). The ZSR method (as expressed in Wexler and Seinfeld, 1991) is used in SEMA to calculate the aerosol water content and solve the growth equation over time. The process is repeated for the sea salt particles. The water content is then calculated for the final distribution.

SEMA calculates the parameters for the condensation equation. The activity coefficients are calculated using published data. The tendency for each section and species is determined, that is, whether the aerosols are growing or shrinking. This information is used with the relative mass increase at the section boundaries to recalculate sections.

### 3. Models and Input Data

All particles are assumed to be in crystal form until the relative humidity reaches the deliquescence point. Hysteresis and dry aerosols are currently not included in the calculations and it has been shown that the model results are not reliable when the RH is lower than 70% (von Salzen, 1997; von Salzen & Schlünzen, 1999b)

The SEMA box-model requires initial gas phase concentrations for HNO<sub>3</sub>, HCl, and NH<sub>3</sub>, as input as well as the initial aerosol concentrations for NO<sub>3</sub><sup>-</sup>, Cl<sup>-</sup>, SO<sub>4</sub><sup>2-</sup>, NH<sub>4</sub><sup>+</sup>, and Na<sup>+</sup>. SEMA is applied in a Lagrangian approach in which the model is initialized with observed concentrations and then prognostically calculates the concentrations at the downwind station by taking into account condensation/ evaporation and approximates deposition and sea salt generation. In this study test runs were made with the box-model where observed concentration taken during the ANICE IOP1 from the measurement site at Weybourne Atmospheric Observatory (WAO) were used to initialize the run, and the results were compared to the observations made at Meetpost Noordwijk (MPN; Figure 3-2). This initialization data and the test runs are discussed in more detail in Section 3.2.

## 3.2 Data Sources and Pre-processing

The above-mentioned models have been prepared for application in the area of the North Sea to simulate the summer 1998 and summer 1999 measuring campaign of ANICE. The model area was chosen to encompass both the MPN and Weybourne (WAO) observation sites as well as the southern ferry route to Harwich. The land use data have been derived from a data set for north-west Europe provided by Smiatek (July, 1998) on a 30" grid, based on the CORINE/PHARE land cover data (EEA) and mapped as described in Smiatek (1998). These data have been aggregated to an 8 by 8 km<sup>2</sup> grid with up to ten different sub-grid-scale land use categories considered in each grid box by application of the blending height concept (von Salzen et al., 1996). Orography data are based on the 30" by 30" GTOPO30 data set (U.S. Geological Survey, 1996) from which averaged heights were calculated for each grid cell.

### 3.2.1 Input for METRAS

Specific days from the 1998 field campaign were chosen when there was connecting flow between the two monitoring stations. Figures 3-2 to 3-4 show the backward wind trajectories for both surface- (solid line) and geostrophic winds (dashed line) for June 16 and 20/21, 1998. These are all days with connecting flow at the surface between MPN and WAO). The lifetime of the backward trajectories is 60hrs except in the case of the geostrophic winds, which extend beyond the region plotted. In this case the minimum lifetime is 19 hours. Figure 3-1 shows connecting flow between the MPN and WAO station. When clean air is coming in from the North Sea before it reaches the WAO station on June 16. For the 20<sup>th</sup> and 21<sup>st</sup> the flow is from MPN to WAO

transporting polluted air from the continent offshore. The connecting flow is well pronounced in the upper layers at June 20 (Figure 3-3). On June 21 (Figure 3-4) westerly flows are found in higher levels (geostrophic wind).

The output from the German Weather Service's forecast model, the Deutschland Model (DM) (Deutscher Wetterdienst, 1998), was used to force the meteorology in METRAS. These large-scale values are initial data for METRAS and influence the model simulations at the lateral and upper boundaries by nudging. A new data pre-processor was developed able to read the DWD-DM data, convert the units to METRAS units, calculate the DM data on the METRAS grid, and prepare a data set that can be used by the METRAS model. The pre-processor was tested by comparing the output with observations, i.e. comparing vertical profiles, surface temperature, wind patterns, etc. These results of the METRAS meteorology model are discussed in more detail in Chapter 4.

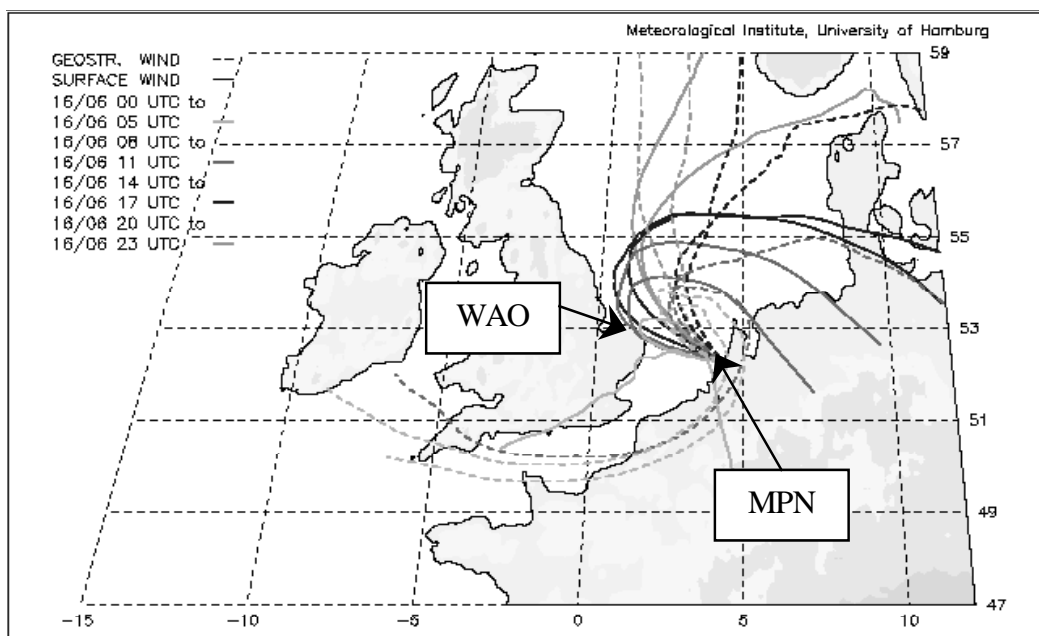


**Figure 3-2.** Surface (S, solid lines) and Geostrophic (G, dashed lines) backward wind trajectories in 3-hour increments for June 16, 1998. The maximum life times of the air parcels represented is 60hrs, the minimum is 24hrs for G winds, and 60 hrs for S winds.

### 3. Models and Input Data

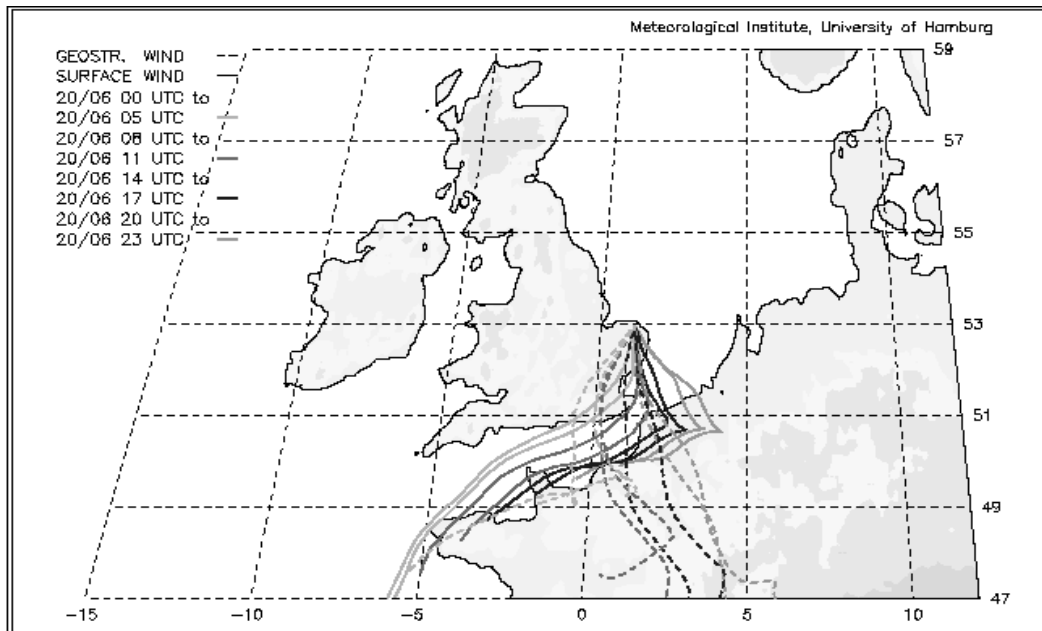


**Figure 3-3.** Surface (S, solid lines) and Geostrophic (G, dashed lines) backward wind trajectories for WAO in 3-hour increments for June 20, 1998. The maximum life times of the air parcels represented is 60hrs, the minimum is 58hrs for G winds, and 23 hrs for S winds.

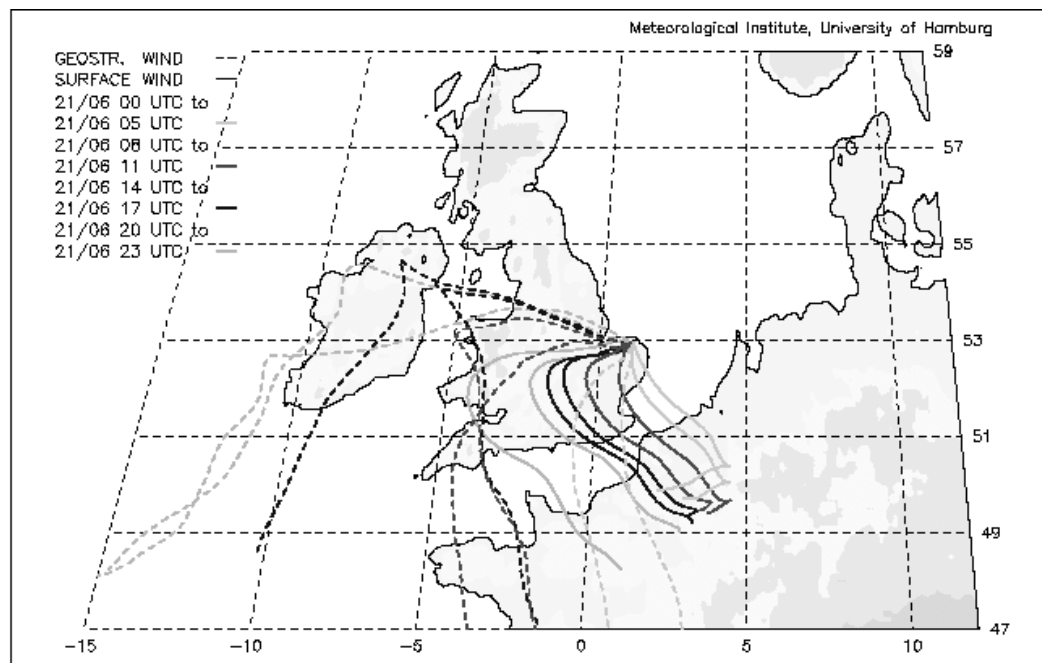


**Figure 3-4.** Surface (S, solid lines) and Geostrophic (G, dashed lines) backward wind trajectories for WAO in 3-hour increment for June 21, 1998. The maximum life times of the air parcels represented is 60 hrs, the minimum is 19 hrs for G winds, and 60 hrs for S winds.

METRAS was used to calculate all necessary meteorological fields with a time resolution of 15 minutes. The horizontal resolution was set to 8 km x 8 km, and the vertical resolution changes from 20 m at the ground with the lowest grid level at 10m above ground to about 1000 m at the top of the model domain. The model domain

height was chosen to be 11 km. The grid was set up as Arakawa-C with terrain-following coordinates. The model area is 352 km x 488 km (171,776 km<sup>2</sup>), and roughly 84,000 km<sup>2</sup> of the modeled region is covered by water.

### 3.2.2 Emission Data and Photolysis Rates for MECTM

Anthropogenic emissions for both point and area sources were obtained from the University of Stuttgart, Institute for Energy Economics and the Rational Use of Energy (Figure 1-1). These include emissions from industry, residential, and a mobile emissions inventory (including running losses, cold-starts, etc.) as well as agriculture (NH<sub>3</sub> emissions).

The emissions were grouped using the aggregation set out by Middleton et al. (1990) and is the same aggregation system used by RADM2 (Stockwell et al. 1990). It has been tailored to use with regional models with polluted atmospheres, and so concentrates on those species most relevant to urban pollution such as nitrogen and sulfur compounds. The emission data were interpolated to the METRAS grid and converted to the units that would be necessary for the gas phase chemistry reactions. The emission species used are listed in Appendix E.

The biogenic emission factors are calculated for MECTM by a program that uses the land use classification data and the emission factors from McKeen et al. (1991). The emission factors are used to calculate emissions for 4 classes of biogenic emissions; isoprene, alpha-pinene, beta-pinene, and OVOC's (other volatile organic compounds). The biogenic emission inventory data file contains the factors stated in kilogram per model grid cell per hour. MECTM uses these factors with the actual radiation and temperature values to calculate the biogenic emissions for each grid cell which are then treated as area emissions by the model.

In order to accurately model and predict the effects of air pollution, photo-dissociation reaction rate estimates must be made. The simulation accuracy of the entire gas phase chemistry system is highly dependant upon the accuracy of the photolysis rates, which are the primary source of radicals in the atmosphere. The current approach taken for setting photolysis rates in the METRAS/MECTM was based on the System for Transfer of Atmospheric Radiation (STAR) model developed by Ruggaber et al. (1994). Before the chemistry model is run, a table of clear-sky photolysis rates was calculated for 21 different gases using a pre-processor which calculates the rates for each photolysis reaction and each hour based on meteorological and land use information extracted from the METRAS runs. The STAR land use classes and the STAR/MECTM land use class relation matrix is shown in Appendix D.

### 3. Models and Input Data

The calculated photolysis rate is the product of the photolysis frequency and the concentration of the dissociating molecular species. RADM2 requires photolysis frequencies ( $J_{\text{gas}}$ ) at each grid point and time step to determine the concentrations of the different species. STAR calculates  $J_{\text{gas}}$  by integrating over all wavelengths the product of the spectral actinic flux  $I_A$ , the spectral absorption cross section  $\sigma_{\text{gas}}$  and quantum yields  $\phi_{\text{gas}}$ . Only the tropospheric wavelengths between 290 and 700 nm are considered.

These rates are then matched to the modified RADM2 mechanism in the chemical transformations during the chemistry run. The spectral absorption cross section  $\sigma_{\text{gas}}$  is corrected for temperature dependence and  $\phi_{\text{gas}}$  is corrected for temperature and pressure dependence at each altitude. The photolysis frequencies in each layer for each hour were calculated and written to a table that was used as input for the MECTM model runs.

Photolysis rates were interpolated from the pre-generated table by the MECTM based on grid cell location and model time. The STAR photolytic reactions and the relation matrix for the RADM2 chemistry mechanism is shown in Appendix F.

#### 3.2.3 Initial Values for MECTM

In order to investigate the effects of gas phase chemistry on concentrations, the MECTM was run for the June 16 to June 20, 1998 period. There was no large-scale chemistry data available so the MECTM was initially run for a 24-hour simulation period using emissions of June 16 to generate background concentrations. For this run prescribed background concentrations were applied (provided by Müller) and then the chemical model was run for a 24-h period using the meteorology results from the METRAS June 16 run. The new concentrations calculated by this initialization run were then applied as background concentrations, and then the model was restarted for June 16 and run for the entire period. A zero-gradient condition was applied to the lateral boundaries.

#### 3.2.4 Initial Values for SEMA Box Model

June 16, 1998 was selected to investigate the effects of transport over the sea on the aerosol size distribution when there was connected flow from the WAO to MPN (Figure 3-2). The box-model was initialized with the measured concentrations at WAO redistributed to 8 different size categories. One of the criteria of SEMA's input concentrations is that the ions must balance. In order to achieve this it was necessary to make assumptions to the measured data as to where the ions are missing and add them accordingly. Since  $\text{Na}^+$  is the only cation included in the model,  $\text{Mg}^{2+}$ ,  $\text{Ca}^{2+}$ , and  $\text{K}^+$  are represented by using an equivalent number of  $\text{Na}^+$  cations according to the ion

balance (von Salzen and Schlünzen, 1999c). After trying various combinations it was decided to replace the remaining missing ions with  $H^+$  in one run and  $Na^+$  in another to analyze the impact that the different additions have on the resulting aerosol concentrations. The gas phase concentrations measured were  $HNO_3$  and  $NH_3$ .  $HCl$  and  $H_2SO_4$  were not measured, so no input value was available. Figure 3-5 presents the measured concentrations (with the modified  $Na^+$ ) in the distribution used as input into the box-model.

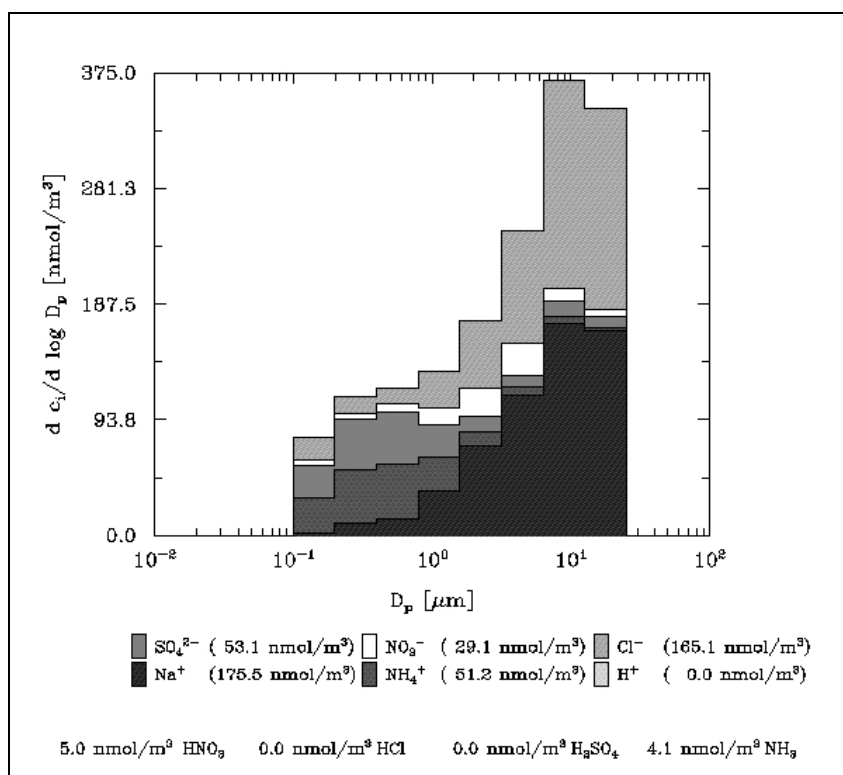


**Figure 3-5.** Measured Concentrations at WAO, June 16, 1998. The original measurements were redistributed to create an input for the SEMA box model. (WAO-12, 8:02h-16:02h, June 16)

The air temperature for the air mass traveling over the North Sea was derived from the water temperature for June 16 and then interpolated to represent the air temperature close to the sea surface. This resulted in an air temperature of  $15.1^{\circ}C$  with a relative humidity of 95%. The wind speed was roughly 5m/s. During the runs the meteorological parameters were held constant. This simplification was necessary for the box-model.

The evaluation of the meteorological runs with METRAS is discussed in Chapter 4 and the results of the runs with chemical transformations (MECTM) are discussed in Chapter 5. Chapter 6 summarizes the effects both the physical and chemical transformations have on deposition for the case studied, June 16 to June 20, 1998.

## **4. The Influence of Coastal Meteorological Phenomena**

### **4.1 Evaluation of METRAS Meteorology Results**

The first phase in the numerical simulations was to utilize the METRAS model to forecast the meteorological conditions for the ANICE IOP1 field experiment dates from June 16 to June 20, 1998. METRAS was nudged at the lateral and upper boundaries to the large-scale meteorology forcing data derived from the Deutsche Wetterdienst Deutschland Model results. A weak nudging was used at the model boundaries. There was no nudging in the inner model domain so that the model could develop mesoscale features of the meteorological fields.

It is important for the meteorology simulations to be accurate in its predictions of such parameters as wind speed, humidity and temperature because the level of accuracy will be reflected in the chemistry runs and increases the confidence in the results (Lenz et al., 2000). The weather data accuracy criteria used to evaluate the results of the METRAS run were taken from an intercomparison study of four U.S. weather forecast models, the Fifth-Generation NCAR / Penn State Mesoscale Model (MM5), the Regional Atmospheric Modeling System (RAMS), the Navy Operational Regional Prediction System Version 6 (NORAPS6), and the US Air Force's mesoscale Relocatable Window Model (RWM) (Cox et al. 1998). One main goal of that study was to determine how well the models operated and could produce forecasts in data-sparse areas and in this case that could be compared to the lack of available data on the North Sea.

The programs applied for evaluation of the METRAS meteorology results interpolate the METRAS results to the locations of the observation stations which regularly collect and report meteorological conditions. 76 stations with valid observations are located within the model domain and more than 6000 surface observations (hourly) were used in the statistical analysis (Table 4-1). The same comparison programs were run using the observation station data from MPN and WAO (Table 4-2). Hit rates are determined by calculating the percent of values which are within the accuracy criteria.

Compared to average results from Cox et al. (1998) (last column of Table 4-1) the METRAS results agree well with measured data. This is especially true for temperature and dew point temperature as well as for wind direction. Even wind speed hit rates are mostly better than found in the Cox et al. study (1998).

**Table 4-1.** Forecast accuracy of METRAS for the period June 16-20, 1998.

Parameter	Accuracy Criteria <sup>1</sup>	Correlation to observations	Hit rate (%)	Avg. hit rate of the models in Cox et al. (1998)
Temperature	2° C	0.91	86	35
Dewpoint depression	2° C	0.85	76	41
Wind speed	1 m/s	0.26	39	30
Wind direction	30°	0.74	67	34
Sea level pressure	1.7 mb	0.68	36	32

<sup>1</sup> taken from Cox et al., 1998

**Table 4-2.** Forecast accuracy of METRAS correlated to the ANICE stations.

Parameter	Accuracy Criteria <sup>1</sup>	Correlation to obs. WAO	Correlation to obs. MPN	WAO Hit rate (%)	MPN Hit rate (%)
Temperature	2° C	0.95	0.89	77	89
Dewpoint depression	2° C	0.91	0.94	87	94
Wind speed	1 m/s	0.21	0.64	34	27
Wind direction	30°	0.78	0.80	74	64
Sea level pressure	1.7 hPa	0.46	0.88	28	50

<sup>1</sup> taken from the Cox et al., 1998

The excellent accuracy of the temperature provides confidence that the boundary heights are being well simulated and will not have a negative impact on the chemistry simulations. The accuracy of the wind direction assures that the deposition patterns will be properly predicted and the influence of the emissions will be seen in the true down-wind areas.

Satellite images and observation data for the modeled period showed that it was mostly cloudy for the entire period, clearing slightly towards the 20<sup>th</sup>. In order to compare the simulated inversion heights to observations rawinsonde data was obtained from the British Atmospheric Data Center (BADC) for three locations within the same grid space as the 3 ANICE locations used in Figure 4-4. The inversion heights were determined by means of calculating  $\partial\theta/\partial z$  from the rawinsonde data and then the gradient was plotted against the mean height. This resulted in an uncertainty of the heights ranging from -360 to +190m. An example of the profile analysis is presented in Figure 4-1.

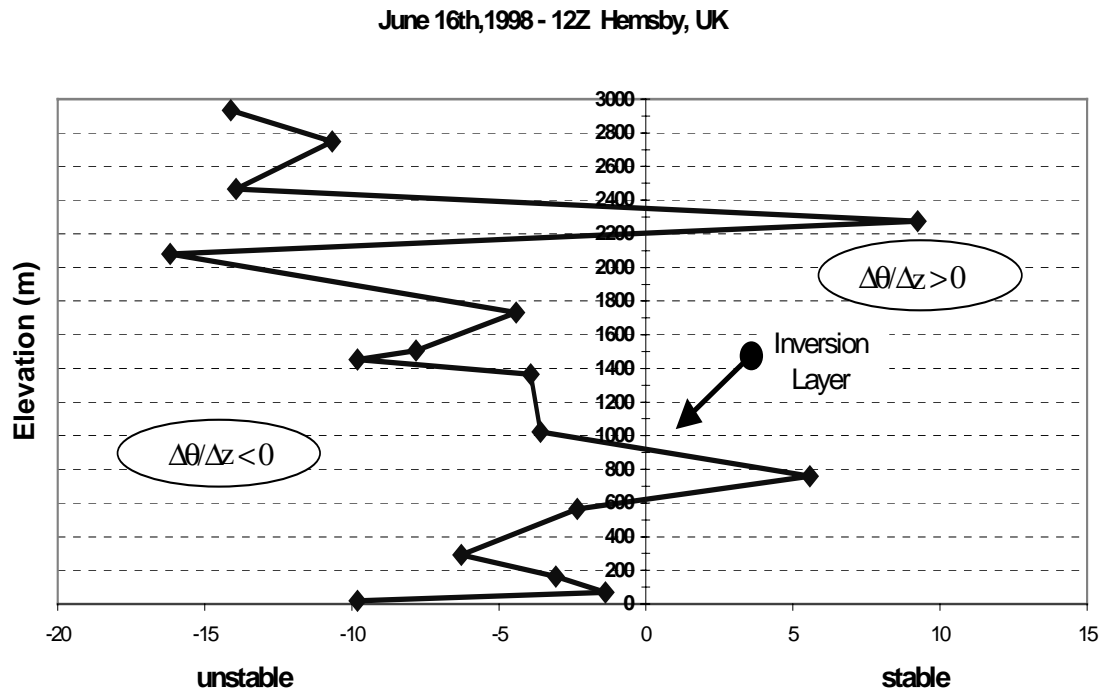


**Figure 4-1.** Stability vs. height based on rawinsonde data for Hemsby, UK, 12Z June 16th, 1998.

Some of the observation data was incomplete so a full comparison was not available. In the case of the rawinsonde data for the regions in the Netherlands (i.e. DeBilt) there were no clear signs of the boundary layer on the profiles. It is important to note that nighttime inversions are difficult to calculate using rawinsonde data because the inversion heights are usually below a hundred meters and rawinsonde data at those heights are not without problems with the soundings at the beginning of the measurement recording periods, i.e. shortly after release (Schlünzen personal communication, 2002). Table 4-3 shows the inversion layers from the BADC data and the corresponding value from the model simulation. On June 18<sup>th</sup>, 1998 Hemsby, UK showed no sign of an inversion layer and the Essen daytime data was complete only for 12Z. All in all the morning and evening inversion heights are quite high and more consistent with daytime inversion heights. Their reliability is thus questionable.

The uncertainty of the inversion layer height varies at each height and is based on the level spacing recorded in the sounding data. The model height is also determined with some uncertainty because it can only be determined at a fixed grid level. The model PBL is determined from the temperature gradient for stable stratification and from the minimum heat flux for unstable stratification. The PBL height is determined at the height where the positive gradient begins, as was used in the analysis of the BADC rawinsonde data. The table includes an error range for each PBL calculated from the soundings and from the model.

**Table 4-3.** Rawinsonde Inversion Heights vs. Modeled (values in parenthesis are the error range)

Date	Time	Hemsby, UK (m)	WAO modeled (m)	Essen, DE (m)	Continental modeled (m)
June 16 <sup>th</sup>	6Z	755 (-65/+200)	525 (-32/+110)		
	12Z	760 (-130/+160)	759 (-123/+42)	1480 (-200/+160)	1574 (-125/+148)
June 17 <sup>th</sup>	6Z	1500 (-25/+70)	290 (-18/+82)		
	12Z	900 (-200/+180)	1259 (-53/+190)	875 (-360/+110)	1590 (-140/+132)
June 18 <sup>th</sup>	12Z			2700 (-65/-60)	1248 (-40/+200)
	12Z	725 (-50/+20)	985 (-184/+6)	1100 (-30/+10)	1082 (-90/+125)
June 19 <sup>th</sup>	18Z	825 (-250/+20)	605 (-112/+30)		
	12Z	875 (-85/+120)	545 (-52/+91)	880 (-90/+170)	1112 (-120/+95)
June 20 <sup>th</sup>	18Z	830 (-65/+125)	169 (-34/+25)		

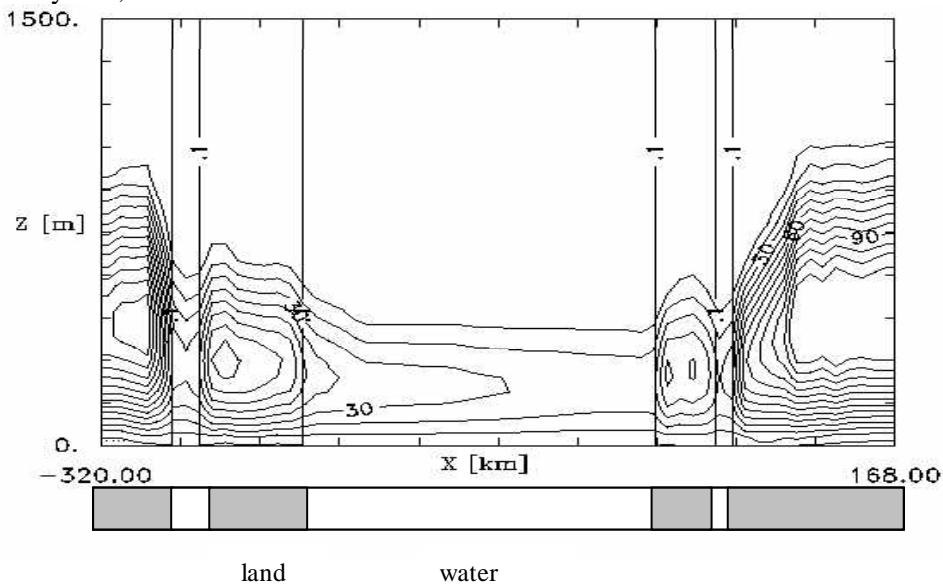
Grey shading denotes no sign of inversion layer from observations.

From Table 4-3 it can be seen that the model sufficiently simulates the PBL height with some variation from observed. A general trend in the comparison can not be derived. However, in several cases the daytime inversion heights are overestimated by the model, while morning and evening boundary layer heights are often simulated lower than the heights derived from the rawinsonde data which are not very reliable, as mentioned before. The overestimation of the daytime inversions could partially be due to the fact that no clouds were included in the model runs and also because the model values are the average over the grid box (8km<sup>2</sup>) as opposed to a single location.

## 4.2 Influence of Meteorology on Pollution Dispersion Mechanisms

Pollution dispersion and deposition are dependent on various meteorological parameters, which include wind speed, temperature stratification and stability, and boundary layer heights. The METRAS simulations were made in order to simulate these parameters and then the information would later be passed on to the MECTM model for the chemistry runs. All 5 days from the 16<sup>th</sup> through the 20<sup>th</sup> were simulated and used in the analysis. The 16<sup>th</sup> has been chosen to illustrate the coastal characteristics because that was a day which had connecting flow between the WAO and MPN observation stations.

a) Daytime, 14:00 LST.



b) Night-time, 23:00 LST.

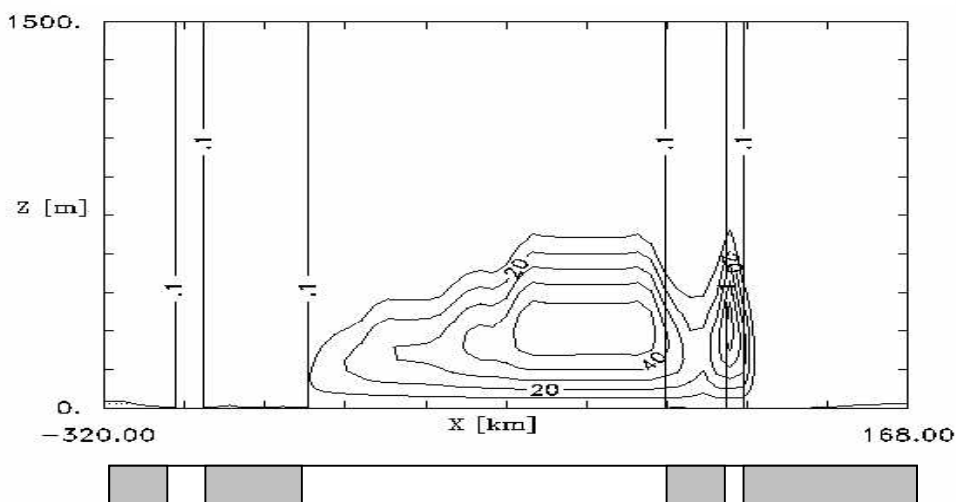


**Figure 4-2.** West-east vertical cross-section to 1500m height of vertical exchange coefficient in  $m^2/s$  at  $53^\circ$  North during the day (a) and during the night (b) for June 16, 1998. The North Sea is situated in the center and is bounded by England and the Netherlands. (Figure not to scale)

The local concentration change of trace gas species is driven by advection and turbulent transport processes as well as by local sources and sinks which are predicted by METRAS. An interesting feature in coastal pollution dispersion is the variation of turbulence and vertical advection between water and land. This was simulated by the METRAS model system (Figure 4-2). During the day (16.6.1998) there is intense vertical mixing over land and weaker mixing over water. During the night the mixing decreases over land to minimal values while over water it doubles, but is still less than half the intensity of the daytime mixing over land.

The potential temperature reflects the diurnal variations in the mixing layer height. During the day there is a well-mixed boundary layer over the entire region with somewhat lower boundary layer heights over the water. At night there is the development of an inversion at the surface over the continent well below the well-mixed planetary boundary layer (PBL) height of the ending day (Figure 4-2). This low inversion layer is resulting from radiative cooling at the surface and has a height of about 40 m only (Figure 4-3). The local influence of this stability acts to limit the vertical mixing of pollutants and contributes to the high concentrations simulated over land for the night.

As noted above the changes in surface concentrations are connected with the vertical mixing and these are connected with the diurnal cycle in the boundary layer height (Figure 4-3). At MPN, WAO and a site just west of Düsseldorf the hourly inversion heights were output from the METRAS and were plotted to study the differences between the two coastal stations and an inland site. In general WAO and the continental station show similar PBL heights, showing the influence of land at WAO. This, however, might be somewhat overestimated since the PBL heights are not interpolated to the measurement site but the average value of the corresponding grid box is taken. The values thus correspond to 4 km inland while WAO is situated only 75 m from the coast.

#### 4. The Influence of Coastal Meteorological Phenomena

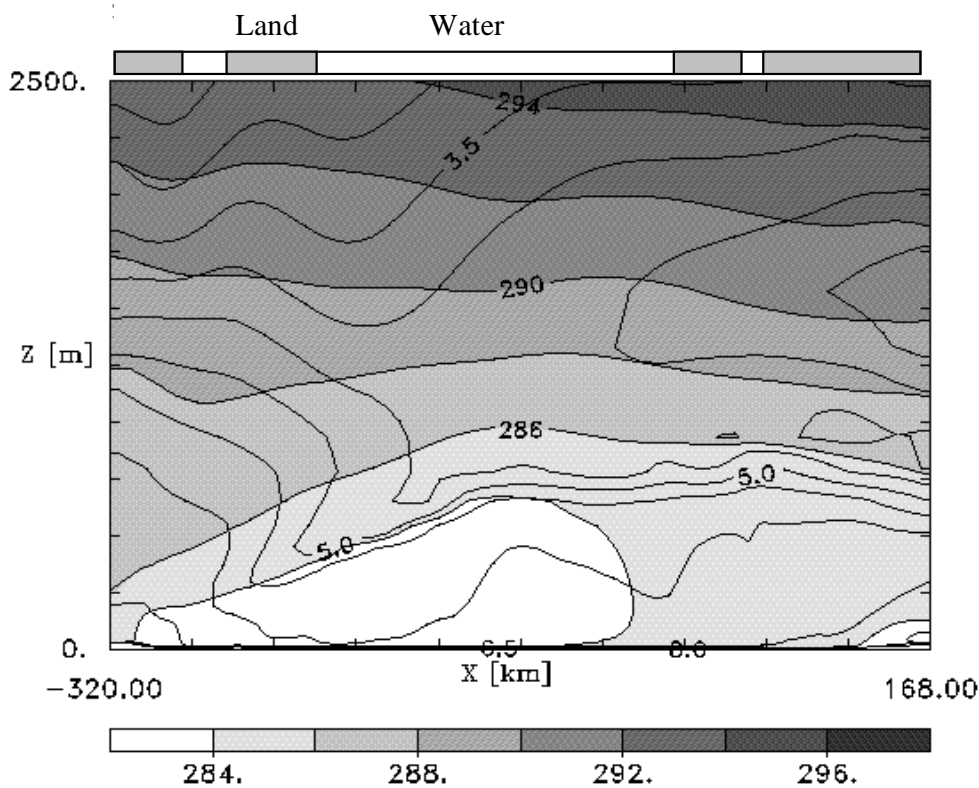


**Figure 4-3.** Vertical cross-section of potential temperature (shaded area) and specific humidity (contour lines) to 2500m height, June 16, 22:00. The cross-section is taken at the same latitude as the MPN site (figure is not to scale). The eastern coast of England is on the far left, and the western coast of the Netherlands on the right side of the plot.

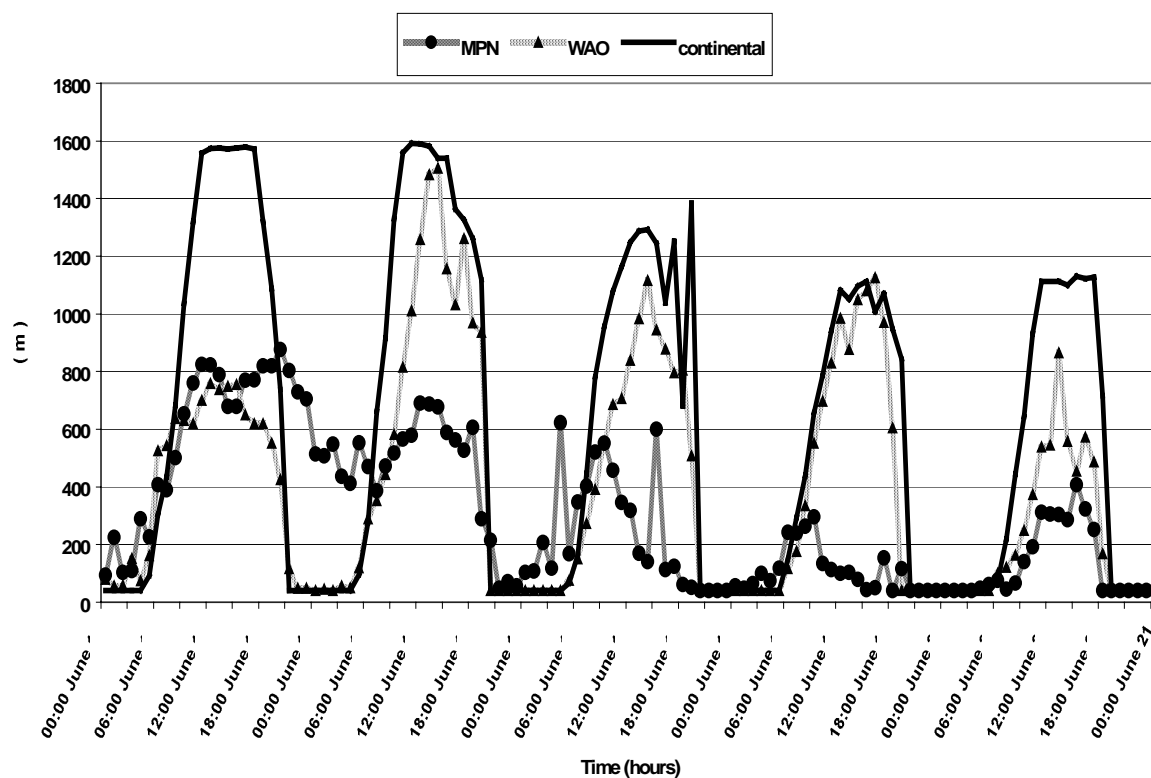


**Figure 4-4.** Boundary layer heights at sites MPN, WAO, and a continental site.

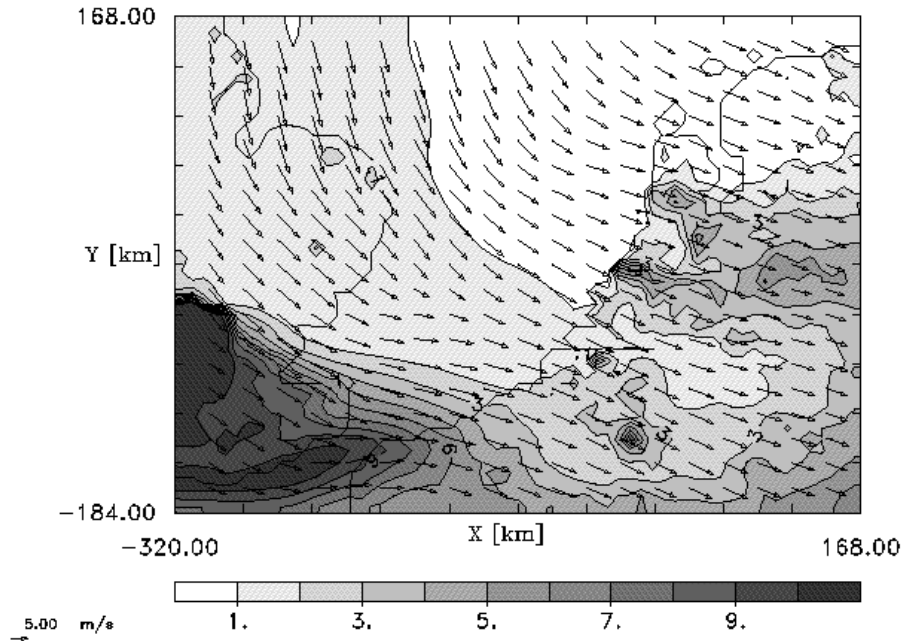
On the 16<sup>th</sup> the effects of the cold air approaching from the northern North Sea are observed at WAO and MPN. This results in unstable stratification giving comparatively high boundary layers at day and night for the marine station MPN. From the 17<sup>th</sup> to the 20<sup>th</sup> the air mass that reached the WAO station was southerly and the effects of passing over England can be noted by the increased inversion height during the day (unstable stratification). The airflow direction over the MPN station changed gradually and remained northwest into the 17<sup>th</sup> and became more southeasterly towards the 20<sup>th</sup>. Again this is reflected in the inversion height pattern which begins to show greater diurnal changes as well as lower heights in the later days of the modeling period when influenced by coast parallel or continental air masses. The continental site receives less influence from the North Sea and shows a diurnal pattern throughout. The more or less continuous decreasing of the PBL height over the platform MPN is also a result of changed air masses: while at the beginning of the experiment cold air was advected by northerly flows, resulting in unstable stratification, the south-easterly flows advected warmer air over the water resulting in lower mixing heights.

### **4.3 Influence of Meteorology on Passive Transport**

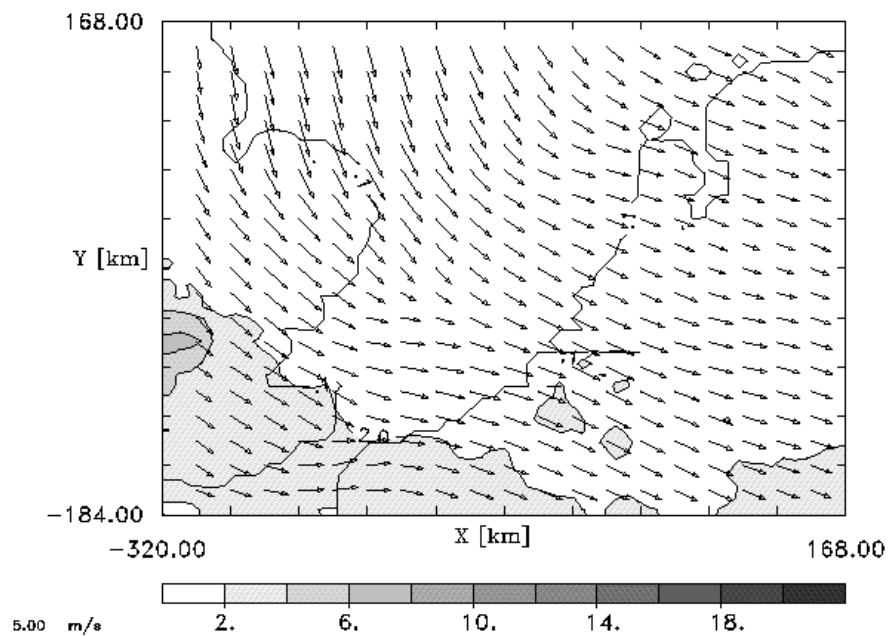
The southern North Sea area was selected to study the influence of meteorology on transport in coastal regions due to its combination of coastline, open water, and urban and agricultural emission sources. Measurements are available for both sides of the water body and over the ocean from the ANICE (Atmospheric Nitrogen Input to the Coastal Environment) experiment, which ran from June 16-20, 1998 and show the transformation from emissions to secondary pollutants. Other available data for that region include routine measurement data and routine weather forecasts. These available data help for judging the model performance.

A series of runs were completed for the ANICE IOP1 that included emissions and meteorology but no chemical reactions in order to study the pure influence of meteorology on the concentrations and deposition. The meteorology simulations showed that during the day there is intense vertical mixing over land, which compensates the higher daytime emissions coming from urban areas around London (NO<sub>x</sub>), and agricultural areas as those located in the Netherlands (NH<sub>3</sub>). Lower concentrations due to this vertical mixing during the afternoon were simulated showing that vertical mixing plays an important role in reducing pollution concentrations at lower levels during the daytime hours. During the night when the mixing over land decreased and the inversion heights were lower (Figure 4-1), the dispersive activity of the pollutants was less resulting in greater concentrations in the lower levels. Figure 4-5 presents minimum (day) concentrations for NO and SO<sub>2</sub>, and Figure 4-6 presents NO, NO<sub>2</sub>, and Figure 4-7 shows SO<sub>2</sub> maximum (night) 10 m concentrations for the 'no gas-phase chemistry' case on June 16<sup>th</sup>, 1998.

#### 4. The Influence of Coastal Meteorological Phenomena



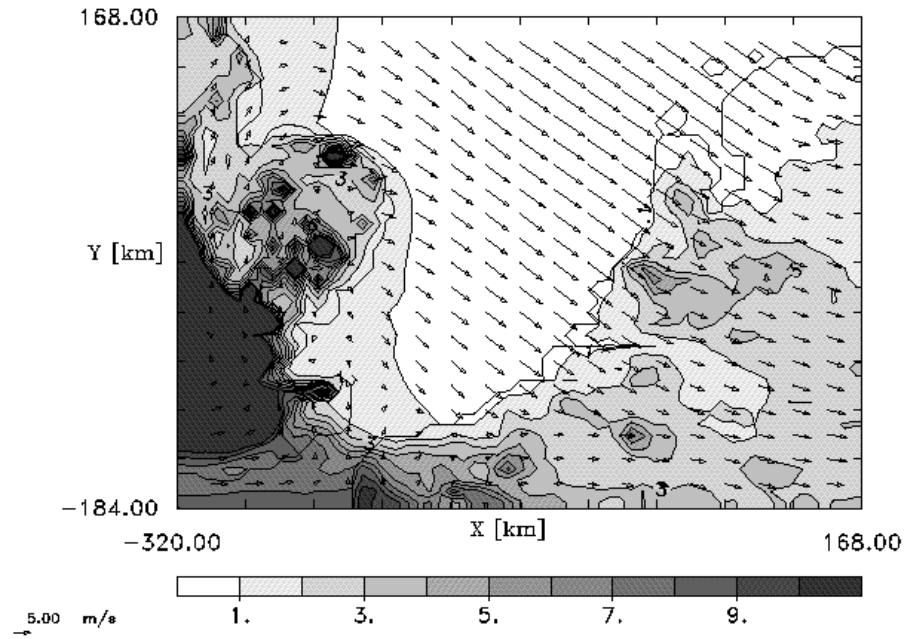
a)  $\text{NO}$  minimum concentration (ppb), 13:00 (scaled to a max of 10 ppb).



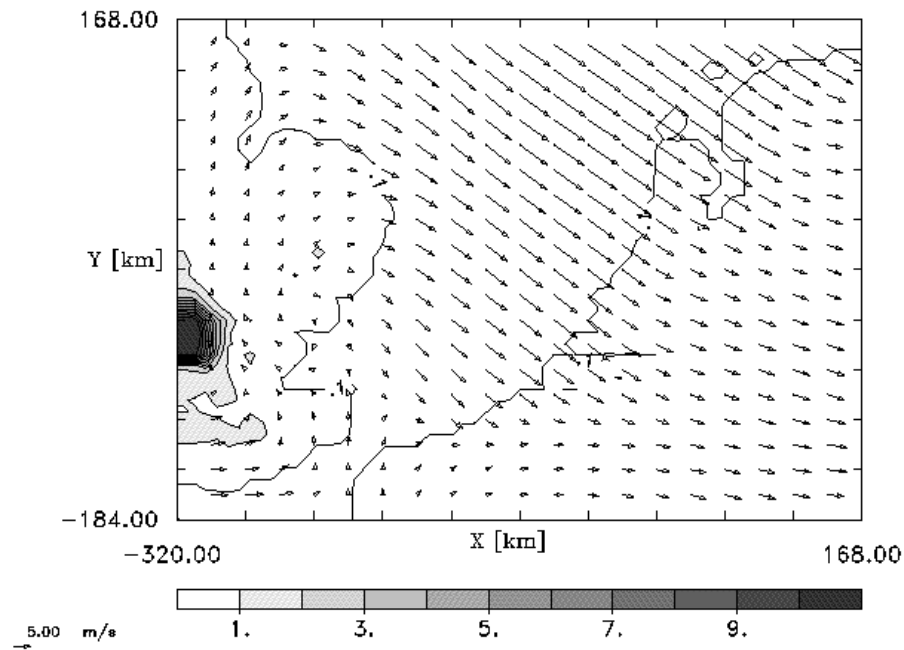
b)  $\text{SO}_2$  minimum concentration (ppb), 13:00 (scaled to a max of 20 ppb).

**Figure 4-5.** Minimum concentrations at a height of 10m, June 16, 1998 (ppb). Runs included emissions and deposition but no chemical reactions.

#### 4. The Influence of Coastal Meteorological Phenomena



a) NO maximum concentration (ppb), 23:00 (scaled to a max of 10 ppb)



b) NO<sub>2</sub> maximum concentration (ppb), 23:00 (scaled to a max of 10 ppb)

**Figure 4-6.** Hourly concentrations at a height of 10m, June 16, 1998 (ppb). Runs included emissions and deposition but no chemical reactions.

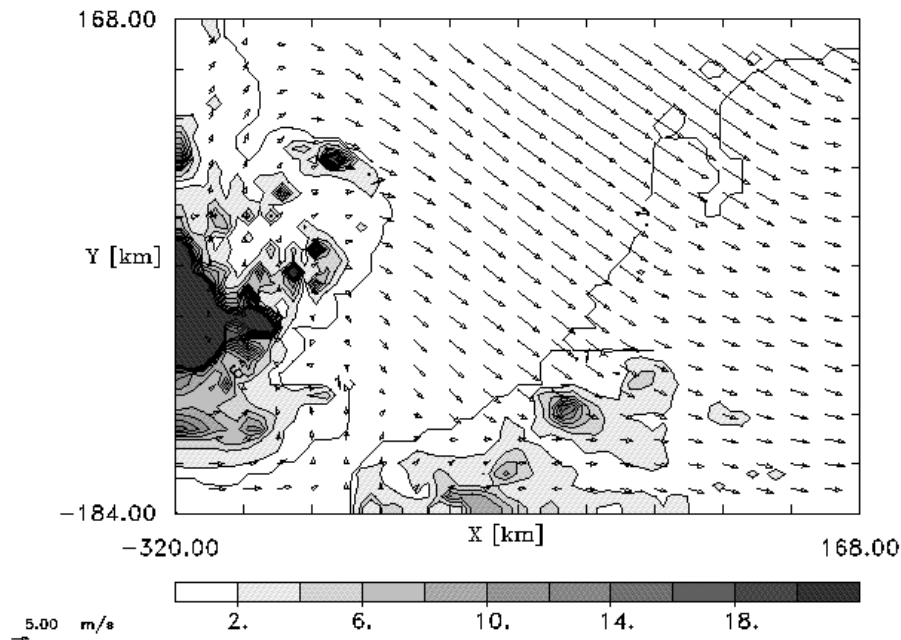


**Figure 4-7.** *SO<sub>2</sub> maximum hourly concentration (ppb), 23:00 (scaled to a max of 20 ppb) at a height of 10m, June 16, 1998. Runs included emissions and deposition but no chemical reactions.*

During the night there was some NO<sub>2</sub> in the vicinity of London due to the large emissions in that area. There is transport over the water in the lower southeast corner of the model area for those chemical compounds which are less soluble and do not deposit to the water (i.e. NO, NO<sub>2</sub>).

The passive tracer runs show how the influence of the land-based emissions can affect the atmosphere over the water from transport. The southern North Sea is situated so that it is impacted by emissions originating in both the UK and continental Europe. It is these primary pollutants that will eventually undergo chemical transformations and then be deposited kilometers away from their source, and much over water as will be shown in Chapters 5 and 6.

## 5. Influence of Chemical Transformations

### 5.1 Influence of Gas Phase Chemistry

In the MECTM runs with gas-phase chemistry performed for the ANICE IOP1 there is the minimum occurring around 1pm (Figure 5-1), at the same time as for the no-chemistry case. This is true for most of the gases; however, the values don't remain the same as in the no-chemistry case. For instance, the minimum values of NO are about halved. In addition to the vertical mixing, the NO<sub>x</sub> concentrations during the day are reduced due to photochemical reactions, e.g. the conversion of NO<sub>2</sub> into HNO<sub>3</sub> reducing the NO<sub>2</sub> concentration. At the same time ozone is formed, resulting in the highest ozone concentrations in the late afternoon (Figure 5-4).

Maximum concentrations for NO, NO<sub>2</sub>, and SO<sub>2</sub> concentrations at 10m occur around midnight (Figures 5-3 and 5-4). Since one of the larger sinks for NO<sub>x</sub> is photolytical reactions, it is understandable that the higher concentrations occur during the night when there is no photolysis but there are emissions. Once the sun began to rise the NO<sub>x</sub> concentrations begin to decrease.

In the chemistry runs it was noticed that NO<sub>x</sub> begins to increase in the afternoon at the same time HNO<sub>3</sub> deposition increases. The peak daytime HNO<sub>3</sub> deposition took place during the late afternoon and corresponded with the time that highest concentrations for HNO<sub>3</sub> were simulated. As the day progressed, the HNO<sub>3</sub> concentrations decreased and the NO<sub>x</sub> increased as the conversion of NO<sub>2</sub> to HNO<sub>3</sub> slowed.

5. The Influence of Chemical Transformations

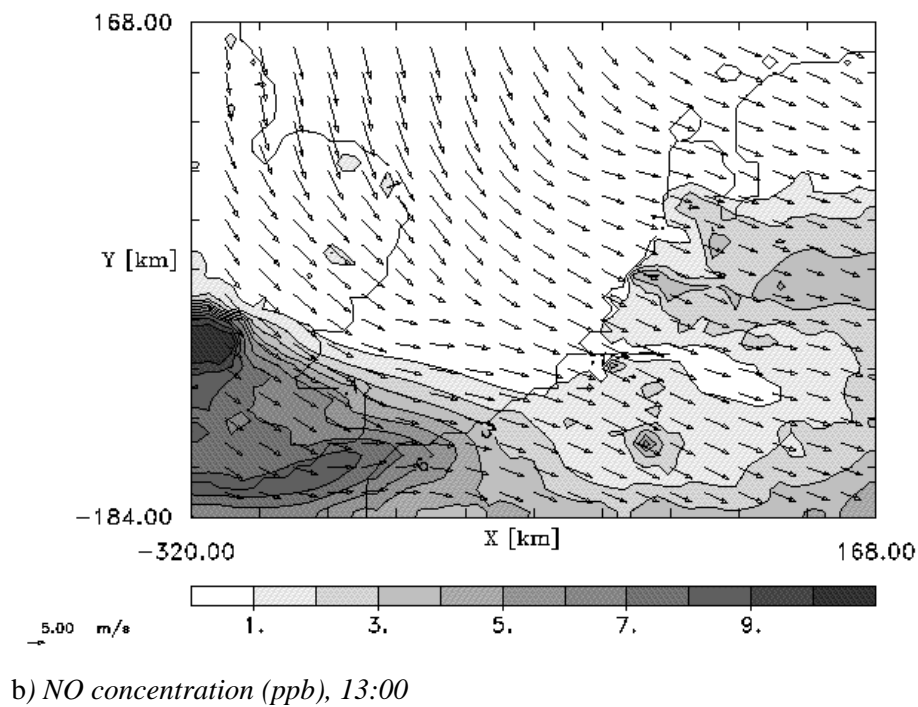
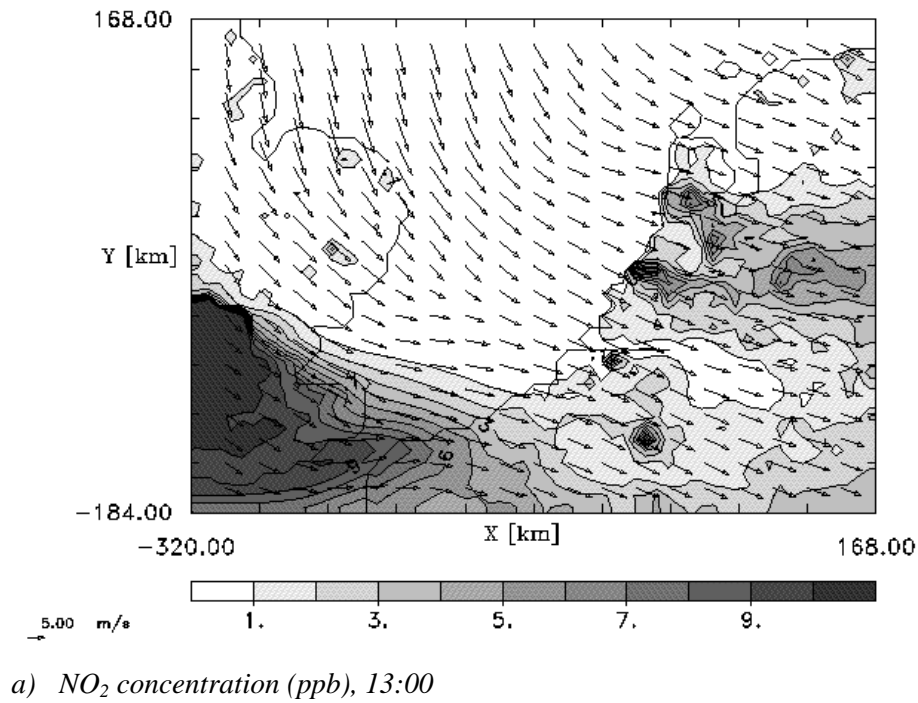


**Figure 5-1.** Minimum hourly concentrations at a height of 10m, June 16, 1998 (ppb) when including chemical reactions.

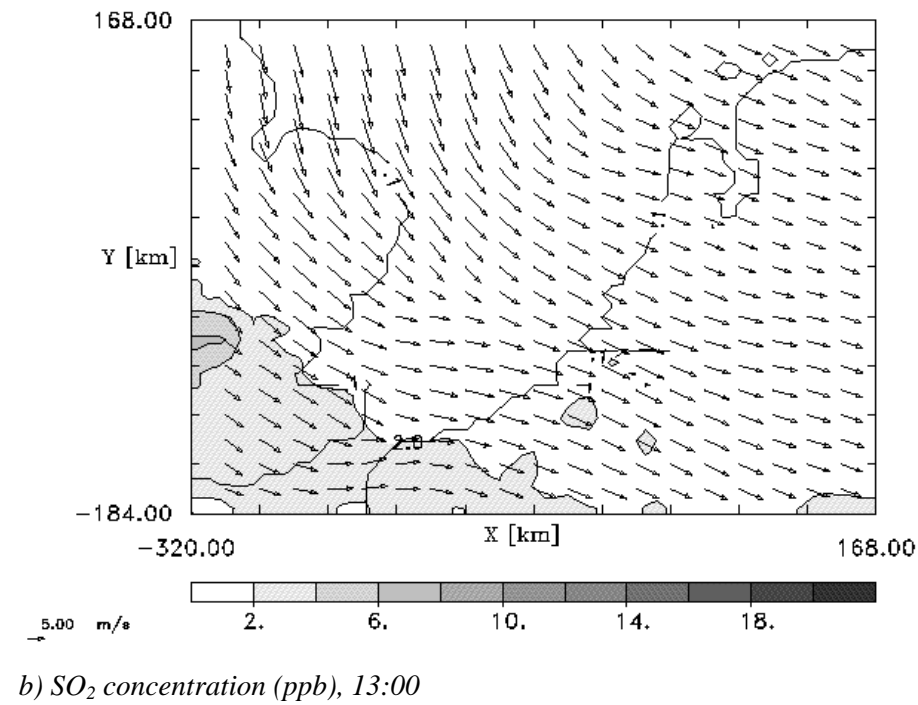
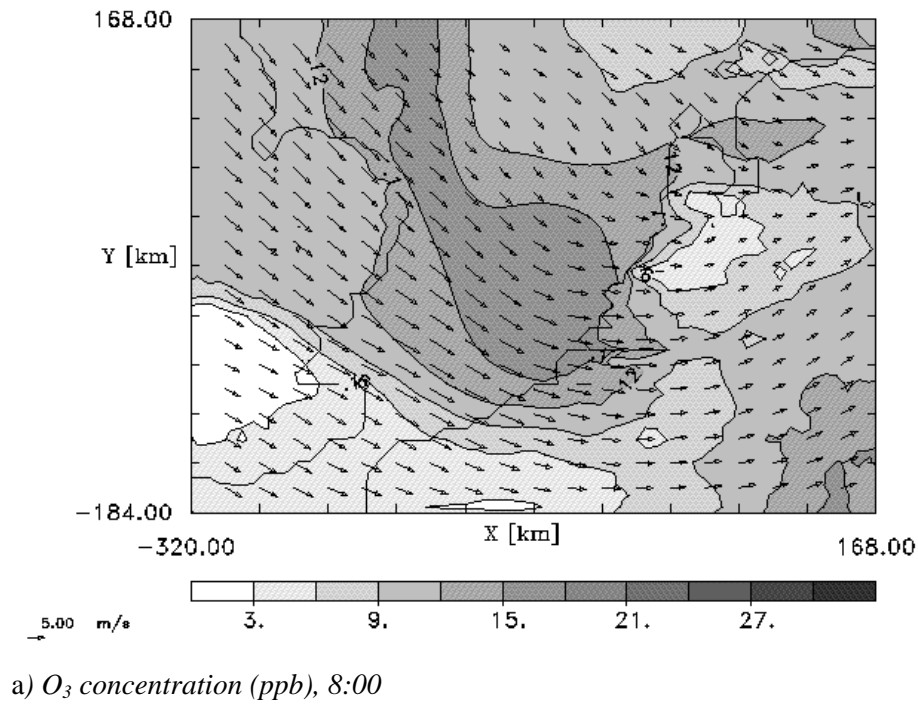
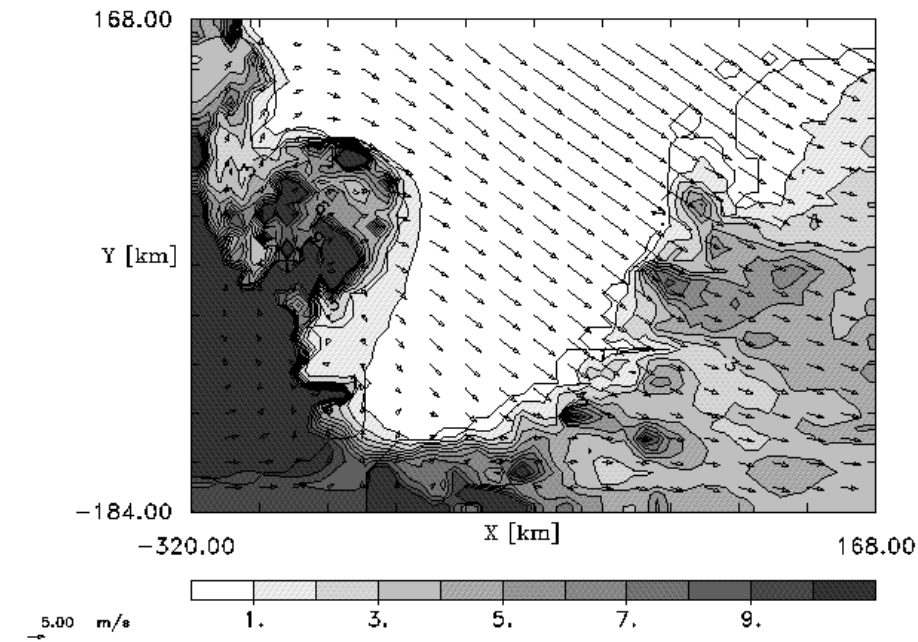


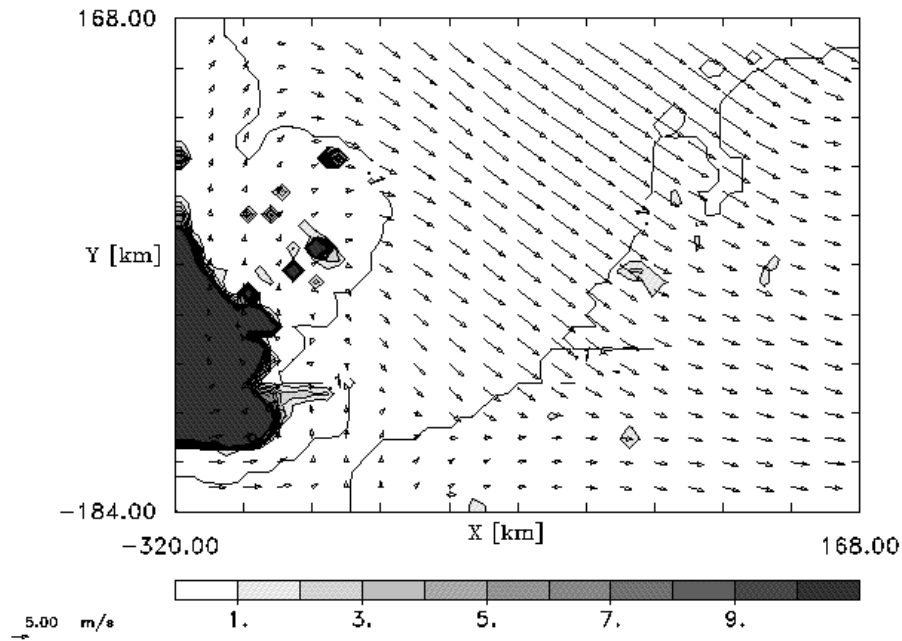
**Figure 5-2.** Same as in Figure 5-1, except for  $O_3$  and  $SO_2$ .

## 5. The Influence of Chemical Transformations

The chemistry runs produced concentrations of ozone due to the inclusion of photochemical processes. The O<sub>3</sub> figures in this section are the result of both formation and deposition processes.

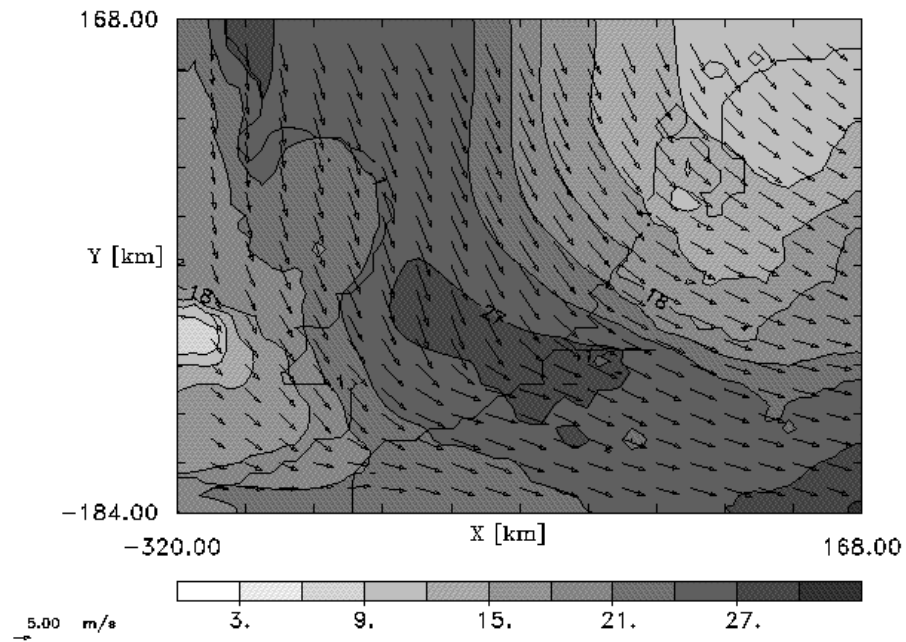


a) NO<sub>2</sub> concentration (ppb), 23:00

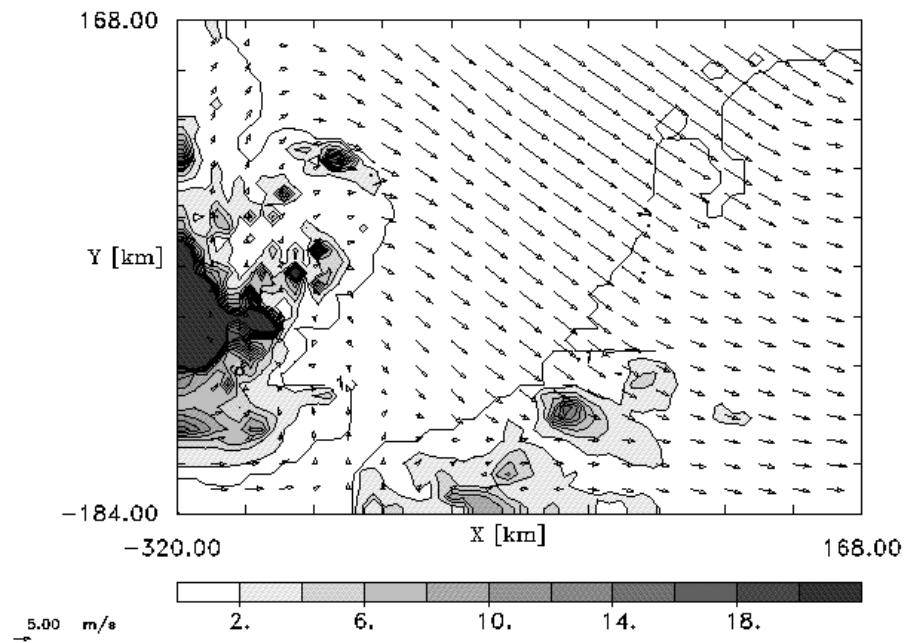


b) NO concentration (ppb), 23:00

**Figure 5-3.** Maximum hourly concentrations at 10m, June 16, 1998(ppb) when including chemical reactions.



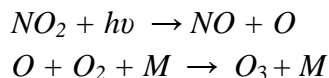
a)  $O_3$  concentration (ppb), 16:00



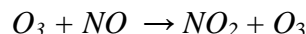
b)  $SO_2$  concentration (ppb), 23:00

**Figure 5-4.** Same as in Figure 5-3, except for  $O_3$  and  $SO_2$ .

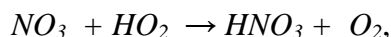
These results compared to the passive tracer runs show a decreased NO concentration and increased NO<sub>2</sub> concentration during the day. Early in the day there is some available NO<sub>2</sub> in the system which, during sunlight hours, photolyzes to form O<sub>3</sub>. (The full set of chemical equations is tabulated in Appendix C and the STAR photolysis reactions are in Appendix F).



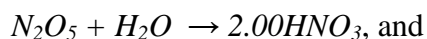
This newly formed O<sub>3</sub>, which was not present in the passive tracer case, and NO react to form NO<sub>2</sub>:



In the gas phase chemistry case the photochemical cycle of NO<sub>x</sub> and O<sub>3</sub> regenerates the NO<sub>x</sub> compounds, whereas in the passive tracer case they are merely removed through deposition (Chapter 6). It will also be shown that these nitrogen compounds will aid in the aggressive nighttime generation of HNO<sub>3</sub> and HNO<sub>3</sub> deposition through reactions such as nitrogen trioxide and the hydroperoxy radical,



dinitrogen pentoxide and water molecules,



the hydroxy radical and nitrogen dioxide,



During the day there is some destruction of HNO<sub>3</sub> through photolysis,



but not at a rate which compensates for the formation.

## 5.2 Influence of Aerosol Phase Chemistry

The box model was allowed to evolve for a period similar to the air mass travel between the monitoring stations, and then the resulting size distributions were compared with the measured data at MPN (Klein et al., 1999a,b, 2001). An empirical deposition/sea salt generation function was included to simulate what may be happening over water (Klein et al., 1999a). The SEMA results show the bi-modal distribution expected (Figures 5-5, 5-6) but with increased intensity compared to measured data (Figure 3-5). All in all, the total concentrations agree reasonably well with the measured data (Table 5-1).

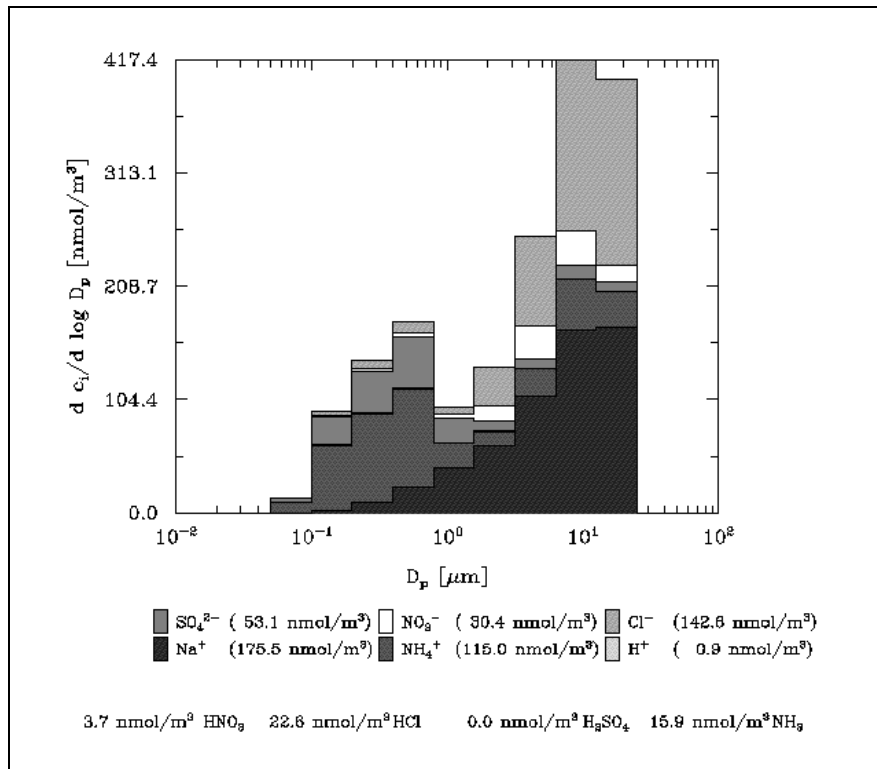


**Figure 5-5.** SEMA results using a relative humidity of 95%, temperature of 15°C, and completing the ion budget with  $\text{H}^+$ .

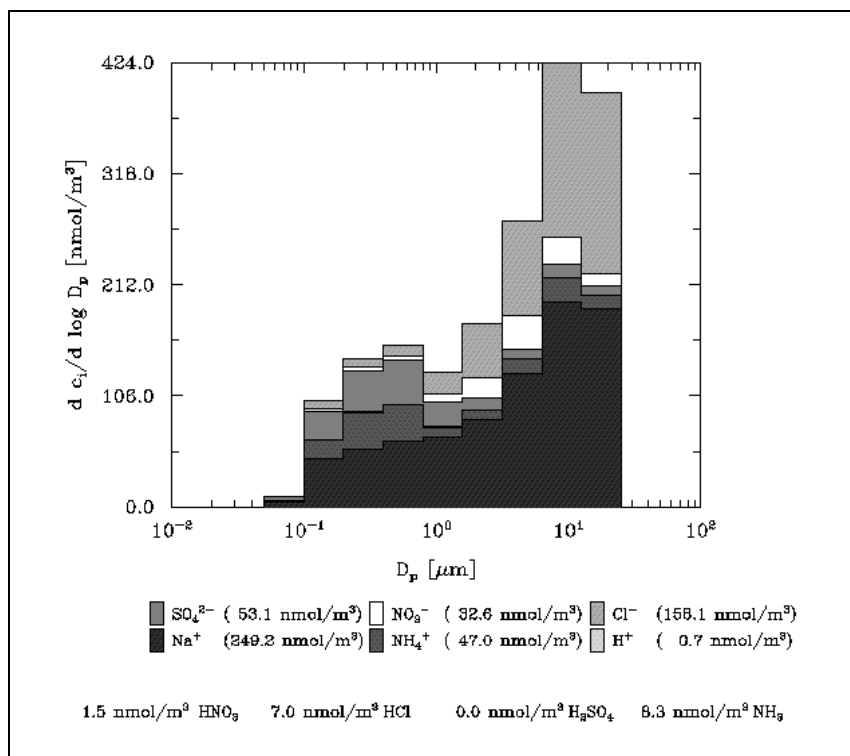


**Figure 5-6.** SEMA results using a relative humidity of 95%, temperature of 15°C, and completing the ion budget with  $\text{Na}^+$ .

5. The Influence of Chemical Transformations

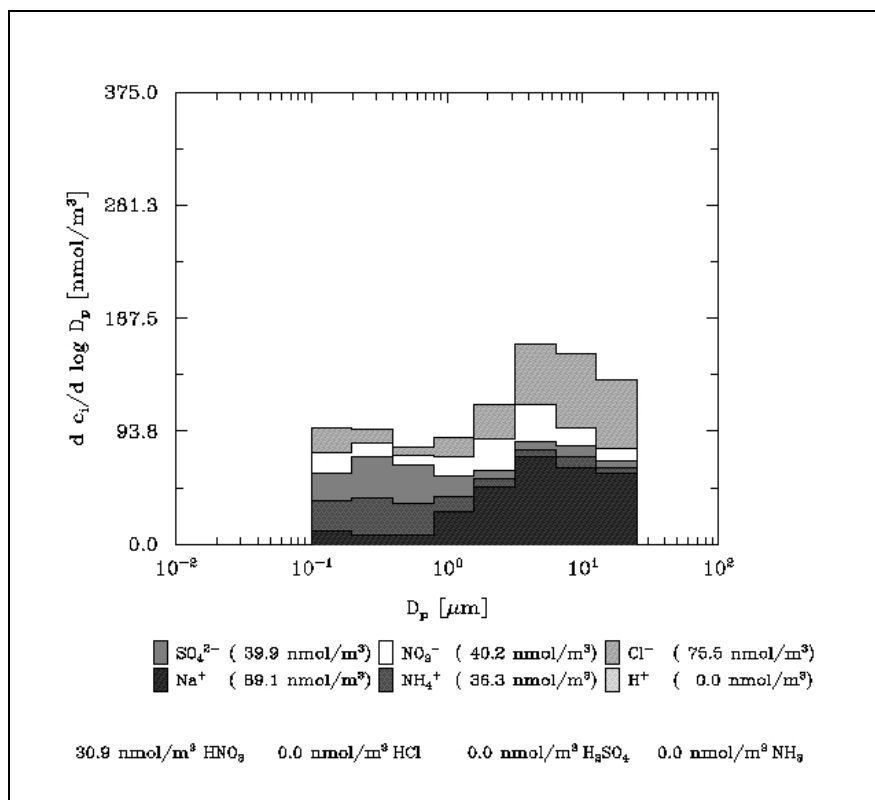


Figure 5-7. MPN-9 measurements taken from 13:12h - 20:44h June 16, 1998.

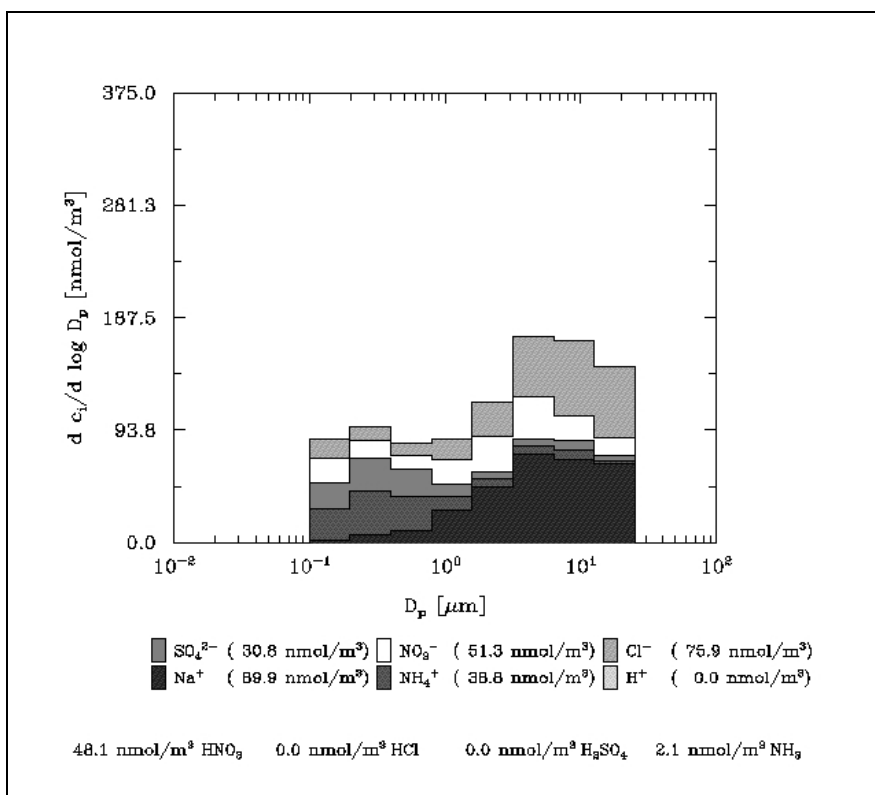


Figure 5-8. MPN-10 measurements taken from 21:38h June 16, 1998 to 12:06h June 17, 1998.

Figures 5-7 and 5-8 show the measured concentrations at MPN for the time periods that would represent the air mass measured in Figure 3-4 if the airflow were connected between the two observation sites. Two sets of MPN data were used to fully capture the air mass, which was estimated to travel the distance in about 12 hours.

Assuming the same air parcel was sampled at both stations the following observations can be made regarding the measured data:

- Chloride concentrations are lower at MPN, the biggest decrease was with the large aerosols so chloride was depleted as it passed over the sea, most likely by a reaction of nitric or sulfuric acid with the sea-salt aerosol, NaCl, to form gaseous HCl, (Pakkanen, 1996) and deposition.
- Sodium was also greatly depleted, sulfate concentrations decreased, and nitrate concentrations increased.
- Ammonium concentrations increased at the largest size and decreased at the smaller sizes.

**Table 5-1.** Total Concentrations, Box-Model Results vs. Observations

	SEMA results (nmol/m <sup>3</sup> ) <sup>1</sup>		Measured Concentrations (nmol/m <sup>3</sup> )	
	H <sup>+</sup>	Na <sup>+</sup>	MPN-9	MPN-10
<b>NO<sub>3</sub><sup>-</sup></b>	30.4	32.6	40.2	51.3
<b>Cl<sup>-</sup></b>	142.6	158.1	75.5	75.9
<b>SO<sub>4</sub><sup>2-</sup></b>	53.1	53.1	39.9	30.6
<b>NH<sub>4</sub><sup>+</sup></b>	115.0	47.0	36.3	38.8
<b>Na<sup>+</sup></b>	175.5	249.2	89.1	89.9
<b>HNO<sub>3</sub></b>	3.7	1.5	30.9	48.1
<b>H<sub>2</sub>SO<sub>4</sub></b>	0.0	0.0	-	-
<b>HCl</b>	22.6	7.0	-	-
<b>NH<sub>3</sub></b>	15.9	8.3	- 0.6	2.1

<sup>1)</sup> Ion balance completed with the listed ions.

Table 5-1 summarizes the total concentrations of the various ions for the SEMA box model runs with the ion budgets completed by H<sup>+</sup> and Na<sup>+</sup> compared to the measurements. The difference in total aerosol nitrate in both cases can be explained by the figures. The measured concentration show higher concentration of fine nitrate ( $D_p < 1 \mu\text{m}$ ) than the modeled results, but similar concentrations of coarse ( $D_p < 1 \mu\text{m}$ )

## 5. *The Influence of Chemical Transformations*

aerosol nitrate. There are differences in the chloride aerosol concentrations because of the different ions chosen to close the ion budget. The available  $\text{H}^+$  reacted easily with the  $\text{Cl}^-$  to form HCl in the  $\text{H}^+$  case and the  $\text{HNO}_3$  concentration remained relatively high. In the  $\text{Na}^+$  case it was the  $\text{HNO}_3$  that reacted with the  $\text{Cl}^-$  to form HCl. This reaction also led to a higher  $\text{NO}_3^-$  aerosol concentration, which is not seen in the  $\text{H}^+$  case. In both SEMA runs the  $\text{Cl}^-$  loss was almost complete for the smaller sea-salt particles, most likely due to the surface reaction mechanism for the reactions. Also in both cases the  $\text{NO}_3^-$  concentrations were much lower than those measured and the remaining ions were much greater. This shows the importance of deposition in the aerosol cycle, which was not sufficiently modeled in these box-model runs. There was a substantial difference between the  $\text{HNO}_3$  modeled by the box-model and measured, a factor of 10, and this is due mainly to emissions and photolytical reactions not being included. Box-models are good for general conclusions but do not fully simulate what is occurring in nature.

One notable difference in the two ion-balance completion schemes is the behavior of  $\text{NH}_4^+$ . The addition of  $\text{H}^+$  results in an overestimation while more consistent values were computed with the  $\text{Na}^+$  completion. The excess  $\text{H}^+$  acts as a catalyst for ammonium formation in the box-model, and this is an issue which must be investigated further before integrating the aerosol code into the chemical model.

A sensitivity analysis was made comprising several runs with varying temperature, relative humidity, and gas phase concentrations (results in Appendix G). This analysis provided useful information on aerosol behavior over the southern North Sea. It was shown that lower temperatures and higher relative humidities corresponded with an increase in concentrations (Klein et al, 1999a,b). The sensitivity study also showed the impact that input data has on results, and the uncertainty involved. Using the relationship between humidity and temperature changes and aerosol formation, and the ratio between the gaseous phase species and aerosol formation, we can get an overall idea of how the aerosols would behave during the study period.

The box study has shown that aerosol transformation results in a loss of  $\text{HNO}_3$ , in this case roughly 20% - 60% depending on which ion was used to complete the necessary balance. What is important here is not the exact number as much as the development of a hypothesis that  $\text{HNO}_3$  will be overestimated by a chemical transport model that does not include aerosol formation. This is an uncertainty that will be carried through to the deposition studies and are extremely important for coastal regions where aerosol formation is prominent.

## 6. Influence of Physical and Chemical Processes on Deposition

The purpose of this research is to determine what is contributing to coastal pollution, specifically nitrogen deposition in coastal regions. This section will show the N deposition patterns and volumes simulated, and the associated causal factors.

There are four main factors governing dry deposition in the atmosphere:

- Concentration in the atmosphere,
- Atmospheric turbulence,
- Chemical properties of the depositing species, and
- Nature of the surface/receptor.

The turbulence near the ground affects the deposition rate to the surface, the solubility and chemical reactivity at the surface may influence the uptake, and surfaces may be non-reactive for gas absorption/adsorption. They may be smooth enough for particles to bounce off, or as in the case of vegetation, may be highly susceptible to deposition. At the coastline these rough and vegetated surfaces are neighboring comparatively smooth water surfaces of the ocean. The water surfaces are a good sink for nitrate and sulfate particles as well as sulfur and some nitrogenous gases (ie.  $\text{HNO}_3$ ), since these are well water-soluble. Due to the differences in the uptake of gases a strong gradient can develop in the deposition at the coastline even for a similar concentration in air. In the model applied, consideration is given to atmospheric transport processes as well as to removal mechanisms and the physical and physiochemical properties of gases (Chapter 3).

### 6.1 Passive Tracer Deposition Studies

The METRAS/MECTM runs that included emissions and meteorology but no chemical reactions (Chapter 4) were analyzed with respect to deposition. The daily deposition for  $\text{NO}$ ,  $\text{NO}_2$ ,  $\text{HNO}_3$ , and  $\text{NH}_3$  are shown in Figure 6-1. The results have all been scaled to a maximum of  $1\text{mg/m}^2/\text{day}$  of N.

Deposition differs over water and over land due to the different surface resistances that are present. The ANICE model area comprised mainly sea surface and agricultural land use, and the effect of the different surfaces on deposition can be seen. The less soluble species have greater deposition over land (i.e.  $\text{NO}_2$ ), while the more soluble species such as  $\text{HNO}_3$  and  $\text{SO}_2$  deposited over the water as well as land with the greater amount entering the North Sea close to the coast (Figures 6-1, 6-2, and 6-3). The greatest deposition occurred downwind from the London urban area as a result of the high concentration of emissions in that region for June 16, 1998.

## 6. Influence of Physical and Chemical Processes on Deposition

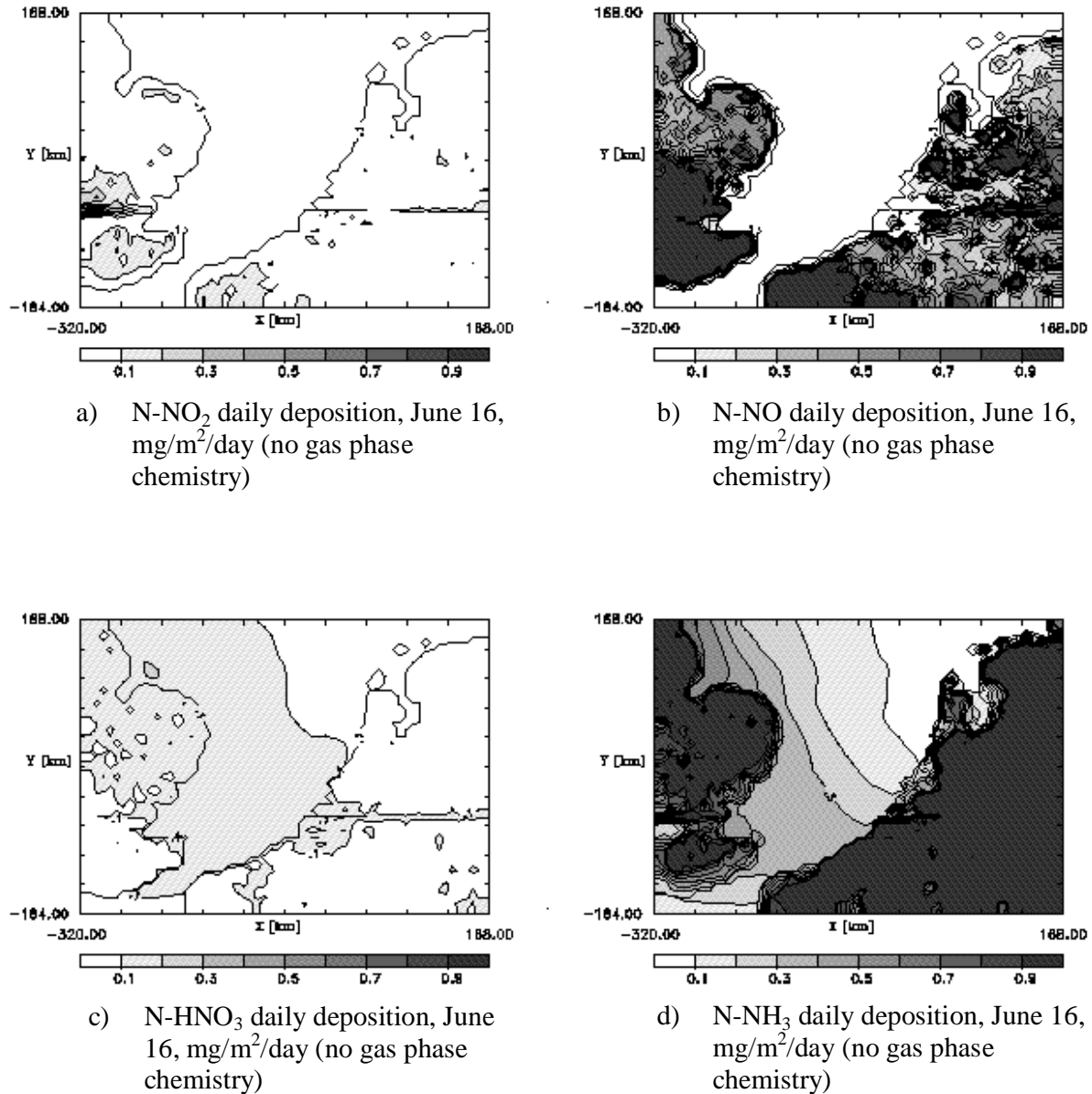


**Figure 6-1.** Daily deposition values for various nitrogen compounds with no gas phase chemistry (only passive tracers), June 16 1998 (mg/m<sup>2</sup>/day).

As would be expected since the NO<sub>2</sub> concentrations are low, the NO<sub>2</sub> deposition values are low for the passive tracer case. The HNO<sub>3</sub> deposition is also very low because there is no input of HNO<sub>3</sub> to the atmosphere from chemical reactions and the deposition is a result of background concentrations.

## 6.2 Gas Phase Chemistry Deposition Studies

During the MECTM runs that included gas phase chemistry, deposition values for hourly and daily amounts were calculated. Figure 6-2 shows the daily deposition values for various nitrogen compounds, again for June 16, 1998. The highest concentration modeled was clearly NO, but the greatest amount deposited to the waterway is HNO<sub>3</sub> due to its solubility in water. The high values of NH<sub>3</sub> deposited over land are largely a result of the emissions from the agricultural regions in the modeled area. The simulated values of 3-8 mg NH<sub>3</sub>/m<sup>2</sup>/day over land fall within previously published studies (Singh et al., 2001).

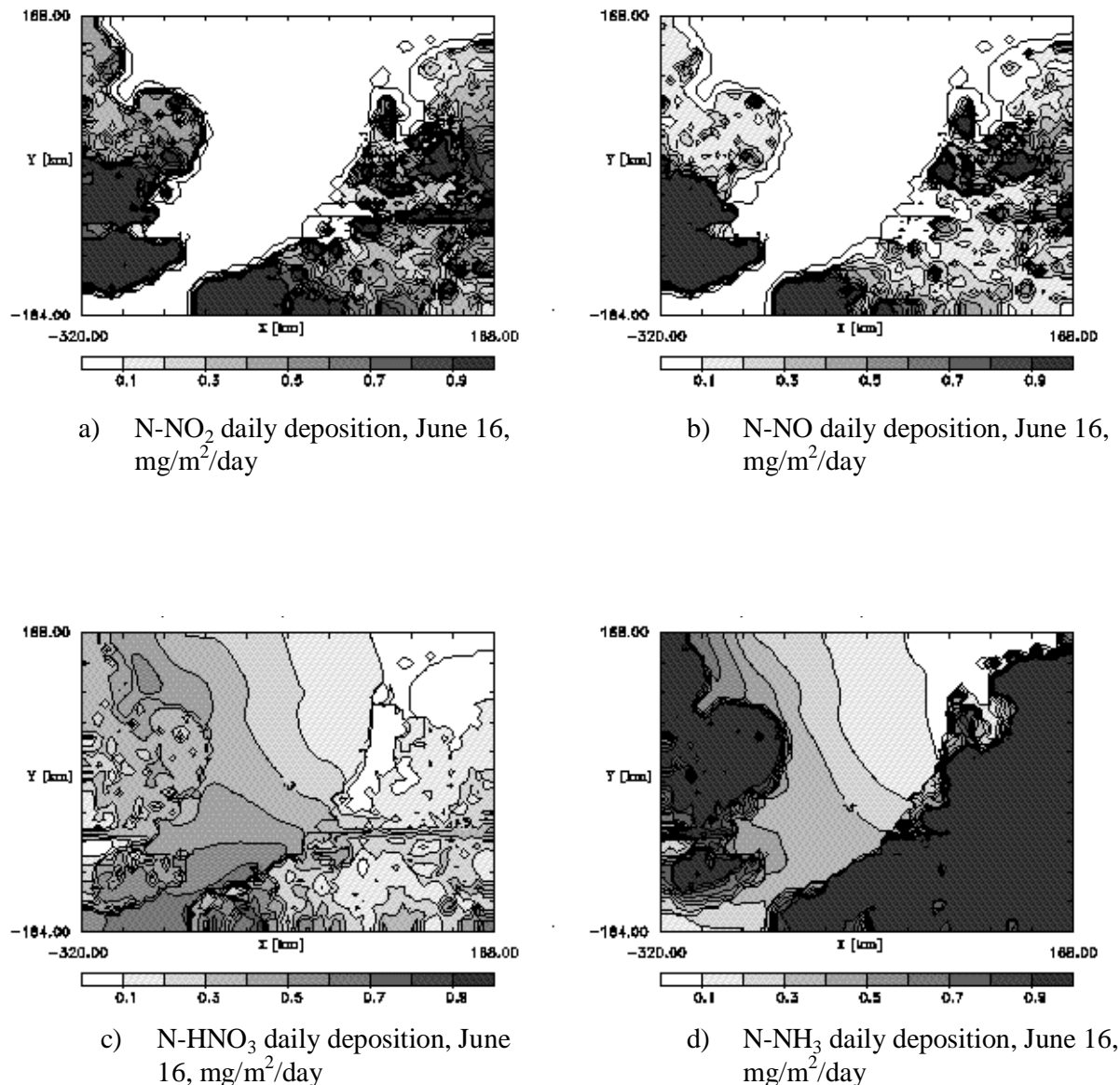


**Figure 6-2.** Daily deposition values for various nitrogen compounds, June 16, 1998 (mg/m<sup>2</sup>/day, scaled to a maximum of 1 mg/m<sup>2</sup>/day N).

## 6. Influence of Physical and Chemical Processes on Deposition

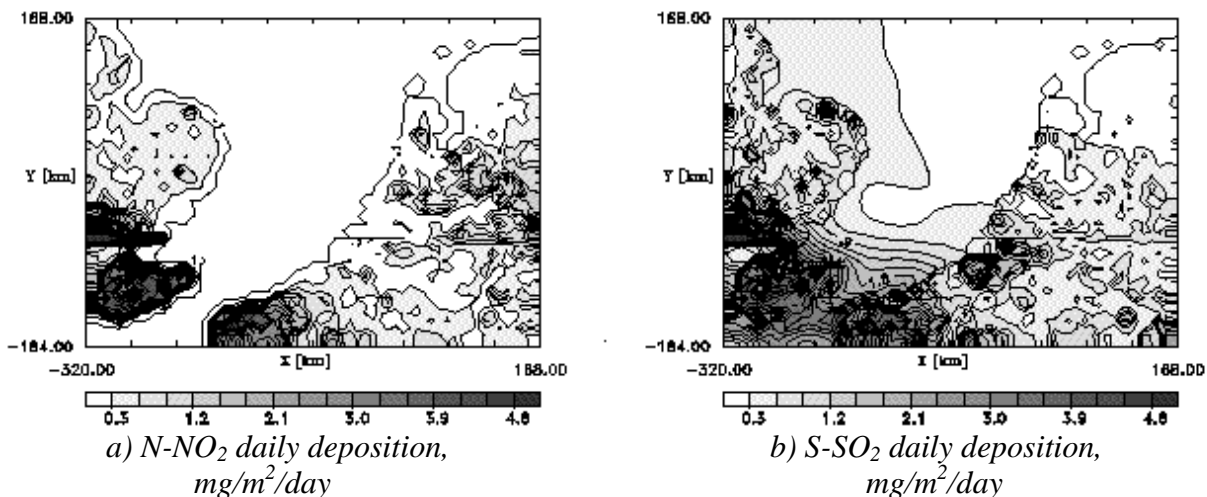


**Figure 6-3:** Hourly deposition values for  $N\text{-NO}_2$  and  $S\text{-SO}_2$ , 14:00, June 16, 1998 ( $\mu\text{g/m}^2/\text{hour}$ , scaled to a maximum of  $5 \mu\text{g/m}^2/\text{hour}$ ).

The winds turned more westerly on the 17<sup>th</sup>, advecting the London plume over the southwestern North Sea (Figure 6-4). Daily deposition values are in the same range as the previous day but the high deposition reaches further north due to the shifting winds. The  $\text{HNO}_3$  deposition values predicted are higher toward the middle of the modeled region. This trend, which continues throughout the modeled period, is due to the slow transformation of  $\text{NO}_x$  to  $\text{HNO}_3$  and has also been observed in a 1999 North Sea observational study which included long-term ferry measurements (DeLeeuw et al. 2002; Tamm & Schulz 2002).

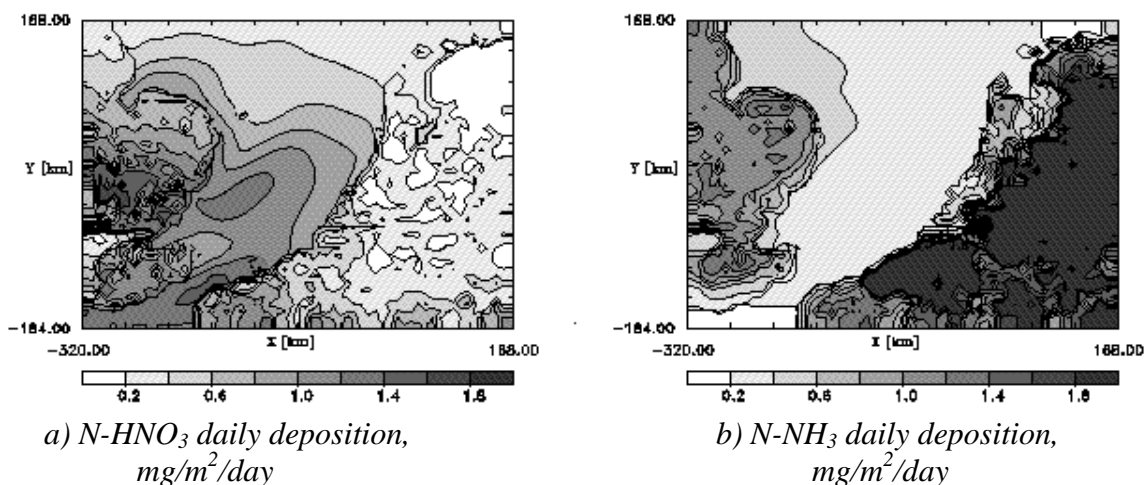


**Figure 6-4.** Daily deposition values for  $N\text{-HNO}_3$  and  $N\text{-NH}_3$ , June 17, 1998 ( $\text{mg/m}^2/\text{day}$ , scaled to a max of  $2 \text{mg/m}^2/\text{day N}$ ).

By the 18<sup>th</sup> the winds had begun to shift to a more southwesterly pattern and were strong during the day, tapering off slightly in the night. The deposition patterns reflect the strong

flow along the coast of the Netherlands, advecting the pollutants northward over the water. There was also increased deposition into the North Sea off the northeast coast of England (Figure 6-5). The very high deposition values are mainly a result of doubled deposition velocities, caused by intensified winds.

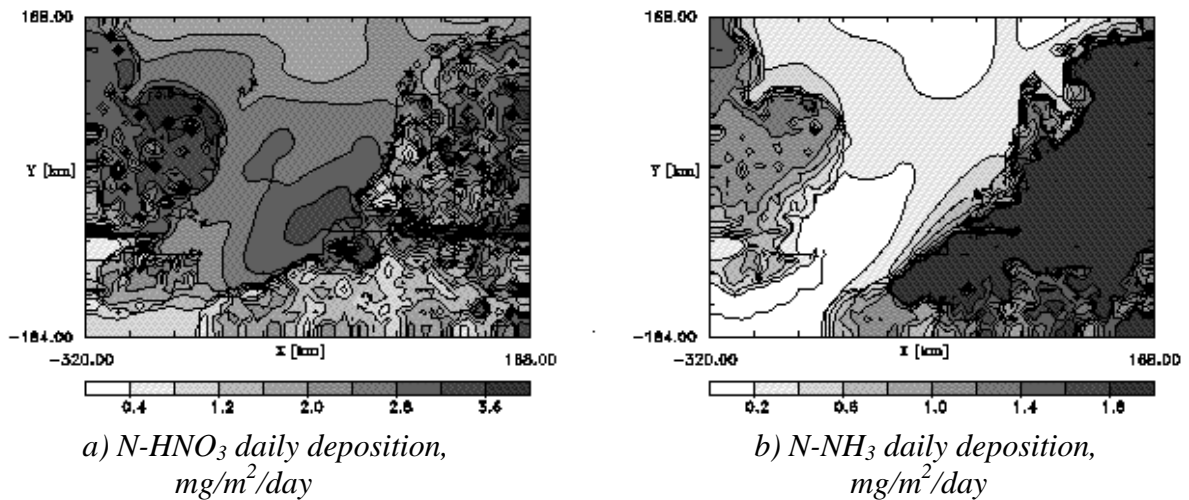


**Figure 6-5.** Daily deposition values for  $N\text{-HNO}_3$  and  $N\text{-NH}_3$ , June 18, 1998 ( $\text{mg/m}^2/\text{day}$ ). ( $N\text{-HNO}_3$  scaled to a max of  $4 \text{ mg/m}^2/\text{day}$  N,  $N\text{-NH}_3$  scaled to a max of  $2 \text{ mg/m}^2/\text{day}$ ).

The airflow patterns on the 19<sup>th</sup> were more complicated. During the day the air moved northeastward along the coast of the Netherlands and northwestward following the English coast. Over the North Sea the winds were northward. During the night there was an off-shore wind from the continent and these winds are also reflected in the deposition pattern where there was a sharp gradient in the  $\text{NH}_3$  deposition in the coastal waters (Figure 6-6). The abrupt changes at the coast cause sharp gradients in the deposition fluxes at the coastline. The deposition of  $\text{NH}_3$  decreases rapidly with distance from the coast, which is consistent with other recent coastal studies (DeLeeuw et al. 2001)

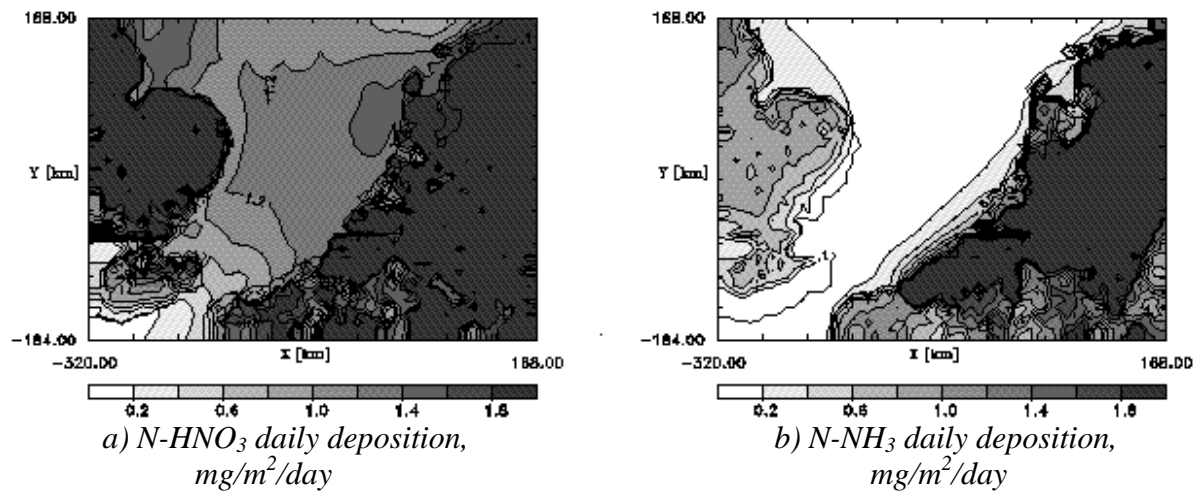


**Figure 6-6.** Daily deposition values for  $N\text{-HNO}_3$  and  $N\text{-NH}_3$ , June 19, 1998 ( $\text{mg/m}^2/\text{day}$ , scaled to a max of  $2 \text{ mg/m}^2/\text{day}$  N).

## 6. Influence of Physical and Chemical Processes on Deposition

On the 20<sup>th</sup> we start to see connected flow between MPN and WAO stations (Figure 3-3) The winds are steady with a strong offshore wind and a correspondingly high daily deposition was modeled for HNO<sub>3</sub>, almost four times the previously modeled levels (Figure 6-7, note: scaled to a max of 4 mg/m<sup>2</sup>/day). This elevated level of NH<sub>3</sub> was also observed at the WAO and MPN stations during the ANICE field campaign (Jickells and Spokes, 1999) and was associated with the heavily polluted continental air.

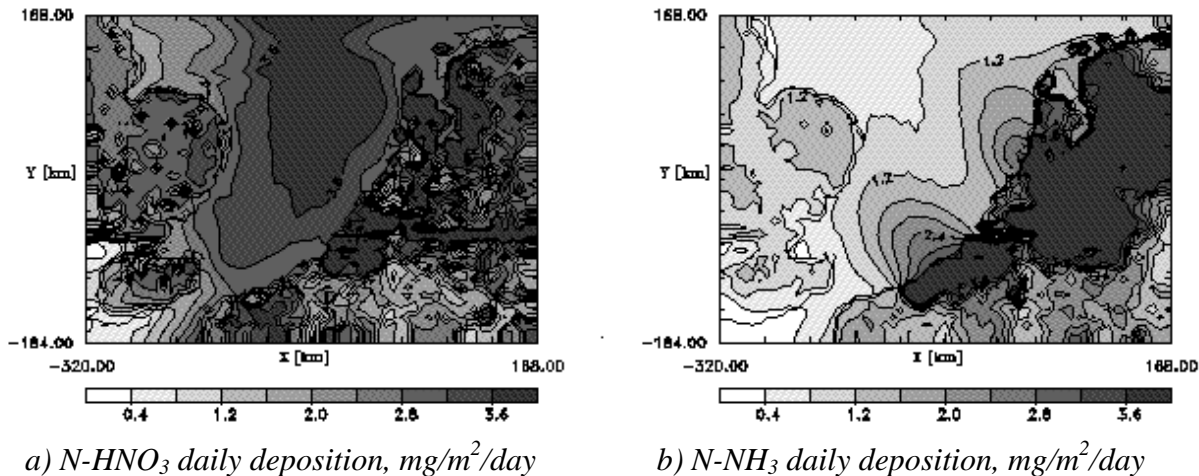


**Figure 6-7.** Daily deposition values for N-HNO<sub>3</sub> and N-NH<sub>3</sub>, June 20, 1998 (mg/m<sup>2</sup>/day, scaled to a max of 4 mg/m<sup>2</sup>/day).

The maximum N deposition values into the water on the 20<sup>th</sup> ranged between 3.1 to 3.8 mg/m<sup>2</sup>/day for N-HNO<sub>3</sub> and 1.2 to 1.8 mg/m<sup>2</sup>/day for N-NH<sub>3</sub>. These high values are the result of the air now coming from the continent carrying high emissions of NO, NO<sub>2</sub>, and NH<sub>3</sub>. The HNO<sub>3</sub> pattern is clearly defined with the peak deposition in the center of the southern North Sea. In Figure 6-7b the deposition is occurring closer to the coast partly because NH<sub>3</sub> is a primary pollutant and does not go through any chemical transformation other than loss due to aerosols. This process, however, is not included in the present simulation.

The total daily N deposition to the southern North Sea (over water) for the modeled domain was calculated for the various nitrogen compounds (Figure 6-8). The greatest source for N loading into the water was HNO<sub>3</sub>, likely due to its high solubility but also partially due to over-estimation by the model. On all days the NO<sub>2</sub> was slightly greater than NO, but still only a fraction of the total N deposited. N loads increased as the winds were more south-westerly (18<sup>th</sup>) coming off of the continent. The wind patterns of the 18<sup>th</sup> saw high values of N input off of both the coast of England and the coast of the Netherlands. The more complicated flow patterns of the 19<sup>th</sup> resulted in lower N loading into the water than the 18<sup>th</sup>, but then by the 20<sup>th</sup> the influence of the strong offshore winds coming from the continent is clearly seen in the figure.

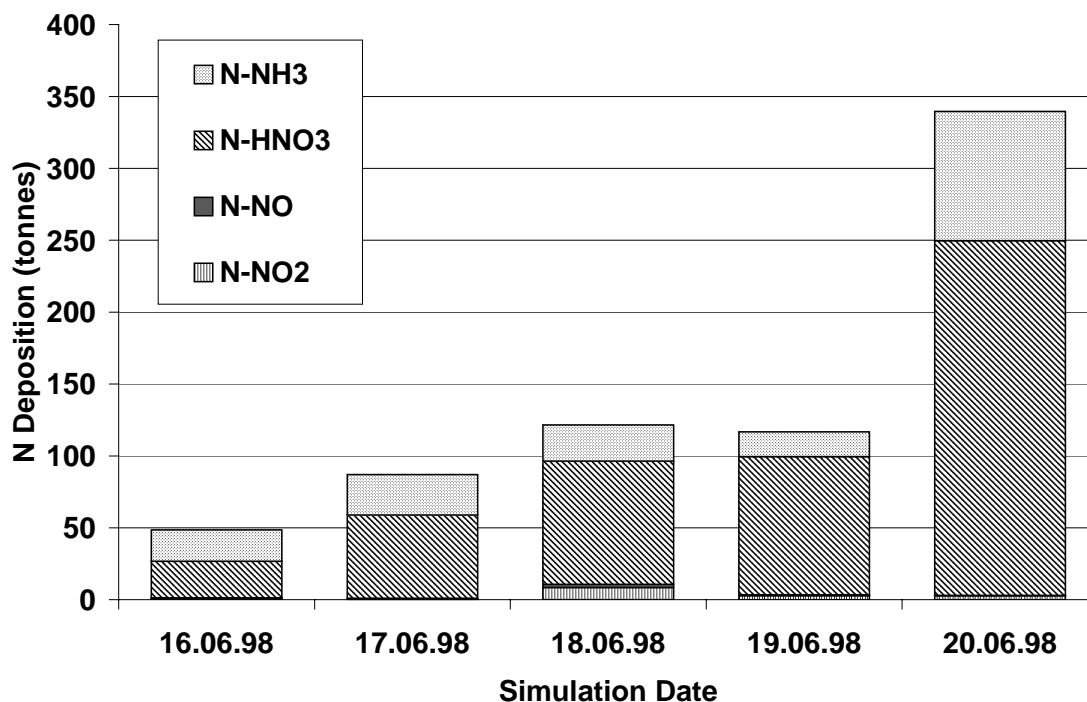


**Figure 6-8.** Total N Deposition to the southern North Sea as modeled by METRAS/MECTM (region covers 83,520 km<sup>2</sup>)

### 6.3 Passive Tracer versus Chemistry Deposition

The total N loading for the passive tracer case was calculated and plotted against the run with chemistry (Figure 6-9). One of the more important observations to be made from this comparison is that when the winds were bringing air from the UK (June 16 and 17), higher deposition of N-NO was found in the passive tracer run. In the chemistry run the NO reacts quickly to create new forms of N. Nitrogen dioxide deposition is greater in the chemistry run regardless of wind direction, but notably so on the 18<sup>th</sup>. On this day the emissions from the UK and the continent are both advected over the water, and the strong winds carry the air parcels further over the North Sea. The advected pollutants spent more time over the sea than on the other four days studied and this provided time for more chemical transformations, and greater values of N-NO<sub>2</sub> deposition. This was not the day with the greatest emissions, so it shows how transport time plays a very important role in total N deposited to the coastal waters. In general, the more oxidized the nitrogen the more water soluble it is, and the higher the dry deposition velocities, especially to the sea. The inclusion of chemistry more than doubles the amount of N-NO and N-NO<sub>2</sub> input to the studied region. In addition, when N-HNO<sub>3</sub> input is considered too (Figure 6-8) the calculated input is increased by about a factor of ten in the chemistry case compared to the passive tracer case.

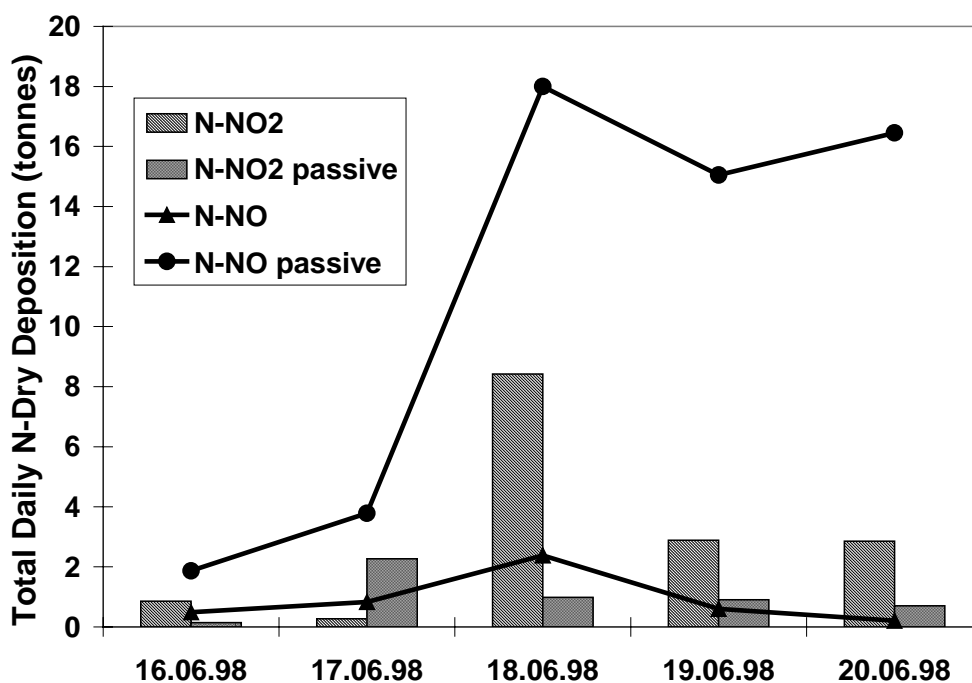


**Figure 6-9:** Total N Deposition to the southern North Sea as Modeled by MET-RAS/MECTM for the Chemistry and No Chemistry cases, June 16<sup>th</sup>, 1998.

In the ‘no gas-phase chemistry’ scenario the bulk of the total N deposition was in the southern North Sea and off the eastern coast of Great Britain while the chemistry case showed the highest deposition to occur over the English Channel. This is most likely a result of the  $\text{NO}_x$  emissions in Great Britain being chemically transformed and then transported south-east by the prevailing wind patterns (Schlünzen et al., 2000; Klein and Schlünzen, 2001).

Two important coastal deposition characteristics were simulated by the MET-RAS/MECTM. The first of these is the effects of composition on deposition patterns. The more highly soluble species ( $\text{HNO}_3$ ) readily deposited to the water surface while the least soluble species ( $\text{NO}$ ,  $\text{NO}_2$ ) mainly deposited on land. The second important feature is the impact of land-based emissions on deposition. When the winds were coming off the coast higher amounts of nitrogen were input to the sea. The winds coming out of the north brought cleaner air and thus lower deposition over the water. The influence of the chemical processes was easily seen by the  $\text{HNO}_3$  deposition results. The creation of  $\text{HNO}_3$  through the photolysis reactions meant that it was available to be removed through deposition. This was most significant on the 20<sup>th</sup> when the winds were coming off the coast carrying the continental  $\text{NO}_x$  emissions, which were transformed into  $\text{HNO}_3$  and then subsequently deposited to the waters.

This study showed a high variability from day to day. The variability is dependent on the meteorological factors as wind speed and wind direction and boundary layer height and the

chemical factors as emissions, chemical transformations and solubility. The 18<sup>th</sup> shows how a combination of physical and chemical parameters has the greatest impact on NO<sub>x</sub> deposition values. When using coastal measurements to calculate atmospheric input it should be remembered to take into consideration the air parcel trajectories **and** the chemical transformations.

The daily variability during this time period modeled shows that the meteorological conditions in the coastal zone, which are highly changeable, are driving factors as to where and how great the impact of land-based pollutants will be. Winds flowing inland will carry most emissions away from the water, minimizing impact to the regional sea, but winds flowing off-shore will carry the polluted air parcels great distances and allow for the formation and deposition of secondary pollutants.

## 7. Discussion and Conclusions

This study has examined the influences of chemical and physical processes on nitrogen deposition to the southern North Sea. The METRAS/MECTM model results show the distribution of concentrations and deposition patterns. They demonstrate the relevance of both the meteorological conditions (wind direction, wind speed, planetary boundary layer height) and atmospheric chemistry for nitrogen inputs to the coastal zone. The strong gradient of  $\text{NH}_3$  deposition from the source along the coastline that has been observed (Plate et al., 1995; de Leeuw et al., 2001) was simulated by the model. Based on the analysis, the daily N input flux can range from 2.1 to 14.7  $\text{mg/m}^2/\text{day}$ , with the maximum occurring on the day when the prevailing winds are off continental Europe due to the increased ammonia input from the Netherlands.

It was also shown that there is a strong relationship between deposition concentrations and the physical coastal processes. The inversion height analysis showed that the trend during this study period was for higher boundary heights over continentally influenced regions. The low boundary layer heights over highly environmentally sensitive coastal areas increase their susceptibility to pollutant input. The comparison between the meteorology runs and the rawinsonde data showed that the model performs well overall in the simulation of the PBL but with some slight weaknesses. For several cases the comparison shows that the model overestimates daytime inversion heights and instability and underestimates morning and evening stability. This could partially be due to the fact that no clouds were included in the model runs and also because the model values are the average over the grid box (8 km x 8 km) as opposed to a single location. The surface meteorological data were simulated very well, as comparisons with meteorological routine data have shown. The overestimation of the boundary layer height during the day potentially leads to a decreased pollutant concentration due to the resultant difference in vertical mixing. Conversely, the lower inversion heights modeled by METRAS could lead to a higher pollutant concentration in the region.

Simulations were performed using background concentrations and emissions both including and neglecting chemical reactions in order to see the effect of gas-phase chemistry on deposition values. The comparisons of the passive tracer runs to the chemistry runs show that chemical transformations in the atmosphere also play a large role in deposition. The amounts that are deposited and the make-up of the N-based compound is heavily dependent upon the transformations that take place after the emission from the source. When comparing the nitrogen compounds the greatest difference was that N- $\text{NO}_2$  was lower than N- $\text{NO}$  by about an order of magnitude. The N-deposition values are about a factor of 10 higher when including gas phase chemi-

cal transformations showing that it is the secondary pollutants that are the danger to the coastal zone

Due to changes in the large-scale meteorological situation when there may be intensified vertical mixing due to increased wind speeds, the input of N to the water can increase by a factor of two (as shown in Chapter 6 for 18 June). When the wind is coming from off the continent the N input is roughly a factor of four greater than that found when the input is from the London plume. The higher ammonia emissions in the Netherlands clearly result in increased N deposition into the southern North Sea. The highest concentration modeled was N-NO, but the greatest amount deposited to the waterway is N-HNO<sub>3</sub> due to its solubility in water and the chemical reactions that take place.

The days of highest total N loading from deposition, 18 and 20 June, show that there is no 'single' factor that contributes the most to nitrogen deposition to the water (Figure 6-9). The 18 June case is mainly a result of the winds along the coasts of the UK and continental Europe picking up some emissions, and then high winds carrying the air parcel towards the center of the North Sea. The pollutants undergo chemical transformations while they are airborne. The 20 June case is a result of high emissions being transported directly from the agricultural and industrial regions of the Netherlands almost perpendicular to the coastline and into the regional waters. The study shows that the physical and chemical processes work in tandem, but on the 18<sup>th</sup> the chemical processes were the main impactor, while on the 20<sup>th</sup> the physical processes were dominant.

The box-model study implied that a gaseous phase chemistry model is insufficient for modeling the coastal zone. The input of nitrogen concentrations modeled here does not reflect the loss of gaseous species to aerosol formation, or the increase in deposition from aerosol species. The box-model showed changes in gas phase before and after formation so there are processes taking place that are not considered in a gas-phase only chemical transport model. This increases the uncertainty of the gas-phase model deposition results.

The meteorology simulation is excellent, and that is the first step to realistic atmospheric chemistry modeling. The chemistry simulations are good, but further testing of the photolysis reactions would be beneficial. A topic worthy of further investigation is the influence of aerosols, which needs to be studied for assessing the impact of aerosol formation on chemical concentrations and deposition to the coastal waters.

It has been shown here through the passive tracer runs analyzed against the full gaseous chemistry runs that a combination of physical and chemical processes is key, and one is not more important than the other. The results obtained for the southern North Sea are transferable to other coastal regions that have large land-based emissions.

## *7. Discussion and Conclusions*

The behavior of the emissions and the resultant secondary pollutants will be similar over coastal waters, and will be highly dependent upon the combination of the local meteorology and chemical transformations in the atmosphere.

## Appendix A: Deposition Factors

**Table A-1:** Conversion factor  $\hat{r}_s^{species}$  and surface parameters  $r_s$  for gaseous species

Species	Symbol	$\hat{r}_s^{species}$	$r_{s,min} = r_{s,max} = r_{s,wet}$ (s/m) (over water)
Sulfur dioxide	SO <sub>2</sub>	1.0	0.
Nitric oxide	NO	1.0	7000.
Nitrogen dioxide	NO <sub>2</sub>	1.0	7000.
Nitrous acid	HNO <sub>2</sub>	1.0	0.
Nitric acid vapor	HNO <sub>3</sub>	0.0	0.
Ammonia	NH <sub>3</sub>	0.2	0.
Ozone	O <sub>3</sub>	1.0 <sup>1</sup>	2000.
Hydrogen peroxide	H <sub>2</sub> O <sub>2</sub>	0.1	0.
Formaldehyde	HCHO	0.5	10.
Acetaldehyde	ALD	2.0	6400.
Formic acid	ORA	1.0	0.
Peroxy radicals	RO <sub>2</sub>	No value	400.
Hydrochloric acid	HCl	1.0	0.
Peroxyacetyl nitrate	PAN <sup>2</sup>	1.0	9999.
Peroxyacetic acid	PAA <sup>2</sup>	No value	180.

Values based on Wesely and Hicks (1977, 1989, 2000) and Pahl (1990)

<sup>1)</sup> based on personal communications with Schlünzen (2001)

<sup>2)</sup> values of  $r_{s,min}$ ,  $r_{s,max}$ , and  $r_{s,wet}$  for PAN and PAA can be found in Tables A-5 and A-6.

The parameters  $r_{s,min}$ ,  $r_{s,max}$ , and  $r_{s,wet}$  for the species in Table A1 can be calculated by multiplying the factors listed in the table corresponding values of SO<sub>2</sub> (Table A2) using the following equations:

$$r_{s,min}^{species} = \hat{r}_s^{species} \cdot r_{s,min}^{SO_2}$$

$$r_{s,max}^{species} = \hat{r}_s^{species} \cdot r_{s,max}^{SO_2}$$

$$r_{s,wet}^{species} = \hat{r}_s^{species} \cdot r_{s,wet}^{SO_2}$$

**Table A-2.** Parameters  $r_{s,min}$ ,  $r_{s,max}$ , and  $r_{s,wet}$  for  $SO_2$ 

Land-use type	Season	Resistance parameters		
		$r_{s,min}$ [ $s\ m^{-1}$ ]	$r_{s,max}$ [ $s\ m^{-1}$ ]	$r_{s,wet}$ [ $s\ m^{-1}$ ]
Water	Spring	0	0	0
	Summer	0	0	0
	Early autumn	0	0	0
	Late autumn	0	0	0
	Winter	0	0	0
Mudflat	Spring	100	100	100
	Summer	100	100	100
	Early autumn	100	100	100
	Late autumn	100	100	100
	Winter	100	100	100
Sand	Spring	1000	1000	1000
	Summer	1000	1000	1000
	Early autumn	1000	1000	1000
	Late autumn	1000	1000	1000
	Winter	1000	1000	1000
Mixed vegetation	Spring	50	100	0
	Summer	70	500	0
	Early autumn	500	500	100
	Late autumn	50	50	50
	Winter	100	100	100
Wet grass	Spring	100	400	0
	Summer	100	500	0
	Early autumn	500	500	100
	Late autumn	500	500	100
	Winter	100	100	100
Heath	Spring	75	250	0
	Summer	100	500	0
	Early autumn	500	500	100
	Late autumn	200	200	100
	Winter	100	100	100
Bushes	Spring	100	1000	0
	Summer	70	1000	0
	Early autumn	800	800	300
	Late autumn	800	1000	300
	Winter	800	800	800
Mixed forest	Spring	100	1000	0
	Summer	60	1000	0
	Early autumn	1000	1000	500
	Late autumn	1000	1000	500
	Winter	1000	1000	1000
Coniferous forest	Spring	150	1000	0
	Summer	150	1000	0
	Early autumn	800	800	100
	Late autumn	800	1000	100
	Winter	500	500	500
Urban areas	Spring	1000	1000	1000
	Summer	1000	1000	0
	Early autumn	1000	1000	1000
	Late autumn	1000	1000	1000
	Winter	200	200	200

**Table A-3.** Parameters  $r_{s,min}$ ,  $r_{s,max}$ , and  $r_{s,wet}$  for PAN

Land-use type	Season	Resistance parameters		
		$r_{s,min}$ [s m <sup>-1</sup> ]	$r_{s,max}$ [s m <sup>-1</sup> ]	$r_{s,wet}$ [s m <sup>-1</sup> ]
Water	Spring	0	0	0
	Summer	0	0	0
	Early autumn	0	0	0
	Late autumn	0	0	0
	Winter	0	0	0
Mudflat	Spring	100	100	50
	Summer	100	100	50
	Early autumn	100	100	50
	Late autumn	100	100	50
	Winter	100	100	50
Sand	Spring	1000	1000	1000
	Summer	1000	1000	1000
	Early autumn	1000	1000	1000
	Late autumn	1000	1000	1000
	Winter	1000	1000	1000
Mixed vegetation	Spring	110	180	60
	Summer	80	290	70
	Early autumn	320	330	70
	Late autumn	160	160	60
	Winter	120	120	120
Wet grass	Spring	220	370	80
	Summer	130	350	80
	Early autumn	400	410	80
	Late autumn	410	420	80
	Winter	120	120	120
Heath	Spring	170	280	70
	Summer	110	300	70
	Early autumn	380	390	80
	Late autumn	230	240	70
	Winter	120	120	120
Bushes	Spring	290	1000	90
	Summer	150	940	90
	Early autumn	580	1300	90
	Late autumn	920	1200	90
	Winter	460	1200	1200
Mixed forest	Spring	250	1100	90
	Summer	110	1000	90
	Early autumn	1300	1400	90
	Late autumn	1100	1100	90
	Winter	980	1000	1000
Coniferous forest	Spring	330	1000	90
	Summer	190	1000	90
	Early autumn	370	1300	90
	Late autumn	730	1300	90
	Winter	380	1300	1300
Urban areas	Spring	590	590	80
	Summer	490	490	80
	Early autumn	490	490	80
	Late autumn	490	490	80
	Winter	210	210	210

**Table A-4.** Parameters  $r_{s,min}$ ,  $r_{s,max}$  and  $r_{s,wet}$  for PAA

Land-use type	Season	Resistance parameters		
		$r_{s,min}$ [s m <sup>-1</sup> ]	$r_{s,max}$ [s m <sup>-1</sup> ]	$r_{s,wet}$ [s m <sup>-1</sup> ]
Water	Spring	0	0	0
	Summer	0	0	0
	Early autumn	0	0	0
	Late autumn	0	0	0
	Winter	0	0	0
Mudflat	Spring	4000	5400	4600
	Summer	4000	5400	4600
	Early autumn	4000	5400	4600
	Late autumn	4000	5400	4600
	Winter	4000	5400	4600
Sand	Spring	9700	9700	9700
	Summer	9700	9700	9700
	Early autumn	9700	9700	9700
	Late autumn	9700	9700	9700
	Winter	9700	9700	9700
Mixed vegetation	Spring	350	1300	1300
	Summer	160	1400	1400
	Early autumn	1100	1400	1300
	Late autumn	1300	1400	1400
	Winter	7700	9999	9999
Wet grass	Spring	570	1700	1600
	Summer	310	1700	1600
	Early autumn	1300	1700	1600
	Late autumn	1300	1700	1700
	Winter	7700	9999	9999
Heath	Spring	510	1600	1500
	Summer	260	1600	1500
	Early autumn	1300	1600	1500
	Late autumn	1400	1600	1500
	Winter	7100	9999	9999
Bushes	Spring	580	3100	2900
	Summer	280	3300	3100
	Early autumn	1100	3400	3100
	Late autumn	1900	3300	3000
	Winter	5000	9999	9999
Mixed forest	Spring	430	2400	2300
	Summer	200	2800	2700
	Early autumn	1800	2600	2400
	Late autumn	1700	2400	2200
	Winter	3900	9700	9700
Coniferous forest	Spring	730	2900	2800
	Summer	350	2800	2700
	Early autumn	730	3000	2800
	Late autumn	1600	3000	2800
	Winter	8500	9999	9999
Urban areas	Spring	3000	3000	3000
	Summer	3000	3000	3000
	Early autumn	3000	3000	3000
	Late autumn	3000	3000	3000
	Winter	6000	6000	6000

**Table A-5.** Conversion factor  $\hat{r}_s^{species}$  (same equations as those above, but using values of  $r_s^{Pb}$ , Table A-6) and surface parameters  $r_s$  for particulate species

Species	Symbol	$\hat{r}_s^{species}$	$r_{s,min} = r_{s,max} = r_{s,wet}$ (s/m) (over water)
Lead	Pb	1.	0.
Sulfate	S(VI)	1.	0.
Ammonium nitrate	NH <sub>4</sub> NO <sub>3</sub>	1.	0.
Ammonium sulfate	NH <sub>4</sub> SO <sub>4</sub>	1.	0.
Nitrate	NO <sub>3</sub>	1.	0.

**Table A-6.** Parameters  $r_{s,min}$ ,  $r_{s,max}$ , and  $r_{s,wet}$  for Pb

Land-use type	Season	Resistance parameters		
		$r_{s,min}$ [s m <sup>-1</sup> ]	$r_{s,max}$ [s m <sup>-1</sup> ]	$r_{s,wet}$ [s m <sup>-1</sup> ]
Water	Spring	0	0	0
	Summer	0	0	0
	Early autumn	0	0	0
	Late autumn	0	0	0
	Winter	0	0	0
Mudflat	Spring	300	400	0
	Summer	200	400	0
	Early autumn	200	400	0
	Late autumn	300	400	0
	Winter	1000	2500	0
Sand	Spring	600	1200	0
	Summer	200	400	0
	Early autumn	400	800	0
	Late autumn	600	1200	0
	Winter	2000	4000	0
Mixed vegetation	Spring	500	1000	0
	Summer	300	600	0
	Early autumn	500	1000	0
	Late autumn	500	1000	0
	Winter	1000	2500	0
Wet grass	Spring	400	600	0
	Summer	300	600	0
	Early autumn	300	600	0
	Late autumn	400	600	0
	Winter	1000	2500	0
Heath	Spring	320	650	0
	Summer	220	450	0
	Early autumn	320	650	0
	Late autumn	320	650	0
	Winter	570	1400	0
Bushes	Spring	400	800	0
	Summer	200	400	0
	Early autumn	350	700	0
	Late autumn	400	800	0
	Winter	1000	2250	0
Mixed forest	Spring	300	600	0
	Summer	100	200	0
	Early autumn	200	400	0
	Late autumn	300	600	0
	Winter	1000	2000	0
Coniferous forest	Spring	140	300	0
	Summer	140	300	0
	Early autumn	140	300	0
	Late autumn	140	300	0
	Winter	140	300	0
Urban areas	Spring	600	1200	0
	Summer	200	400	0
	Early autumn	400	800	0
	Late autumn	600	1200	0
	Winter	2000	4000	0

## Appendix B: MECTM Chemical Species

**Table B-1:** MECTM Species List

	Species	Definition
1	NO <sub>2</sub>	Nitrogen dioxide
2	NO	Nitric oxide
2	O <sub>3</sub>	Ozone
4	HONO	Nitrous acid
5	HNO <sub>3</sub>	Nitric acid
6	HNO <sub>4</sub>	Pernitric acid
7	NO <sub>3</sub>	Nitrogen trioxide
8	H <sub>2</sub> O <sub>2</sub>	Hydrogen peroxide
9	HCHO	Formaldehyde
10	CO	Carbon monoxide
11	ALD	Acetaldehyde
12	OP1	Methyl hydrogen peroxide
13	OP2	Higher organic peroxides
14	PAA	Peroxyacetic acid and higher analogs
15	KET	Ketones
16	GLY	Glyoxal
17	MGLY	Methylglyoxal and other $\alpha$ -carbonyl aldehydes
18	DCB	Unsaturated dicarbonyls
19	ONIT	Organic nitrate
20	N <sub>2</sub> O <sub>5</sub>	Dinitrogen pentoxide
21	SO <sub>2</sub>	Sulfur dioxide
22	SULF	Sulfuric acid
23	CH <sub>4</sub>	Methane
24	ETH	Ethane
25	HC3	Alkanes, alcohols, esters, and alkynes with HO rate constant (298 K, 1atm) less than $3.4 \times 10^{-12} \text{ cm}^3 \text{ s}^{-1}$
26	HC5	Alkanes, alcohols, esters, and alkynes with HO rate constant (298 K, 1atm) between $3.4 \times 10^{-12}$ and $6.8 \times 10^{-12} \text{ cm}^3 \text{ s}^{-1}$
27	HC8	Alkanes, alcohols, esters, and alkynes with HO rate constant (298 K, 1atm) greater than $6.8 \times 10^{-12} \text{ cm}^3 \text{ s}^{-1}$
28	OL2	Ethene
29	OLT	Terminal Alkenes
30	OLI	Internal Alkenes
31	TOL	Toluene and less reactive aromatics
32	CSL	Cresol and other hydroxy substituted aromatics
33	XYL	Xylene and more reactive aromatics

	Species	Definition
34	PAN	Peroxyacetyl nitrate and higher saturated PANs
35	ISO	Isoprene
36	TPAN	Unsaturated PANs
37	ORA1	Formic acid
38	ORA2	Acetic acid and higher acids
39	HO <sub>2</sub>	Hydroperoxy radical
40	MO <sub>2</sub>	Methyl peroxy radical
41	OLN	NO <sub>3</sub> -alkene adduct
42	ACO <sub>3</sub>	Acetyl peroxy and higher saturated acyl peroxy radicals
43	TCO <sub>3</sub>	Unsaturated acyl peroxy radicals
44	HO	Hydroxy radical
45	ETHP	Peroxy radical formed from ETH
46	HC3P	Peroxy radical formed from HC3
47	HC5P	Peroxy radical formed from HC5
48	HC8P	Peroxy radical formed from HC8
49	OL2P	Peroxy radicals formed from OL2
50	OLTP	Peroxy radicals formed from OLT
51	OLIP	Peroxy radicals formed from OLI
52	TOLP	Peroxy radicals formed from TOL
53	XYLP	Peroxy radicals formed from XYL
54	KETP	Peroxy radicals formed from KET
55	XNO <sub>2</sub>	Additional NO to NO <sub>2</sub> conversions
56	XO <sub>2</sub>	Additional HO to HO <sub>2</sub> conversions
57	NH <sub>3</sub>	Ammonia
58	HCl	Hydrochloric acid

## Appendix C: Chemical Mechanism Reactions

**Table C-1.** MECTM's Modified RADM2 Mechanism Reactions

Reaction Number	Reaction
<b>Photolysis Reactions <sup>1</sup></b>	
1	$\text{NO}_2 \rightarrow \text{O}^3\text{P} + \text{NO}$
2	$\text{O}_3 \rightarrow \text{O}^1\text{D} + \text{O}_2$
3	$\text{O}_3 \rightarrow \text{O}^3\text{P} + \text{O}_2$
4	$\text{HONO} \rightarrow \text{HO} + \text{NO}$
5	$\text{HNO}_3 \rightarrow \text{HO} + \text{NO}_2$
6	$\text{HNO}_4 \rightarrow \text{HO}_2 + \text{NO}_2$
7	$\text{NO}_3 \rightarrow \text{NO} + \text{O}_2$
8	$\text{NO}_3 \rightarrow \text{NO}_2 + \text{O}^3\text{P}$
9	$\text{H}_2\text{O}_2 \rightarrow \text{HO} + \text{HO}$
10	$\text{HCHO} \rightarrow \text{H}_2 + \text{CO}$
11	$\text{HCHO} \rightarrow \text{HO}_2 + \text{HO}_2 + \text{CO}$
12	$\text{ALD} \rightarrow \text{MO}_2 + \text{HO}_2 + \text{CO}$
13	$\text{OP1} \rightarrow \text{HCHO} + \text{HO}_2 + \text{HO}$
14	$\text{OP2} \rightarrow \text{ALD} + \text{HO}_2 + \text{HO}$
15	$\text{PAA} \rightarrow \text{MO}_2 + \text{CO}_2 + \text{HO}$
16	$\text{KET} \rightarrow \text{ACO}_3 + \text{ETHP}$
17	$\text{GLY} \rightarrow 0.13\text{HCHO} + 1.87\text{CO}$
18	$\text{GLY} \rightarrow 0.45\text{HCHO} + 1.55\text{CO} + 0.80\text{HO}_2$
19	$\text{MGLY} \rightarrow \text{ACO}_3 + \text{HO}_2 + \text{CO}$
20	$\text{DCB} \rightarrow 0.98\text{HO}_2 + 0.02\text{ACO}_3 + \text{TCO}_3$
21	$\text{ONIT} \rightarrow 0.20\text{ALD} + 0.80\text{KET} + \text{HO}_2 + \text{NO}_2$
22	$\text{ONIT} \rightarrow 2.0 \text{NO}_2$
<b>Inorganic Reactions</b>	
23	$\text{O}^3\text{P} + \text{O}_2 \rightarrow \text{O}_3$
24	$\text{O}^3\text{P} + \text{NO}_2 \rightarrow \text{NO} + \text{O}_2$
25	$\text{O}^1\text{D} + \text{N}_2 \rightarrow \text{O}^3\text{P} + \text{N}_2$
26	$\text{O}^1\text{D} + \text{O}_2 \rightarrow \text{O}^3\text{P} + \text{O}_2$
27	$\text{O}^1\text{D} + \text{H}_2\text{O} \rightarrow \text{HO} + \text{HO}$
28	$\text{O}_3 + \text{NO} \rightarrow \text{NO}_2 + \text{O}_2$
29	$\text{O}_3 + \text{HO} \rightarrow \text{HO}_2 + \text{O}_2$
30	$\text{O}_3 + \text{HO}_2 \rightarrow \text{HO} + 2.00\text{O}_2$
31	$\text{HO}_2 + \text{NO} \rightarrow \text{NO}_2 + \text{HO}$
32	$\text{HO}_2 + \text{NO}_2 \rightarrow \text{HNO}_4$
33	$\text{HNO}_4 \rightarrow \text{HO}_2 + \text{NO}_2$

Reaction Number	Reaction
34	$\text{HO}_2 + \text{HO}_2 \rightarrow \text{H}_2\text{O}_2$
35	$\text{HO}_2 + \text{HO}_2 + \text{H}_2\text{O} \rightarrow \text{H}_2\text{O}_2$
36	$\text{H}_2\text{O}_2 + \text{HO} \rightarrow \text{HO}_2 + \text{H}_2\text{O}$
37	$\text{NO} + \text{HO} \rightarrow \text{HONO}$
38	$\text{NO} + \text{NO} + \text{O}_2 \rightarrow \text{NO}_2 + \text{NO}_2$
39	$\text{O}_3 + \text{NO}_2 \rightarrow \text{NO}_3$
40	$\text{NO}_3 + \text{NO} \rightarrow \text{NO}_2 + \text{NO}_2$
41	$\text{NO}_3 + \text{NO}_2 \rightarrow \text{NO} + \text{NO}_2 + \text{O}_2$
42	$\text{NO}_3 + \text{HO}_2 \rightarrow \text{HNO}_3 + \text{O}_2$
43	$\text{NO}_3 + \text{NO}_2 \rightarrow \text{N}_2\text{O}_5$
44	$\text{N}_2\text{O}_5 \rightarrow \text{NO}_2 + \text{NO}_3$
45	$\text{N}_2\text{O}_5 + \text{H}_2\text{O} \rightarrow 2.00\text{HNO}_3$
46	$\text{HO} + \text{NO}_2 \rightarrow \text{HNO}_3$
47	$\text{HO} + \text{HNO}_3 \rightarrow \text{NO}_3 + \text{H}_2\text{O}$
48	$\text{HO} + \text{HNO}_4 \rightarrow \text{NO}_2 + \text{H}_2\text{O}$
49	$\text{HO} + \text{HO}_2 \rightarrow \text{H}_2\text{O} + \text{O}_2$
50	$\text{HO} + \text{SO}_2 \rightarrow \text{SULF} + \text{HO}_2$
51	$\text{CO} + \text{HO} \rightarrow \text{HO}_2 + \text{CO}_2$

### HO + Organic Compounds

52	$\text{CH}_4 + \text{HO} \rightarrow \text{MO}_2 + \text{H}_2\text{O}$
53	$\text{ETH} + \text{HO} \rightarrow \text{ETHP} + \text{H}_2\text{O}$
54	$\text{HC3} + \text{HO} \rightarrow 0.83\text{HC3P} + 0.17\text{HO}_2 + 0.009 \text{HCHO}$
55	$\text{HC3} + \text{HO} \rightarrow 0.075 \text{ALD} + 0.025 \text{KET} + \text{HO}_2$
56	$\text{HC5} + \text{HO} \rightarrow \text{HC5P} + 0.25\text{XO}_2 + \text{H}_2\text{O}$
57	$\text{HC8} + \text{HO} \rightarrow \text{HC8P} + 0.75\text{XO}_2 + \text{H}_2\text{O}$
58	$\text{OL2} + \text{HO} \rightarrow \text{OL2P}$
59	$\text{OLT} + \text{HO} \rightarrow \text{OLT P}$
60	$\text{OLI} + \text{HO} \rightarrow \text{OLIP}$
61	$\text{TOL} + \text{HO} \rightarrow 0.75\text{TOLP} + 0.25\text{CSL} + 0.25\text{HO}_2$
62	$\text{XYL} + \text{HO} \rightarrow 0.83\text{XYLP} + 0.17\text{CSL} + 0.17\text{HO}_2$
63	$\text{CSL} + \text{HO} \rightarrow 0.10\text{HO}_2 + 0.90\text{XO}_2 + 0.90\text{TCO}_3$
64	$\text{CSL} + \text{HO} \rightarrow \text{CSL}$
65	$\text{HCHO} + \text{HO} \rightarrow \text{HO}_2 + \text{CO} + \text{H}_2\text{O}$
66	$\text{ALD} + \text{HO} \rightarrow \text{ACO}_3 + \text{H}_2\text{O}$
67	$\text{KET} + \text{HO} \rightarrow \text{KETP} + \text{H}_2\text{O}$
68	$\text{GLY} + \text{HO} \rightarrow \text{HO}_2 + 2.00\text{CO} + \text{H}_2\text{O}$
69	$\text{MGLY} + \text{HO} \rightarrow \text{ACO}_3 + \text{CO} + \text{H}_2\text{O}$
70	$\text{DCB} + \text{HO} \rightarrow \text{TCO}_3 + \text{H}_2\text{O}$
71	$\text{OP1} + \text{HO} \rightarrow 0.50\text{MO}_2 + 0.50\text{HCHO} + 0.50\text{HO}$

Reaction Number	Reaction
72	$OP2 + HO \rightarrow 0.50HC3P + 0.50ALD + 0.50HO$
73	$PAA + HO \rightarrow ACO_3 + H_2O$
74	$PAN + HO \rightarrow HCHO + NO_3 + XO_2$
75	$ONIT + HO \rightarrow HC3P + NO_2$
76	$ISO + HO \rightarrow OLTP$

### Peroxyacylnitrate Formation and Decomposition

77	$ACO_3 + NO_2 \rightarrow PAN$
78	$PAN \rightarrow ACO_3 + NO_2$
79	$TCO_3 + NO_2 \rightarrow TPAN$
80	$TPAN \rightarrow TCO_3 + NO_2$

### NO + Organic Peroxy Radicals

81	$MO_2 + NO \rightarrow HCHO + HO_2 + NO_2$
82	$HC3P + NO \rightarrow 0.75ALD + 0.25KET + 0.09HCHO$
83	$HC3P + NO \rightarrow 0.036 ONIT + 0.964 NO_2 + 0.964HO_2$
84	$HC5P + NO \rightarrow 0.38ALD + 0.69KET + 0.08ONIT$
85	$HC5P + NO \rightarrow 0.92NO_2 + 0.92HO_2$
86	$HC8P + NO \rightarrow 0.35ALD + 1.06KET + 0.04HCHO$
87	$HC8P + NO \rightarrow 0.24 ONIT + 0.76NO_2 + 0.76 HO_2$
88	$OL2P + NO \rightarrow 1.60HCHO + HO_2 + NO_2$
89	$OL2P + NO \rightarrow 0.2 ALD$
90	$OLTP + NO \rightarrow ALD + HCHO + HO_2$
91	$OLTP + NO \rightarrow NO_2$
92	$OLIP + NO \rightarrow HO_2 + 1.45ALD + 0.28HCHO$
93	$OLIP + NO \rightarrow 0.1KET + NO_2$
94	$ACO_3 + NO \rightarrow MO_2 + NO_2$
95	$TCO_3 + NO \rightarrow NO_2 + 0.92HO_2 + 0.89GLY$
96	$TCO_3 + NO \rightarrow 0.11 MGLY + 0.05 ACO_3 + 0.95 CO$
97	$TCO_3 + NO \rightarrow 2.00 XO_2$
98	$TOLP + NO \rightarrow NO_2 + HO_2 + 0.17MGLY$
99	$TOLP + NO \rightarrow 0.16 GLY + 0.70DCB$
100	$XYLP + NO \rightarrow NO_2 + HO_2 + 0.45MGLY$
101	$XYLP + NO \rightarrow 0.806 DCB$
102	$ETHP + NO \rightarrow ALD + HO_2 + NO_2$
103	$KETP + NO \rightarrow MGLY + NO_2 + HO_2$
104	$OLN + NO \rightarrow HCHO + ALD + 2.00NO_2$

Reaction Number	Reaction
<b>NO<sub>3</sub> + Organic Compounds</b>	
105	HCHO + NO <sub>3</sub> → HO <sub>2</sub> + HNO <sub>3</sub> + CO
106	ALD + NO <sub>3</sub> → ACO <sub>3</sub> + HNO <sub>3</sub>
107	GLY + NO <sub>3</sub> → HNO <sub>3</sub> + HO <sub>2</sub> + 2.00CO
108	MGLY + NO <sub>3</sub> → HNO <sub>3</sub> + ACO <sub>3</sub> + CO
109	DCB + NO <sub>3</sub> → HNO <sub>3</sub> + TCO <sub>3</sub>
110	CSL + NO <sub>3</sub> → HNO <sub>3</sub> + XNO <sub>2</sub> + 0.50CSL
111	OL2 + NO <sub>3</sub> → OLN
112	OLT + NO <sub>3</sub> → OLN
113	OLI + NO <sub>3</sub> → OLN
114	ISO + NO <sub>3</sub> → OLN
<b>O<sub>3</sub> + Organic Compounds</b>	
115	OL2 + O <sub>3</sub> → HCHO + 0.42CO + 0.40ORA1
116	OL2 + O <sub>3</sub> → 0.12 HO <sub>2</sub>
117	OLT + O <sub>3</sub> → 0.53HCHO + 0.50ALD + 0.33CO
118	OLT + O <sub>3</sub> → 0.20ORA1 + 0.20 ORA2 + 0.23 HO <sub>2</sub>
119	OLT + O <sub>3</sub> → 0.22 MO <sub>2</sub> + 0.10 HO + 0.06 CH <sub>4</sub>
120	OLI + O <sub>3</sub> → 0.18HCHO + 0.72ALD + 0.10KET
121	OLI + O <sub>3</sub> → 0.23 CO + 0.06 ORA1 + 0.29 ORA2
122	OLI + O <sub>3</sub> → 0.09 CH <sub>4</sub> + 0.26HO <sub>2</sub> + 0.14 HO
123	OLI + O <sub>3</sub> → 0.31 MO <sub>2</sub>
124	ISO + O <sub>3</sub> → 0.53HCHO + 0.50ALD + 0.33CO
125	ISO + O <sub>3</sub> → 0.20ORA1 + 0.20 ORA2 + 0.23 HO <sub>2</sub>
126	ISO + O <sub>3</sub> → 0.22 MO <sub>2</sub> + 0.10 HO
<b>HO<sub>2</sub> + Organic Peroxy Radicals</b>	
127	HO <sub>2</sub> + MO <sub>2</sub> → OP1
128	HO <sub>2</sub> + EHP → OP2
129	HO <sub>2</sub> + HC3P → OP2
130	HO <sub>2</sub> + HC5P → OP2
131	HO <sub>2</sub> + HC8P → OP2
132	HO <sub>2</sub> + OL2P → OP2
133	HO <sub>2</sub> + OLTP → OP2
134	HO <sub>2</sub> + OLIP → OP2
135	HO <sub>2</sub> + KETP → OP2
136	HO <sub>2</sub> + ACO <sub>3</sub> → PAA
137	HO <sub>2</sub> + TOLP → OP2

Reaction Number	Reaction
138	$\text{HO}_2 + \text{XYLP} \rightarrow \text{OP2}$
139	$\text{HO}_2 + \text{TCO}_3 \rightarrow \text{OP2}$
140	$\text{HO}_2 + \text{OLN} \rightarrow \text{ONIT}$
<b>Methyl Peroxy Radical + Organic Peroxy Radical</b>	
141	$\text{MO}_2 + \text{MO}_2 \rightarrow 1.50\text{HCHO} + \text{HO}_2$
142	$\text{MO}_2 + \text{ETHP} \rightarrow 0.75\text{HCHO} + \text{HO}_2 + 0.75 \text{ALD}$
143	$\text{MO}_2 + \text{HC3P} \rightarrow 0.84\text{HCHO} + \text{HO}_2 + 0.77 \text{ALD}$
144	$\text{MO}_2 + \text{HC3P} \rightarrow 0.26 \text{KET}$
145	$\text{MO}_2 + \text{HC5P} \rightarrow 0.77 \text{HCHO} + \text{HO}_2 + 0.41 \text{ALD}$
146	$\text{MO}_2 + \text{HC5P} \rightarrow 0.75 \text{KET}$
147	$\text{MO}_2 + \text{HC8P} \rightarrow 0.80 \text{HCHO} + \text{HO}_2 + 0.46 \text{ALD}$
148	$\text{MO}_2 + \text{HC8P} \rightarrow 1.39 \text{KET}$
149	$\text{MO}_2 + \text{OL2P} \rightarrow 1.55 \text{HCHO} + \text{HO}_2 + 0.35 \text{ALD}$
150	$\text{MO}_2 + \text{OLTP} \rightarrow 1.25 \text{HCHO} + \text{HO}_2 + 0.75 \text{ALD}$
151	$\text{MO}_2 + \text{OLIP} \rightarrow 0.89 \text{HCHO} + \text{HO}_2 + 0.73 \text{ALD}$
152	$\text{MO}_2 + \text{OLIP} \rightarrow 0.55 \text{KET}$
153	$\text{MO}_2 + \text{KETP} \rightarrow 0.75 \text{HCHO} + \text{HO}_2 + 0.75 \text{MGLY}$
154	$\text{MO}_2 + \text{ACO}_3 \rightarrow \text{HCHO} + 0.50\text{HO}_2 + 0.50\text{MO}_2$
155	$\text{MO}_2 + \text{ACO}_3 \rightarrow 0.5 \text{ORA2}$
156	$\text{MO}_2 + \text{TOLP} \rightarrow \text{HCHO} + 2.00 \text{HO}_2 + 0.17 \text{MGLY}$
157	$\text{MO}_2 + \text{TOLP} \rightarrow 0.16 \text{GLY} + 0.70 \text{DCB}$
158	$\text{MO}_2 + \text{XYLP} \rightarrow \text{HCHO} + 2.00\text{HO}_2 + 0.45 \text{MGLY}$
159	$\text{MO}_2 + \text{XYLP} \rightarrow 0.806 \text{DCB}$
160	$\text{MO}_2 + \text{TCO}_3 \rightarrow 0.50\text{HCHO} + 0.50\text{ORA2} + 0.46\text{HO}_2$
161	$\text{MO}_2 + \text{TCO}_3 \rightarrow 0.445 \text{GLY} + 0.055 \text{MGLY} + 0.025 \text{ACO}_3$
162	$\text{MO}_2 + \text{TCO}_3 \rightarrow 0.475\text{CO} + \text{XO}_2$
163	$\text{MO}_2 + \text{OLN} \rightarrow 1.75\text{HCHO} + 0.50\text{HO}_2 + \text{ALD}$
164	$\text{MO}_2 + \text{OLN} \rightarrow \text{NO}_2$
<b>Acetyl Radical + Organic Peroxy Radicals</b>	
165	$\text{ETHP} + \text{ACO}_3 \rightarrow \text{ALD} + 0.50\text{HO}_2 + 0.50\text{MO}_2$
166	$\text{ETHP} + \text{ACO}_3 \rightarrow 0.5 \text{ORA2}$
167	$\text{HC3P} + \text{ACO}_3 \rightarrow 0.77 \text{ALD} + 0.26 \text{KET} + 0.50 \text{HO}_2$
168	$\text{HC3P} + \text{ACO}_3 \rightarrow 0.5 \text{MO}_2 + 0.5 \text{ORA2}$
169	$\text{HC5P} + \text{ACO}_3 \rightarrow 0.41 \text{ALD} + 0.75 \text{KET} + 0.50 \text{HO}_2$
170	$\text{HC5P} + \text{ACO}_3 \rightarrow 0.50 \text{MO}_2 + 0.50 \text{ORA2}$
171	$\text{HC8P} + \text{ACO}_3 \rightarrow 0.46\text{ALD} + 1.39\text{KET} + 0.50 \text{HO}_2$
172	$\text{HC8P} + \text{ACO}_3 \rightarrow 0.50\text{MO}_2 + 0.50 \text{ORA2}$

Reaction Number	Reaction
173	$OL2P + ACO_3 \rightarrow 0.80HCHO + 0.60ALD + 0.50 HO_2$
174	$OL2P + ACO_3 \rightarrow 0.50 MO_2 + 0.50 ORA2$
175	$OLTP + ACO_3 \rightarrow ALD + 0.50 HCHO + 0.50 HO_2$
176	$OLTP + ACO_3 \rightarrow 0.50MO_2 + 0.50 ORA2$
177	$OLIP + ACO_3 \rightarrow 0.73ALD + 0.55KET + 0.14 HCHO$
178	$OLIP + ACO_3 \rightarrow 0.50HO_2 + 0.50MO_2 + 0.50 ORA2$
179	$KETP + ACO_3 \rightarrow MGLY + 0.50HO_2 + 0.50 MO_2$
180	$KETP + ACO_3 \rightarrow 0.50ORA2$
181	$ACO_3 + ACO_3 \rightarrow 2.00MO_2$
182	$ACO_3 + TOLP \rightarrow MO_2 + 0.17MGLY + 0.16 GLY$
183	$ACO_3 + TOLP \rightarrow 0.70DCB + HO_2$
184	$ACO_3 + XYLP \rightarrow MO_2 + 0.45 MGLY + 0.806 DCB$
185	$ACO_3 + XYLP \rightarrow HO_2$
186	$ACO_3 + TCO_3 \rightarrow MO_2 + 0.92HO_2 + 0.89 GLY$
187	$ACO_3 + TCO_3 \rightarrow 0.11 MGLY + 0.05 ACO_3 + 0.95 CO$
188	$ACO_3 + TCO_3 \rightarrow 2.00 XO_2$
189	$ACO_3 + OLN \rightarrow HCHO + ALD + 0.50 ORA2$
190	$ACO_3 + OLN \rightarrow NO_2 + 0.5 MO_2$
191	$OLN + OLN \rightarrow 2.00 HCHO + 2.00ALD + 2.00NO_2$

### Operator Reactions

192	$XO_2 + HO_2 \rightarrow OP2$
193	$XO_2 + MO_2 \rightarrow HCHO + HO_2$
194	$XO_2 + ACO_3 \rightarrow MO_2$
195	$XO_2 + XO_2 \rightarrow$
196	$XO_2 + NO \rightarrow NO_2$
197	$XNO_2 + NO_2 \rightarrow ONIT$
198	$XNO_2 + HO_2 \rightarrow OP2$
199	$XNO_2 + MO_2 \rightarrow HCHO + HO_2$
200	$XNO_2 + ACO_3 \rightarrow MO_2$
201	$XNO_2 + XNO_2 \rightarrow$

Note: <sup>1</sup> Relation table for STAR Photolysis Reaction Rates in Appendix F

## Appendix D: Landuse Classes

**Table D-1:** *METRAS/MECTM Landuse Classes*

Class	Definition
1	Water
2	Mudflats
3	Sand
4	Mixed land use
5	Meadows
6	Heath
7	Bushes
8	Mixed forest
9	Coniferous forest
10	Urban area

**Table D-2:** STAR photolysis rate Landuse classes (adapted from Ruggaber, 1991)

Class	Definition
1	Grass Summer
2	Grass Spring
3	Forest
4	Water
5	Sand
6	Snow Old
7	Fresh Fallen Snow

**Table D-3:** *Biogenic Emission Factors Landuse Classes (Adapted from McKeen et al., 1991)*

Class	Definition
1	Oak Forest
2	Corn
3	Deciduous forest
4	Coniferous Forest
5	Rice, peanuts
6	Tobacco
7	Grass
8	Hay
9	Potatoes
10	Sorghum
11	Barley
12	Oats
13	Wheat
14	Soybean
15	Water

**Table D-4:** *Relation Matrices for METRAS/MECTM Landuse Classes with Photolysis Rates (STAR) and Biogenic Emission Factors*

METRAS/MECTM Class	METRAS/MECTM Definition	STAR Landuse Class	Biogenic Emissions Landuse Class
1	Water	4 (water)	15 (water)
2	Mudflats	4 (water)	15 (water)
3	Sand	5 (sand)	15 (water)
4	Mixed land use	3 (forest)	$1/7*(2+7+8+9+11+12+13)$ (corn, grass, hay, potatoes, barley, oats, wheat)
5	Meadows	3 (forest)	7 (grass)
6	Heath	1 (grass summer)	7 (grass)
7	Bushes	1 (grass summer)	3 (deciduous forest)
8	Mixed forest	3 (forest)	$1/2*(3+4)$ (deciduous forest, coniferous forest)
9	Coniferous forest	3 (forest)	4 (coniferous forest)
10	Urban area	3 (forest)	15 (water)

## Appendix E: Emission Chemical Species

**Table E-1:** *Emission Species used for MECTM*

Species	Definition
SO <sub>2</sub>	Sulfur dioxide
NO <sub>2</sub>	Nitrogen dioxide
NO	Nitric oxide
CO	Carbon monoxide
ALD	Acetaldehyde
HCHO	Formaldehyde
ORA2	Acetic acid and higher acids
HC3	Alkanes, alcohols, esters, and alkynes with HO rate constant (298 K, 1atm) less than $3.4 \times 10^{-12} \text{ cm}^3 \text{ s}^{-1}$
HC5	Alkanes, alcohols, esters, and alkynes with HO rate constant (298 K, 1atm) between $3.4 \times 10^{-12}$ and $6.8 \times 10^{-12} \text{ cm}^3 \text{ s}^{-1}$
HC8	Alkanes, alcohols, esters, and alkynes with HO rate constant (298 K, 1atm) greater than $6.8 \times 10^{-12} \text{ cm}^3 \text{ s}^{-1}$
ETH	Ethane
OL2	Ethene
OLT	Terminal Alkenes
OLI	Internal Alkenes
TOL	Toluene and less reactive aromatics
XYL	Xylene and more reactive aromatics
KET	Ketones
CSL	Cresol and other hydroxy substituted aromatics
NH <sub>3</sub>	Ammonia
CH <sub>4</sub>	Methane

## Appendix F: STAR Photolytic Reactions

Table F-1. STAR photolytic reactions and relation to the MECTM chemistry

	Reaction	Relation matrix for the RADM2 chemistry mecha- nism used in the MECTM <sup>1</sup>
1	$O_3 + hv \rightarrow O^1D + O_2$	2
2	$O_3 + hv \rightarrow O^3P + O_2$	3
3	$NO_2 + hv \rightarrow O^3P + NO$	1
4	$NO_3 + hv \rightarrow NO + O_2$	7
5	$NO_3 + hv \rightarrow NO_2 + O$	8
6	$HONO + hv \rightarrow HO + NO$	4
7	$HNO_3 + hv \rightarrow HO + NO_2$	5
8	$HNO_4 + hv \rightarrow HO_2 + NO_2$	6
9	$H_2O_2 + hv \rightarrow 2 HO$	9
10	$HCHO + hv \rightarrow 2 HO_2 + CO$	11
11	$HCHO + hv \rightarrow H_2 + CO$	10
12	$CH_3CHO + hv \rightarrow CH_3O_2 + HO_2 + CO$	12
13	$CH_3COCH_3 + hv \rightarrow CH_3CO_3 + C_2H_5O_2$	16
14	$CH_3COC_2H_5 + hv \rightarrow CH_3CO_3 + C_2H_5O_2$	-1
15	$CHOCHO + hv \rightarrow 0.13 HCHO + 1.87 CO$	17
16	$CH_3COCHO + hv \rightarrow CH_3CO_3 + HO_2 + CO$	19
17	$HCOCH = CHCHO + hv \rightarrow 0.98 HO_2$ $+ H(CO)CH = CHCO_3 + 0.02CH_3CO_3$	20
18	$CH_3O_2H + hv \rightarrow HCHO + HO_2 + HO$	13
19	$CH_3COO_2H + hv \rightarrow CH_3O_2 + CO_2 + HO$	15
20	$CH_3ONO_2 + hv \rightarrow 0.2 CH_3CHO + 0.8CH_3COCH_3 +$ $HO_2 + NO_2$	21
21	$HCOCHO_2 + hv \rightarrow 0.45 HCHO + 1.55 CO + 0.8 HO_2$	18
22	$Cl_2 + hv \rightarrow Cl + Cl$	-1
23	$ClNO + hv \rightarrow Cl + NO$	-1
24	$ClNO_2 + hv \rightarrow Cl + NO_2$	-1
25	$ClO + hv \rightarrow Cl + O$	-1
26	$ClONO_2 + hv \rightarrow Cl + NO_3$	-1
27	$HOCl + hv \rightarrow Cl + HO$	-1
28	$OCIO + hv \rightarrow ClO + O$	-1
29	$Cl_2O_3 + hv \rightarrow ClO + OClO$	-1
30	$BRO + hv \rightarrow BR + O$	-1
31	$BRONO_2 + hv \rightarrow BR + NO_3$	-1
32	$HOBR + hv \rightarrow BR + HO$	-1
33	$BR_2O + hv \rightarrow BR + O$	-1

Reaction	Relation matrix for the RADM2 chemistry mechanism used in the MECTM <sup>1</sup>
34 $\text{BR}_2 + hv \rightarrow \text{BR} + \text{BR}$	-1
35 $\text{BRCl} + hv \rightarrow \text{BR} + \text{Cl}$ (same as $\text{BR}_2\text{O} + hv$ )	-1
36 $\text{BRNO}_2 + hv \rightarrow \text{BR} + \text{NO}_2$ (same as $\text{ClNO}_2 + hv = \text{Cl} + \text{NO}_2$ )	-1

<sup>1)</sup> A -1 value denotes that this reaction is not used in the MECTM chemistry.

The STAR pre-processor calculates the photolysis rates, and then the relation matrix is used to integrate this information into the chemistry mechanism as listed in Appendix C.

## Appendix G: SEMA Box-model Sensitivity Analysis

**Table G-1.** SEMA Results vs. Measurements (hit rates based on deviations <50% of measured data in 8 sections)

SEMA run	MPN-9 (13:12-20:44 16/06)					MPN-10 (21:38 16/06 - 12:06 17/06)				
	NO <sub>3</sub> <sup>-</sup>	Cl <sup>-</sup>	SO <sub>4</sub> <sup>2-</sup>	NH <sub>4</sub> <sup>+</sup>	Na <sup>+</sup>	NO <sub>3</sub> <sup>-</sup>	Cl <sup>-</sup>	SO <sub>4</sub> <sup>2-</sup>	NH <sub>4</sub> <sup>+</sup>	Na <sup>+</sup>
<b>Base Run</b> *	5/8	6/8	4/8	0/8	6/8	4/8	6/8	3/8	0/8	7/8
<b>T increased 5°C</b>	3/8	6/8	4/8	0/8	5/8	4/8	6/8	4/8	0/8	7/8
<b>RH decreased 5%</b>	4/8	6/8	5/8	0/8	5/8	4/8	6/8	3/8	0/8	7/8
<b>HCl increased to 11 nmol/m<sup>3</sup></b>	5/8	6/8	4/8	0/8	6/8	4/8	6/8	3/8	0/8	7/8
<b>H<sub>2</sub>SO<sub>4</sub> increased to 40 nmol/m<sup>3</sup></b>	4/8	2/8	2/8	0/8	3/8	2/8	2/8	2/8	0/8	2/8
<b>No deposition or sea salt generation</b>	3/8	3/8	5/8	0/8	3/8	2/8	3/8	2/8	0/8	4/8
<b>Ion balance completed with Na<sup>+</sup></b>	6/8	7/8	5/8	4/8	2/8	4/8	7/8	3/8	5/8	3/8

\* Base run initialized with WAO measured and redistributed to SEMA input, Temperature = 15°C, RH = 95%, ion balance closed by adding H<sup>+</sup>, HCl = 0, H<sub>2</sub>SO<sub>4</sub> = 0

This sensitivity study shows the dependence of aerosol formation on varying meteorology and varying gaseous specie concentrations. It shows the relevance of proper meteorological data, and meteorological numerical simulations, for aerosol simulation, especially since temperature and relative humidity dependence is so great. The study also identifies some of the uncertainties that can arise from the input data, be it from observations or numerical forecasting. If the input data is even slightly different from the real situation large changes in the output can occur which can degrade the quality of the results.

## List of Symbols

Symbol	Definition
$C_i$	Pollutant concentration
$D_p$	Particle diameter
$K_{vert}$	Vertical exchange coefficient for momentum
$K_{vert,\chi}$	Vertical exchange coefficient for scalar quantities
$r_a$	Aerodynamic resistance
$r_b$	Viscous sub layer resistance
$r_s$	Surface resistance
$u_*$	Friction velocity
$V$	Magnitude of horizontal wind
$V_g$	Geostrophic wind in south-north direction
$v_d$	Deposition velocity
$v_g$	Gravitational settling velocity
$w$	Vertical velocity
$z$	Height
$\theta$	Potential temperature
$\partial\theta/\partial z$	Environmental Lapse Rate (ELR)
$\kappa$	von Karman constant
$\rho$	Density of air
$\tau$	Characteristic time constant

## **Acknowledgements**

I would like to express my sincere gratitude to Frau Priv. Doz. Dr. K. Heinke Schlünzen for her guidance and encouragement throughout this project. As well, I would like to thank Dr. Guy Brasseur for accepting to act as a second reviewer of this work and Prof. Dr. Michael Schatzmann for his support during my work in Hamburg.

My colleagues at the Meteorologisches Institut are gratefully acknowledged for their aid in many aspects; Dipl.-Met. Silke Dierer, Dipl.-Met. Frank Schimmel, and Dipl.-Phys. Alfred Trukenmüller for their helpful discussions, Volker Reinhardt for his assistance in meteorological data acquisition, Dr. Otto Böhringer for his help and patience in program debugging, and those attending Dr. Schlünzen's Friday Work Group meetings providing a forum to test new ideas. I would also like to thank those who were with the Work Group during my time in Hamburg; Dr. Heiko Panskus, Dr. Claus-Jürgen Lenz, Dr. Frank Müller, and Dr. Sheng Lifang for their help large and small.

The modeling portion of this project could not have taken place without Dr. Knut von Salzen's SEMA box-model and guidance in using it, as well as Dr. Frank Müller for an earlier version of the gas phase chemistry model MECTM. Data and support were generously provided by the ANICE 'crew', particularly Suzanne Tamm who provided measurement data and useful discussion. Meteorological data was provided by the German Weather Service, sounding from the British Atmospheric Data Center (BADC), and thanks also to Burkhard Wickert of University of Stuttgart, Institute for Energy Economics and the Rational Use of Energy for providing emission data sets for the study region.

This research was supported by the University of Hamburg and the European Commission under contract number ENV4-CT97-0594 (ANICE).

## References

- Ackermann, I. J., H. Hass, M. Memmesheimer, A. Ebel, F. S. Binkowski, and U. Shankar. Modal aerosol dynamics model for Europe: development and first applications. *Atmospheric Environment*, **32**, 2981–2999, 1998.
- Ackermann, I. J., H. Hass, M. Memmesheimer, C. Ziegenbein, and A. Ebel. The parameterization of the Sulfate–Nitrate–Ammonia aerosol system in the long-range transport model EURAD, *Meteorol. Atmos. Phys.*, **57**, 101–114, 1995.
- Andronopoulos, S., A. Passamichali, N. Gounaris, and J. G. Bartzis. Evolution and Transport of Pollutants over a Mediterranean Coastal Area: The Influence of Biogenic Volatile Organic Compound Emissions on Ozone Concentrations, *J. Appl. Meteorol.*, **39**, 526–545, 2000.
- Aneja, V. P., P. A. Roelle, G. C. Murray, J. Southerland, J. W. Erisman, D. Fowler, W. A. H. Asman, and N. Patni. Atmospheric nitrogen compounds II: emissions, transport, transformation, deposition and assessment. *Atmospheric Environment*, **35**, 1903–1911, 2001.
- Angevine, W. M., M. Trainer, S.A. McKeen, and C. M. Berkowitz. Mesoscale meteorology of the New England Coast, Gulf of Maine, and Nova Scotia: Overview. *J. Geophys. Res.*, **101**, 28,893–28,901, 1996a.
- Angevine, W. M., J. S. Holloway, M. L. Trainer, D. D. Parrish, J. I. MacPherson, G. L. Kok, R. D. Schillawski, and D. H. Bowlby. Local meteorological features affecting chemical measurements at a North Atlantic coastal site. *J. Geophys. Res.*, **101**, 28935–28946, 1996b.
- Ansari, A. S., and S. N. Pandis. Prediction of multicomponent inorganic atmospheric aerosol behavior. *Atmospheric Environment*, **33**, 745–757, 1999.
- Asman, W. A. H., and R. Berkowicz. Atmospheric Nitrogen deposition to the North Sea, *Marine Pollution Bulletin*, **29**, 426–434, 1994.
- Atkinson, B.W. *Mesoscale Atmospheric Circulations*. Academic Press, New York City, 1981.
- Binkowski, F. S., and U. Schankar. The regional particulate matter model, 1: Model description and preliminary results. *J. Geophys. Res.*, **100**, 26191–26209, 1995.
- Blanchard, D. C., and R. J. Cipriano. Biological Regulation of Climate. *Nature*, **330**, 526, 1987.
- Blanchard, D. C., and A. H. Woodcock. The production, concentration and vertical distribution of sea-salt aerosol. *Ann. New York Acad. Sci.*, **338**, 330–347, 1980.

- Clegg, S. L., P. Brimblecombe, and A. S. Wexler. A thermodynamic model of the system  $\text{H}^+ - \text{NH}_4^+ - \text{Na}^+ - \text{SO}_4^{2-} - \text{NO}_3^- - \text{Cl}^- - \text{H}_2\text{O}$  at 298.15K. *Journal of Physical Chemistry*, **102**, 2155–2171, 1998a.
- Clegg, S. L., P. Brimblecombe, and A. S. Wexler. A thermodynamic model of the system  $\text{H}^+ - \text{NH}_4^+ - \text{Na}^+ - \text{SO}_4^{2-} - \text{NO}_3^- - \text{Cl}^- - \text{H}_2\text{O}$  at Tropospheric temperatures. *Journal of Physical Chemistry*, **102**, 2137–2154, 1998b.
- Clegg, S. L., K. S. Pitzer, and P. Brimblecombe. Thermodynamics of multicomponent, miscible, ionic solutions. II. Mixture including unsymmetrical electrolytes. *Journal of Physical Chemistry*, **96**, 9470–9479, 1992.
- Clegg, S. L., K. S. Pitzer, and P. Brimblecombe. (Additions and corrections for their published papers). *Journal of Physical Chemistry*, **98**, 1368, 1994.
- Clegg, S. L., K. S. Pitzer, P. and Brimblecombe. (Additions and corrections for their published papers). *Journal of Physical Chemistry*, **99**, 6755, 1995.
- Cox, R., B. L. Bauer, and T. Smith. A Mesoscale Model Intercomparison. *Bulletin of the American Meteorological Society*, **79**, 265–283, 1998.
- Davies, H. C. A lateral boundary formulation for multi-level prediction models. *Quart. J. R. Meteor. Soc.*, **102**, 405–418, 1976.
- Defant, F., Theorie der Land und Seewinde *Arch. Met. Geophys. Bioklim. A*, **2**, 404–425, 1950.
- de Leeuw, G., L. Cohen, G. J. Kunz, M. Moerman, G. Geernaert, O. Hertel, B., Jensen, B. Pedersen, E. Vignati, L-L. Sorensen, S. Lund, T. Jickells, L. Spokes, H. Schlünzen, L. Klein, K. von Salzen, M. Scully, S. Tamm. Atmospheric Nitrogen Inputs into the Coastal Ecosystem (ANICE): The southern North Sea as a Study Area. *J. Aerosol Science*, **30**, Suppl. 1, pp. S185–S186, 1999a.
- de Leeuw, G., G.J. Kunz, M. Moerman, L.H. Cohen, H. Schlünzen, L. Klein, F. Müller, K. von Salzen, M. Schulz, S. Tamm, E. Plate, G. Geernaert, O. Hertel, E. Vignati, L. Frohn, B. Pedersen, B. Jensen, L.L. Sørensen, S. Lund, T. Jickells and L. Spokes. ANICE: Atmospheric Nitrogen Inputs into the Coastal Ecosystem. Book of abstracts, ELOISE 3rd Open Science Meeting, 1–4 December 1999, Noordwijkerhout, The Netherlands, p. 46, 1999b.
- de Leeuw, G., G.J. Kunz, M. Moerman, L.H. Cohen, H. Schlünzen, L. Klein, F. Müller, K. von Salzen, M. Schulz, S. Tamm, E. Plate, G. Geernaert, O. Hertel, E. Vignati, L. Frohn, B. Pedersen, B. Jensen, L.L. Sørensen, S. Lund, T. Jickells and L. Spokes. Atmospheric nitrogen inputs into the coastal ecosystem (ANICE) ENV4-CT97-0594. First annual report (February 1, 1998 – January 31, 1999). *TNO-Report Fel-99-C123*, pp.60., 1999c.
- de Leeuw, G., G.J. Kunz, M. Moerman, L.H. Cohen, H. Schlünzen, L. Klein, F. Müller, K. von Salzen, M. Schulz, S. Tamm, E. Plate, G. Geernaert, O. Her-

- tel, E. Vignati, L. Frohn, B. Pedersen, B. Jensen, L.L. Sørensen, S. Lund, T. Jickells and L. Spokes. Atmospheric nitrogen inputs into the coastal ecosystem (ANICE) ENV4-CT97-0594. Second annual report (February 1, 1999 – January 31, 2000). *TNO-Report Fel-00-C125*, pp.104., 2000.
- de Leeuw, G., L. Spokes, T. Jickells, C. A. Skjoth, O. Hertel, E. Vignati, S. Tamm, M. Schulz, L-L Sorensen, B. Pedersen, L. Klein and K. H. Schlünzen. Atmospheric Nitrogen Inputs into the North Sea: Effect on Productivity. In preparation for submission to NCO for the 2002 Special issue for ELOISE, March 2002.
- Despiau, S., J. Gourdeau, O. LeCalve, L. Massouh, M. Mallet, K. Sellegri, and G. Tedeschi. Characterization of marine aerosol source during FETCH experiment, 2d workshop "CAPMAN-EUROTRAC2", 3–5 February, 1999, Roskilde, Denmark.
- Deutscher Wetterdienst. Quarterly Report of the Operational NWP-Model of the Deutscher Wetterdienst, Business Area Research and Development, DWD, Offenbach a.M., Germany. 1998.
- Dierer S. und Schlünzen K. H. The influence of a cyclone on the ice drift – nudged simulation with the model METRAS coupled with a sea ice model. *Third international SRNWP, Workshop " Nonhydrostatic modelling", Deutscher WetterdienstInstitution, Offenbach a. Main, (25.bis 27.10.1999)*, pp 1, 1999.
- Duce, R. The input of atmospheric chemicals to the ocean. *WMO Bulletin*, **47**, 51–60, 1998.
- Fitzgerald, J. W. Marine aerosols: a review. *Atmospheric Environment*, **25A**, 533–546, 1991.
- Gelbhard, F., and J.H. Seinfeld. Simulation of multicomponent aerosol dynamics, *J. Colloid Interface Sci.*, **78**, 485–501, 1980.
- Harkel, M. J. T. The effects of particle-size distribution and chloride depletion of sea-salt aerosols on estimating atmospheric deposition at a coastal site. *Atmospheric Environment*, **31**, 417–427, 1997.
- Harrison, R. M., M. I. Msibi, A.-M. N. Kitto and S. Yamulki . Atmospheric chemical transformations of nitrogen compounds measured in the North Sea Experiment, September 1991. *Atmospheric Environment*, **28**, 1593–1599, 1994.
- Hobbs, P., and M. P. McCormick, Eds., *Aerosols and Climate* Deepak Publ. Co., Hampton, Virginia 486 pp., 1988.
- Holtslag, A., and C-H. Moeng, Eddy diffusivity and countergradient transport in the convective atmospheric boundary layer. *J. Atmo. Sci.*, **48**, 1690–1698, 1991.

## References

- Jacobson, M. Z. Development and application of a new air pollution modeling system – II. Aerosol module structure and design. *Atmospheric Environment*, **31**, 131–144, 1997.
- Jacobson, M. Z. *Fundamentals of Atmospheric Modeling*. Cambridge University Press, New York, 1999a.
- Jacobson, M. Z. Studying the effects of calcium and magnesium on size distributed nitrate and ammonium with EQUISOLV II. *Atmospheric Environment*, **33**, 3635–3649, 1999b.
- Jacobson M. Z., R. P. Turco, E. J. Jensen and O. B. Toon. Modeling coagulation among particles of different composition and size. *Atmospheric Environment*, **28A**, 1327 – 1338, 1994.
- Jaenicke, R. Tropospheric aerosols. In: *Aerosol–cloud–climate interactions*. Academic Press, International Geophysics Series, **54**, 1–31, 1993.
- Jickells, T., and L. Spokes. First annual report of the individual partners: partner 4. In: *Atmospheric Nitrogen Inputs into the coastal Ecosystem (ANICE) ENV4-CT97-0594. First Annual Report (February 1, 1998 – January 31, 1999)*. TNO report FEL-99-C123, TNO Physics and Electronics Laboratory, The Hague, The Netherlands, 1999.
- Katoshevski, D., A. Nenes and J. H. Seinfeld. A study of processes that govern the maintenance of aerosols in the marine boundary layer, *J. Aerosol Sci.*, **30**, 503–532, 1999.
- Katsoulis, B. D. Some Meteorological Aspects of Air Pollution in Athens, Greece. *Meteorol. Atmos. Phys.*, **39**, 203–212, 1988.
- Kerminen, V-M., A. S. Wexler. Growth behavior of the marine submicron boundary layer aerosol. *J. Geophys. Res.*, **102**, 18,813–18,825, 1997.
- Kim, Y. P., and J. H. Seinfeld. Atmospheric gas–aerosol equilibrium III: thermodynamics of crustal elements  $\text{Ca}^{2+}$ ,  $\text{K}^+$ , and  $\text{Mg}^{2+}$ . *Aerosol Science and Technology*, **22**, 93–110, 1995.
- Kim, Y. P., J. H. Seinfeld, and P. Saxena. Atmospheric Gas–Aerosol Equilibrium I. Thermodynamic Model. *Aerosol Sci. Technol.*, **19**, 157–181, 1993a.
- Kim, Y. P., J. H. Seinfeld, and P. Saxena. Atmospheric Gas–Aerosol Equilibrium II. Analysis of Common Approximations and Activity Coefficient Calculation Methods. *Aerosol Sci. Technol.*, **10**, 182–198, 1993b.
- Klein L. and K. H. Schlünzen. Simulation of coastal atmospheric processes including aerosols. *CAPMAN annual report, international scientific secretariat; GSF–Forschungszentrum für Umwelt und Gesundheit GMBH*, pp 5, 2001.

- Klein L., K. H. Schlünzen, K. von Salzen, M. Schulz, L. Spokes and S. Tamm. Aerosol size distribution in the atmosphere – modeled vs. measured. *Proceedings from the EUROTRAC Symposium 2000*, Midgley, P.M.; Reuther, M.; Williams, M. (Eds.), Springer Verlag Berlin, Heidelberg 2001, pp 4, 2001.
- Klein, L., K. von Salzen, M. Schulz, L. Spokes, S. Tamm, and H. Schlünzen. Simulated aerosol size distribution over the North Sea using the aerosol model SEMA. *J. Aerosol Science*, **30**, Suppl. 1, S197–S198, 1999a.
- Klein, L., K. von Salzen, M. Schulz, L. Spokes, S. Tamm, and H. Schlünzen. Comparison of simulated and measured size distributions in a coastal area using the aerosol model SEMA. Book of abstracts, ELOISE 3rd Open Science Meeting, 1–4 December 1999, Noordwijkerhout, The Netherlands, p. 124, 1999b.
- Kleinman, L. I., P. H. Daum, Y-N. Lee, S. R. Springston, L. Newman, W. R. Leitch, C. M. Banic, G. A. Isaac, and J. I. MacPherson. Measurement of O<sub>3</sub> and related compounds over southern Nova Scotia 1. Vertical distributions, *J. Geophys. Res.*, **101**, 29,042–29,060, 1996.
- Lenz, C.-J., F. Müller, and K. H. Schlünzen. The sensitivity of mesoscale chemistry transport model results to boundary values. *Environmental Monitoring and Assessment*, **65**, 287–295, 2000.
- Lüpkes, C., and K. H. Schlünzen. Modelling the arctic convective boundary-layer with different turbulence parameterizations. *Boundary Layer Meteorol.*, **79**, 107–130, 1996.
- Lyons, W. A. The Climatology and Prediction of the Chicago Lake-breeze. *J. Appl. Meteorol.*, **11**, 1259–1270, 1972.
- McKeen, S. A., E.-Y. Hsie, M. Trainer, R. Tallamraju, and S. C. Liu. A Regional Model Study of the Ozone Budget in the Eastern United States. *J Geophys. Res.* **96**: 10,809–10,845. 1991.
- Melas, D., G. Abbate, D. Haralampopoulos, and A. Kelesidis. Estimation of Meteorological Parameters for Air Quality Management: Coupling of Sodar Data with Simple Numerical Models. *J. Appl. Meteorol.*, **39**, 509–515, 2000a.
- Melas, D., A. Lavagnini, and A-M. Sempreviva. An Investigation of the Boundary Layer Dynamics of Sardinia Island under Sea-Breeze Conditions. *J. Appl. Meteorol.*, **39**, 516–524, 2000b.
- Meng, Z., J. H. Seinfeld, P. Saxena, and Y. P. Kim. Atmospheric gas–aerosol equilibrium, IV: thermodynamics of carbonates. *Aerosol Science and Technology*, **23**, 131–154, 1995.
- Merrill, J. T., and J. L. Moody. Synoptic meteorology and transport during the North Atlantic Regional Experiment (NARE) intensive: Overview, *J. Geophys. Res.*, **101**, 28,903–28,921, 1996.

## References

- Michaels, A. F., D.A. Siegel, R. J. Johnson, A. . Knap and J. N. Galloway. Episodic inputs of atmospheric nitrogen to the Sargasso Sea: Contributions to new production and phytoplankton blooms. *Global Biogeochem. Cycles*, **7**, 339–351, 1993.
- Middleton, P., W. R. Stockwell, and W. P. L. Carter. Aggregation and analysis of volatile organic compound emissions for regional modeling. *Atmospheric Environment*, **24A**, 1107–1133, 1990.
- Millan., M. M., E. Mantilla, R. Salvador, A. Carratala, and M. J. Sanz. Ozone Cycles in the Western Mediterranean Basin: Interpretation of Monitoring Data in Complex Coastal Terrain. *J. Appl. Meteorol.*, **39**, 487–508, 2000.
- Monahan, E. C., C. W. Fairall, K. L. Davidson, and P. Jones-Boyle. Observed interrelations between 10m winds, ocean whitecaps and marine aerosols. *Q. J. R. Meteorol. Soc.*, **109**, 379–392, 1983.
- Müller F., K. H. Schlünzen, and M. Schatzmann. Test of numerical solvers for chemical reaction mechanisms in 3D air quality models. *Environmental Modelling Software*, **15**, 639 – 646, 2000.
- Müller, F., K. H. Schlünzen, and M. Schatzmann. Evaluation of the chemistry–transport model MECTM using TRACT measurements – effect of different solvers for the chemical mechanism. *Air Pollution Modeling and Its Application*, **XIV**, 583–590, 2001.
- Nenes, A., S. N. Pandis, and C. Pilinis. Continued development and testing of a new thermodynamic aerosol module for urban and regional air quality models. *Atmospheric Environment*, **33**, 1553–1560, 1999.
- O'Dowd, C. D. and M. H. Smith. Physicochemical properties of aerosols over the Northeast Atlantic: Evidence for wind-speed-related submicron sea-salt aerosol production. *J. Geophys. Res.*, **98**, 1127–1149, 1993.
- O'Dowd, C. D., M. E. Smith, I. E. Consterding, and J. A. Lowe. Marine aerosol, sea-salt, and the marine sulphur cycle: A short review. *Atmospheric Environment*, **31**, 73–80, 1997.
- Ottley, C. J. and R. M. Harrison. The spatial distribution and particle size of some inorganic nitrogen, sulphur and chlorine species over the North Sea, *Atmospheric Environment*, **26**, 1989–1699, 1992.
- Owens, N.P., J.N. Galloway and R.A. Duce, 1992: Episodic atmospheric nitrogen deposition to oligotrophic oceans. *Nature*, **357**, 397–399.
- Pahl S. Parameterisierung der trockenen Deposition in einem mesoskaligen Transport- und Stroemungsmodell. Diploma paper. Meteorologisches Institut der Universitaet Hamburg.

- Pakkanen, T.A. Study of formation of coarse particle nitrate aerosol. *Atmospheric Environment*, **30**, 2475–2482, 1996.
- Pilinis, C. Derivation and numerical solution of the species mass distribution equations for multicomponent particulate systems. *Atmospheric Environment*, **24A**, 1923–1928, 1990.
- Pilinis, C., J. H. Seinfeld, and D. Grosjean. Water content of atmospheric aerosols. *Atmospheric Environment*, **23**, 1601–1606, 1989.
- Pilinis, C. and J. H. Seinfeld. Continued development of a general equilibrium model for inorganic multicomponent atmospheric aerosols. *Atmospheric Environment*, **21**, 2453–2466, 1987.
- Pio, C. A., T. V. Nunes, and R. M. Leal. Kinetic and thermodynamic behavior of volatile ammonium compounds in industrial and marine atmospheres. *Atmospheric Environment*, **26A**, 505–512, 1992.
- Pitzer, K. S. *Activity Coefficients in Electrolyte Solutions*, 2nd Edn. CRC Press, Boca Raton, FL., 536 pp., 1981.
- Plate, E., T. Stahlschmidt, M. Schulz, and W. Dannecker. The influence of air–sea-exchange on the partitioning of N-species during transport over sea, In: Jaehne, B., Monahan, E.C. (Eds.), third Int. Symp. On Air–Water Gas Transfer. AEON-Verlag, Hanau, 735–744, 1995.
- Pruppacher, H.R. and J.D. Klett. *Microphysics of Clouds*. D.Reidel, 714 pp., 1978.
- Pryor, S. C., and R. J. Barthelmie. Particle Dry Deposition to Water Surfaces: Processes and Consequences. *Marine Pollution Bulletin*, **41**, 220–231, 2000.
- Ruggaber, A., R. Dlugi, and T. Nakajima. Modelling Radiation Quantities and Photolysis Frequencies in the Troposphere. *J. Atmos. Chem.*, **18**, 171–210, 1994.
- Savoie, D. L. and J. M. Prospero. Comparison of oceanic and continental sources of non-sea-salt sulfate over the Pacific Ocean. *Nature*, **339**, 685–687, 1989.
- Schimmel, F. Parametrisierung der Wolkentropfenbildung für mehrdimensionale Atmosphärenmodelle. Diplomarbeit am Meteorologisches Institut, Universität Hamburg, 1999.
- Schlünzen, K.H. Numerical studies on the inland penetration of sea breeze fronts at a coastline with tidally flooded mudflats. *Beitr. Phys. Atmosph.*, **63**, 243–256, 1990.
- Schlünzen, K.H. Mesoscale modelling in complex terrain – an overview on the German nonhydrostatic models. *Beitr. Phys. Atmosph.*, **67**, 243–253, 1994.
- Schlünzen K. H. Model inventory for EUROTRAC2 subproject SATURN. Proceedings from the EUROTRAC2 Symposium 2000, Midgley, P.M.; Reuther, M.; Williams, M. (Eds.), Springer Verlag Berlin, Heidelberg, 2001.

- Schlünzen, K. H., K. Bigalke, C. Lüpkes, U. Niemeier, and K. von Salzen. Concept and realization of the mesoscale transport- and fluid-model METRAS. Meteorologisches Institut, Universität Hamburg, METRAS Techn. Rep. 5, 156 pp, 1996.
- Schlünzen K.H., L. Klein, C.J. Lenz, F. Müller, and K. von Salzen. Simulation of coastal atmospheric processes including aerosols. *CAPMAN annual report, international scientific secretariat; GSF– Forschungszentrum für Umwelt und Gesundheit GMBH*, 63 – 67, 2000.
- Schlünzen, K. H. and U. Krell. Mean and local transport in air, In: Sündermann, J. (ed.): "Circulation and contaminant fluxes in the North Sea", *Springer Verlag, Berlin*, 344 pp, 1994.
- Schlünzen, K.H., T. Stahlschmidt, A. Rebers, U. Niemeier, M. Kriews, W. Dannecker, Atmospheric input of lead into the German Bight – A high resolution measurement and model case study for April 23rd to 30th, 1991. *Mar. Ecol. Prog. Ser.*, **156**, 299–309, 1997.
- Schlünzen, K. H., and S. Pahl. Modification of dry deposition in a developing sea-breeze circulation – a numerical case study, *Atmospheric Environment*, **26 A**, 51–61, 1992.
- Schulz, M. Synthesis and new conception of North Sea Research (SYCON) External Expertise: Overview on measurements and monitoring of air–sea exchange of anthropogenic inorganic compounds in the North Sea region, *Ber. ZMK Z* **13**, 2001.
- Seinfeld, J. H. "Atmospheric Chemistry and Physics of Air Pollution". John Wiley and Sons, New York, 738 pp., 1986.
- Seinfeld, J. H. and S. N. Pandis. "Atmospheric Chemistry and Physics". John Wiley and Sons, New York, 1360 pp., 1998.
- Singh, S. P., G. S. Satsangi, P. Khare, A. Lakhani, K. Maharaj Kumari, and S. S. Srivastava. Multiphase measurement of atmospheric ammonia. *Chemosphere–global Change Sci.*, **3**, 107–116, 2001.
- Slinn, S., and W. Slinn. Predictions for particle deposition on natural waters. *Atmospheric Environment*, **14**, 1013–1016, 1980.
- Smiatek G. Mapping land use for modelling biogenic and anthropogenic emissions. Proceedings of the EUROTRAC2 Symposium 1998.
- Spokes L., T. Jickells, A. Rendell, M. Schulz, A. Rebers, W. Dannecker, O. Krueger, M. Leermakers, and W. Baeyens. High Atmospheric Nitrogen Deposition Events Over the North Sea. *Marine Pollution Bulletin*, **26**, 698–703, 1993.

- Stockwell, W. R., P. Middleton, J. S. Chang, and X. Tang. The Second Generation Regional Acid Deposition Model Chemical Mechanism for Regional Air Quality Modeling. *J. Geophys. Res.*, **95**, 16343–16367, 1990.
- Stokes, R. H., and R. A. Robinson. Interactions in Aqueous Nonelectrolyte Solutions. I. Solute–Solvent Equilibria. *J. Phys. Chem.*, **70**, 2126–2130, 1966.
- Sun, Q., and A. S. Wexler. Modeling urban and regional aerosols near acid neutrality – application to the June 24–25 SCAQS episode. *Atmospheric Environment*, **32**, 3533–3542, 1998.
- Tamm, S. and Schulz, M. Open ocean aerosol composition obtained during 15 months on a North sea ferry. Submitted for publication in *Atmospheric Environment*, 2002.
- Tang, I. N, and H. R. Munkelwitz. Composition and temperature dependence of the deliquescence properties of hygroscopic aerosols, *Atmospheric Environment*, **27A**, 467–473, 1993.
- Tang, I. N. Thermodynamic and optical properties of mixed-salt aerosols of atmospheric importance. *J. Geophys. Res.*, **102**, 1883–1893, 1997.
- Turco, R. "Atmospheric chemistry," Chapter 7, *Climate System Modeling*, K. E. Trenberth, Ed., Cambridge University Press, 201–240, 1993.
- USGeological Survey. S: Global digital elevation model GTOPO30. U.S. Geological Survey, EROS Data Center in Sioux Falls, South Dakota. 1996.
- Von Salzen K., Claussen M., and Schlünzen K.H. Application of the concept of blending height to the calculation of surface fluxes in a mesoscale model. *Meteorol. Zeitschrift*, **5**, 60–66, 1996.
- Von Salzen K. Entwicklung und Anwendung eines Modells für die Dynamik und Zusammensetzung des sekundären und marinen Aerosols. *Ber. aus dem Zentrum f. Meeres- und Klimaforschung, Meteorologisches Institut, Universität Hamburg*, **30**, 167 pp., 1997.
- Von Salzen, K., and K. H. Schlünzen. A Prognostic Physico–Chemical Model of Secondary and Marine Inorganic Multicomponent Aerosols: Part I. Model Description. *Atmospheric Environment*, **33**, 567–576, 1999a .
- Von Salzen, K., and K. H. Schlünzen. A Prognostic Physico–Chemical Model of Secondary and Marine Inorganic Multicomponent Aerosols: Part II. Model Tests. *Atmospheric Environment*, **33**, 1543–1552, 1999b .
- Von Salzen, K., and K. H. Schlünzen. Simulation of the dynamics and composition of secondary and marine inorganic aerosols in the coastal atmosphere. *J. Geophys. Res.*, **104**, 30,201–30,217, 1999c.

## References

- Wesely, M.L. Parameterization of surface resistance to gaseous dry deposition in regional scale numerical models. *Atmospheric Environment*, **23**, 1293–1304, 1998.
- Wesely, M. L., and B. B. Hicks. Some factors that affect the deposition rates of sulfur dioxide and similar gases on vegetation. *Journal of the Air Pollution Control Association*, **27**, 1110–1117, 1977.
- Wesely, M. L., and B. B. Hicks. A review of the current status of knowledge on dry deposition. *Atmospheric Environment*, **34**, 2261–2282, 2000.
- Wexler, A. S., F. W. Lurmann, and J. H. Seinfeld. Modelling urban and regional aerosols – I. Model development. *Atmospheric Environment*, **28**, 531–546, 1994.
- Wexler, A. S. and J. H. Seinfeld. The distribution of ammonium salts among a size and composition dispersed aerosol. *Atmospheric Environment*, **24A**, 1231–1246, 1990.
- Wexler, A. S. and J. H. Seinfeld. Second-generation inorganic aerosol model. *Atmospheric Environment*, **25A**, 271–2748, 1991.
- Wickert, B. (2000) personnel communication, 06.04.00.
- Wu Zengmao and K. H. Schlünzen. Numerical study on the local wind structures forces by the complex terrain of Qingdao Area. *Acta Meteorologica Sinica*, **6**, 355–366, 1992.
- Young, T. R. and J. P. Boris, A Numerical Technique for Solving Ordinary Differential Equations Associated with the Chemical Kinetics of Reactive-Flow Problems. *J. Physical Chemistry*, **81**, 2424–2427, 1977.
- Zhang Y., C. Seigneur, J. H. Seinfeld, M. Jacobson, S. L. Clegg, and F. S. Binkowski. A comparative review of inorganic aerosol thermodynamic equilibrium modules: similarities, differences, and their likely causes. *Atmospheric Environment*, **34**, 117–137, 2000.
- Zufall, M. J., M. H. Bergin, and C. I. Davidson, Effects of Non-Equilibrium Hygroscopic Growth of  $(\text{NH}_4)_2\text{SO}_4$  on Dry Deposition to Water Surfaces. *Environm. Sci. Technol.*, **32**, 584–590, 1998